

2016

Bioavailability and Transformation of Silver Nanoparticles in the Freshwater Environment

Seth W. Brittle

Wright State University - Main Campus

Follow this and additional works at: https://corescholar.libraries.wright.edu/etd_all



Part of the [Chemistry Commons](#), and the [Environmental Sciences Commons](#)

Repository Citation

Brittle, Seth W., "Bioavailability and Transformation of Silver Nanoparticles in the Freshwater Environment" (2016). *Browse all Theses and Dissertations*. 2412.

https://corescholar.libraries.wright.edu/etd_all/2412

This Dissertation is brought to you for free and open access by the Theses and Dissertations at CORE Scholar. It has been accepted for inclusion in Browse all Theses and Dissertations by an authorized administrator of CORE Scholar. For more information, please contact library-corescholar@wright.edu.

BIOAVAILABILITY AND TRANSFORMATION OF
SILVER NANOPARTICLES
IN THE FRESHWATER ENVIRONMENT

A dissertation submitted in partial fulfillment of the
requirements for the degree of
Doctor of Philosophy

By

SETH WILLIAM BRITTLE

B.S., Marist College, 2012

2016
Wright State University

WRIGHT STATE UNIVERSITY
GRADUATE SCHOOL

December 9, 2016

I HEREBY RECOMMEND THAT THE DISSERTATION PREPARED UNDER MY SUPERVISION BY Seth William Brittle ENTITLED Bioavailabilty and Transformation of Silver Nanoparticles in the Freshwater Environment BE ACCEPTED IN PARTIAL FULFILMENT OF THE REQUIREMENTS FOR THE DEGREE OF Doctor of Philosophy.

Ioana E. Sizemore, Ph.D.
Dissertation Director

Don Cipollini, Ph.D.
Director, Environmental Sciences
Ph.D. Program

Robert E. W. Fyffe, Ph.D.
Vice President for Research and
Dean of the Graduate School

Committee on
Final Examination

Ioana E. Sizemore, Ph.D.

Steven R. Higgins, Ph.D.

David A. Dolson, Ph.D.

Lynn K. Hartzler, Ph.D.

Sushil R. Kanel, Ph.D.

ABSTRACT

Brittle, Seth William Ph.D., Environmental Science Ph.D. Program, Department of Chemistry, Wright State University, 2016. Bioavailability and Transformation of Silver Nanoparticles in the Freshwater Environment.

The proliferation of silver nanoparticles (AgNPs) in consumer products and industrial applications has generated many environmental concerns since the chemistry of silver changes at the nanoscale and the very properties that make them desirable – their unique reactivity – may pose environmental risks. This dissertation addresses these concerns from three different angles. First, freshwater crayfish is demonstrated as a potential benthic indicator of Ag pollution since Ag accumulation depends on the form of Ag. The uptake and distribution of Ag (from AgNPs or Ag^+) in tissue samples were measured by inductively coupled plasma optical emission spectroscopy (ICP-OES). The hepatopancreas ($1.5\text{-}17.4\ \mu\text{g of Ag g}^{-1}$ of tissue) was identified as the best tissue-indicator of AgNP pollution, while the gills ($4.5\text{-}22.0\ \mu\text{g g}^{-1}$) and hepatopancreas ($2.5\text{-}16.7\ \mu\text{g g}^{-1}$) complementarily monitored the presence of Ag^+ . Next, label-free and labeled-enhanced Raman imaging is proposed as a method to characterize AgNPs adsorption behavior and distribution to minerals. The results of this study demonstrate that label-free Raman can detect direct chemical interactions (Ag-O stretching at $241\ \text{cm}^{-1}$) while Label-enhanced Raman can reveal AgNPs distribution, when no molecular interactions are spectroscopically detected, through a SERS-probe. Lastly, an educational laboratory module developed to introduce undergraduate and graduate STEMM students to AgNPs, ICP-OES, and US EPA endorsed calibration methods is shown to be effective with the assessment of laboratory skills and class assignments. Together these studies offer insight into AgNPs future and how to compromise between nanotechnological progress and unfamiliar environmental risks.

TABLE OF CONTENTS

	Page
1. CHAPTER 1	
AN INTRODUCTION TO THE HISTORY, CHEMISTRY, AND TOXICITY OF SILVER NANOPARTICLES AND ENVIRONMENTAL CONCERNS ASSOCIATED WITH THEIR RELEASE INTO FRESHWATER.....	1
Background.....	2
History.....	4
Chemistry.....	7
Toxicity.....	11
Environmental Concerns.....	12
Gaps of Knowledge and Main Goals.....	17
Referencess.....	18
2. CHAPTER 2	
FRESHWATER CRAYFISH: A POTENTIAL BENTHIC-ZONE INDICATOR OF NANOSILVER AND IONIC SILVER POLLUTION.....	22
Copyright Permission.....	23
Summary of Involvement.....	23

Graphical Abstract	24
Abstract	24
Keywords	25
Introduction.....	25
Materials and Methods.....	28
Results and Discussion.....	34
Conclusion	47
Acknowledgements.....	47
References.....	48
Associated Content	60

3. CHAPTER 3

A RAMAN-BASED MOLECULAR IMAGING METHODOLOGY FOR CHARACTERIZING THE ADSORPTION BEHAVIOR AND DISTRIBUTION OF SILVER NANOPARTICLES TO HYDRATED MINERAL SURFACES	84
--	----

Copyright Permission.....	85
Summary of Involvement	85
Abstract	86
Keywords	87
Introduction.....	87

Materials and Methods.....	91
Results and Discussion.....	96
Conclusion	106
Acknowledgements.....	106
References.....	107
Associated Content	112

4. CHAPTER 4

MEASURING THE SILVER COMPOSITION OF NANOCOLLOIDS BY INDUCTIVELY COUPLED PLASMA– OPTICAL EMISSION SPECTROSCOPY: A LABORATORY EXPERIMENT FOR CHEMISTRY AND ENGINEERING STUDENTS	117
Copyright Permission.....	118
Summary of Involvement	118
Abstract.....	119
Keywords	120
Introduction.....	120
Materials and Methods.....	122
Results and Discussion.....	125
Conclusion	130

Acknowledgements.....	131
References.....	132
Associated Content	134
5. CHAPTER 5	
CONCLUSIONS AND FUTURE WORK	157
6. CHAPTER 6	
CURRICULUM VITAE.....	160

LIST OF FIGURES

Figure 1.1 Number of listed nanomaterial products by inventory date.	6
Figure 1.2 Number of indicated nanomaterials per material.....	6
Figure 1.3 Subcategories of nanosilver applications.....	7
Figure 2.1 Schematic showing the separation of the two Ag species (AgNPs and Ag ⁺) from the HRW in the aquaria at day 1 and day 14 after the AgNP exposure via CPE and centrifugation, and their subsequent quantification for total Ag by ICP-OES	36
Figure 2.2 Total Ag accumulation within Ag-exposed tissues from <i>P. clarkii</i> and <i>O.</i> <i>virilis</i>	40
Figure 2.3 Schematic showing the possible exposure routes to environmental Ag pollution	43
Figure 2.4 Degree of DNA damage quantified through comet lengths	45
Figure 2.5 Histological cross sections of hepatopancreas tissues	46
Figure 2.S1 Schematic of the experimental design.....	61
Figure 2.S2 Summary of previous research on the biological impact of nanosilver and ionic Ag ⁺ in freshwater organisms.....	62

Figure 2.S3 Summary of current (2015) silver regulations within various government agencies.....	62
Figure 2.S4 Spectroscopic characterization of AgNPs	65
Figure 2.S5 Pictures of the CPE experimental set-up.....	66
Figure 2.S6 UV-Vis absorbance spectra.....	67
Figure 2.S7 Water metrics measured daily before and during the <i>P. clarkii</i> experiment	68
Figure 2.S8 Water metrics measured daily before and during the <i>O. virilis</i> experiment	69
Figure 2.S9 Average percent weight change for A) <i>P. clarkii</i> and B) <i>O. virilis</i>	72
Figure 2.S10 Average fear response assigned using a ranking scale of 1 to 7	72
Figure 2.S11 ICP-OES calibration curves	74
Figure 2.S12 Percent of Ag distribution	76
Figure 2.S13 Sample epifluorescent images from Single-Cell Gel Electrophoresis comet assays on neural complex tissue (encephalon and ganglion) from <i>P. clarkii</i>	78
Figure 2.S14 Histological cross sections of the encephalon tissue stained with hematoxylin and eosin in both crayfish species.....	79
Figure 2.S15 Comparison of crayfish gill architecture in <i>P. clarkii</i>	79
Figure 3.1 Chemical images of large corundum samples	98
Figure 3.2 Raman spectra and statistical analysis of micro-sized corundum at all experimental pH values Chemical images of large corundum samples	100

Figure 3.3 Visual complexation scheme of adsorption mechanisms	101
Figure 3.4 Average percent adsorption of AgNPs to α -Al ₂ O ₃	102
Figure 3.5 AFM images of macro-sized corundum windows.....	103
Figure 3.6 10 μ M 10 ⁻³ M R6G dried on freshly cleaved muscovite and both AgNPs and 10 μ M 10 ⁻⁴ M R6G dried on freshly cleaved muscovite	105
Figure 3.S1 Raman map of bare muscovite surface.....	115
Figure 3.S2 Silver nanoparticle colloid on muscovite	116
Figure 4.1 Sample calibration curves.....	126

LIST OF TABLES

Table 1.1 Criteria and appropriate characterization methods proposed by the USEPA to appropriately characterize nanomaterials.	10
Table 2.S1 Summary of physical changes observed throughout experiments.....	71
Table 2.S2 Total Ag detected in digested tissue samples.	75
Table 2.S3 Summary of all measured DNA comets for both species and amongst all treatments.....	77
Table 3.S1 Summary of controls and samples for both minerals and the instrumental method they were analyzed with.....	112
Table 3.S2 Vibrational modes, and tentative assignments of Muscovite.....	113
Table 3.S.3 Tentative assignments of the Raman vibrational modes observed for α - Al_2O_3	114
Table 4.1 Class average values and standard deviations for the total Ag composition of Creighton colloids as obtained by students through ICP-OES	128
Table 4.2 Results of the anonymous evaluations of laboratory skills (S1-S6) performed by the instructors in the <i>Experimental Nanomaterials and Nanoscience</i> course.....	130

Table 4.3 Results of the anonymous, student evaluations of several laboratory aspects (Q1-Q3) in the two courses.....	130
Table 4.S1 Tentative time schedule for the proposed laboratory experiment.....	149
Table 4.S2 Average percent errors (%) from each course, calibration method, and wavelength.	150
Table 4.S3 Percent differences (%) calculated for each student group, for the 328.068 nm emission line of Ag.....	151
Table 4.S4 Percent differences (%) between the primary and secondary emission lines of Ag-based off course averages	152

CHAPTER 1

AN INTRODUCTION TO THE HISTORY, CHEMISTRY, AND TOXICITY OF SILVER NANOPARTICLES AND ENVIRONMENTAL CONCERNS ASSOCIATED WITH THEIR RELEASE INTO FRESHWATER

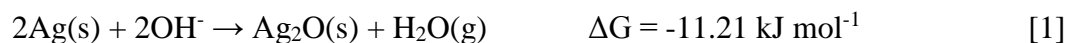
BACKGROUND

Elemental Silver: As with any other element, the location on the periodic table helps define a set of inherent properties that set elements apart from one another. Silver is located in group 11 (IB) and period 5 of the periodic table and is therefore classified as a transition metal. Group 11 elements are commonly referred to as the coinage metals (when the synthetically made roentgenium is ignored) because they all exhibit unique physiochemical properties that make them desirable for monetary purposes. Together with copper and gold, coinage metals have been cherished for their stability, durability, and luster, making them easily commutable materials of value. Silver's residence in period 5 places it vertically between copper and gold with five electron shells. Contrary to expectations, silver is more stable when it fills the $4d$ shell before the $5s$, leaving one lone electron in the $5s$ orbital. With an ionization energy of $730.8 \text{ kJ mol}^{-1}$, the most important silver ion is Ag^+ (also written as Ag(I)). Although Ag(II) and Ag(III) are possible, they are extremely rare as their ionization energies are much higher: $2,072.6$ and $3,359.4 \text{ kJ mol}^{-1}$, respectively¹. Therefore, the most environmentally relevant forms of silver are Ag(0) and Ag(I) . The zero-valent form of silver, Ag(0) , is not very reactive as it is merely the same metallic form monetarily revered throughout history. Also, silver is located fairly low in the reactivity series for metals, but silver surfaces can react (tarnish) with oxygen to form a silver oxide (Ag_2O). Since the focus here is AgNPs, which are known to release Ag^+ ions, the Ag(I) ion demands further attention as it is quite stable against reduction to Ag(0) in aqueous solutions. As a monovalent cation, Ag^+ is one of the most competitive cation exchangers in soil solutions since it has one of the smallest hydrated radii: 2.77\AA resulting in greater polarizability². It can function as a Lewis acid in solution by binding to a ligand,

such as a sulfide, and accepting its electrons. Ligands are found commonly in freshwater environments (in abiotic and biotic soil components) thus silver complexes are more common than Ag^+ alone. The oxidation of silver to Ag^+ becomes an extremely important biogeochemical process because the affinity of Ag^+ towards ligands will impact the fate and transportation of many anthropogenic silver sources - from silver compounds to nanosilver.

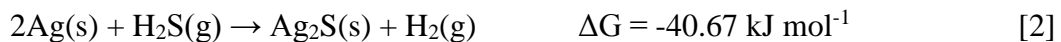
Mineral Silver: As a precious metal, silver has historically existed in a dynamic balance of supply and demand that has helped define countless cultures and economies. Its luster and rarity have been cherished for over 5 millennia³, but before silver ended up on fingers and dinner tables, it existed in the earth's crust. As only a minor constituent, silver occurs at an average concentration of 0.1 mg kg^{-1} throughout the world⁴ and is only the 67th most abundant metal in the earth's crust⁵. Traditionally, silver was mined alongside other metals as minerals. Argentite (a sulfide) and chlorargyrite (a chloride) are the most common, but silver has also been produced as a byproduct of refining for gold, copper, or lead⁵. Silver is then refined, smelted into its purest form, and sold to countless consumers for a variety of purposes.

Metallic Silver: The wonderful feature of silver metal is that its inherent value makes it rarely disposed of. Even in the modern manufacturing process, most waste is recovered and reused to eliminate financial losses. However, silver surfaces may eventually oxidize, as shown below [1]⁶.



Although aesthetically altered, only a negligible thickness of the surface is affected. Silver will more readily turn to silver sulfide as seen below [2]. This occurs when atmospheric

hydrogen sulfide is available, perhaps from industrial processes or decaying organic matter⁷.



Silver sulfide is also not particularly reactive (with no free ion) or soluble and is basically the same form commonly seen in nature (argentite). Furthermore, the formation of Ag_2S helps prevent further oxidation of the silver metal.

Nanosilver: Silver's strength, malleability, ductility, conductivity, reflectance, and reactivity may make it valuable in many industrial processes, but its employment as a nanomaterial has generated a whole other realm of irreplaceable applications. In the simplest sense, silver nanotechnology can be defined as the exploitation of silver's unique properties that exist in nanoscale dimensions⁸. As a bulk material and a compound, silver has already proven itself useful; but at the nanoscale, silver exhibits unique properties that are truly invaluable. Its chemical reactivity changes with smaller dimensions, and this becomes crucial in many consumer products. This growth into over 400 consumer products is best explained by looking at AgNPs' history¹⁶.

HISTORY

Although AgNPs seem relatively new, they have been around for a lot longer than the recent label will suggest. The term "nano" was first used to describe particle size in 1914 by Richard Adolf Zsigmondy, but he was describing particles that already existed⁹. The earliest evidence of using nanomaterials was the Lycurgus cup from ancient Rome. It is a depiction of a scene from Homer's Iliad, and a unique example of ancient dichroic glass - different colors are illuminated depending where the light source is. Transmission electron microscopy has revealed that this phenomenon is attributable to gold and AgNPs

incorporated into the glass¹⁰. Similarly, during the medieval period, monks inadvertently incorporated nanoparticles into stained glass. Modern technologies revealed that different shapes and sizes of Au- and Ag-NPs offer varied surface plasmon resonances (SPR) leading to multiple colors¹¹ (discussed later). The next incident of AgNPs incorporated them into the Deruta Ceramics. Here, AgNPs were used to create the very particular luster. Ultraviolet-visible absorbance spectroscopy (UV-Vis) confirmed absorbances around 420–440 nm, which are indicative of the nanosilver SPR.¹²

The history of nanosilver continued in scarcity until 1889 when M. C. Lea reported the first synthesis of colloidal silver. She was developing on Faraday's silver solution and improved it to remain stable^{13,14}. By the end of the 19th century, the first commercially manufactured nanosilver was sold over the counter as a biocide marketed under the name Collargol¹³. A few more products were developed, and all were marketed as medicinal biocides, but their popularity was soon overshadowed by more readily available antibiotics, such as penicillin¹⁵. Colloidal silver returned in 1954 as a chlorine alternative for residential swimming pools. Algaedyn became the first regulated silver product under the Federal Insecticide, Fungicide, and Rodenticide (FIFRA) as an algaecide¹³. Nanotechnologies have now found their way into over 1600 consumer products – a 400% increase since 2005 (Figure 1.1)¹⁶. From fabrics to electronics, AgNPs are now incorporated into a wide variety of products. Nanosilver alone accounts for over half of the total products listed on the consumer products inventory from the project on emerging nanotechnologies (Figure 1.2). The largest subcategory of nanosilver applications is the health and fitness sector almost exclusively because of AgNPs antimicrobial properties (Figure 1.3).

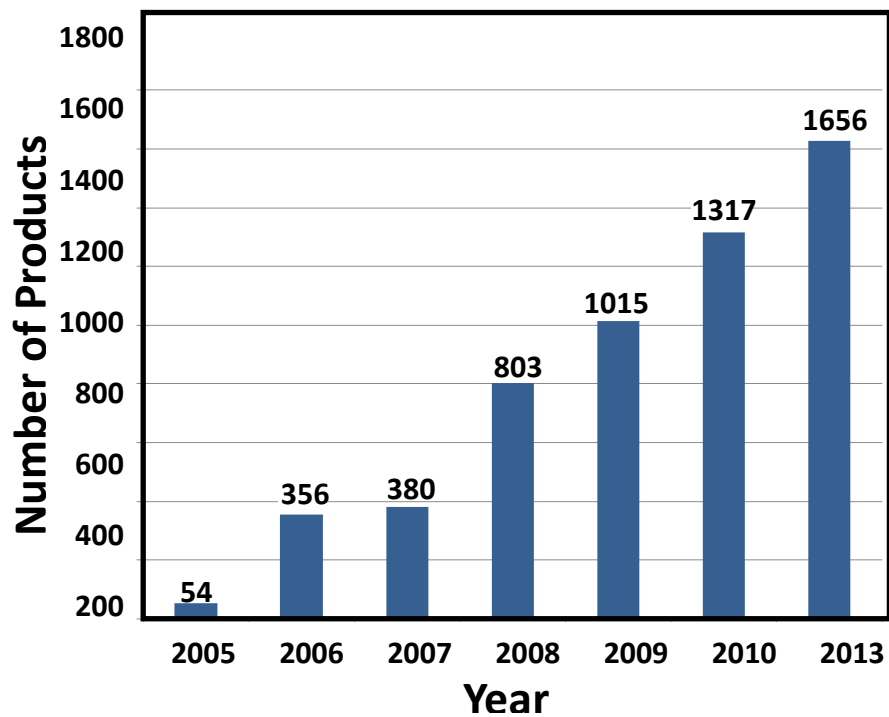


Figure 1.1 Number of listed nanomaterial products by inventory date.¹⁶

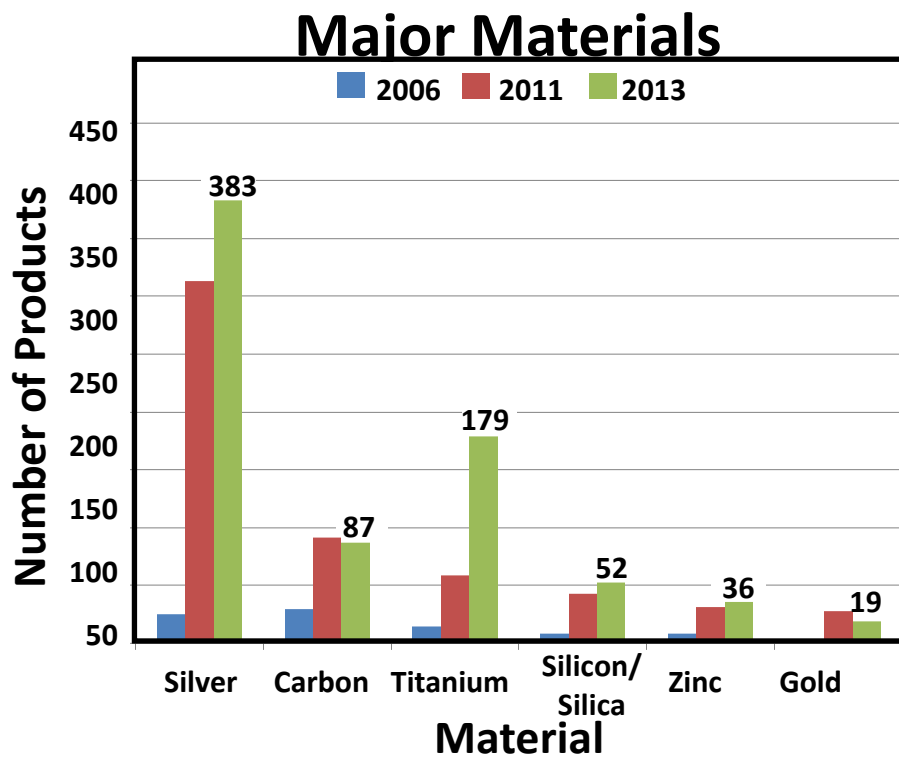


Figure 1.2 Number of indicated nanomaterials per material¹⁶.

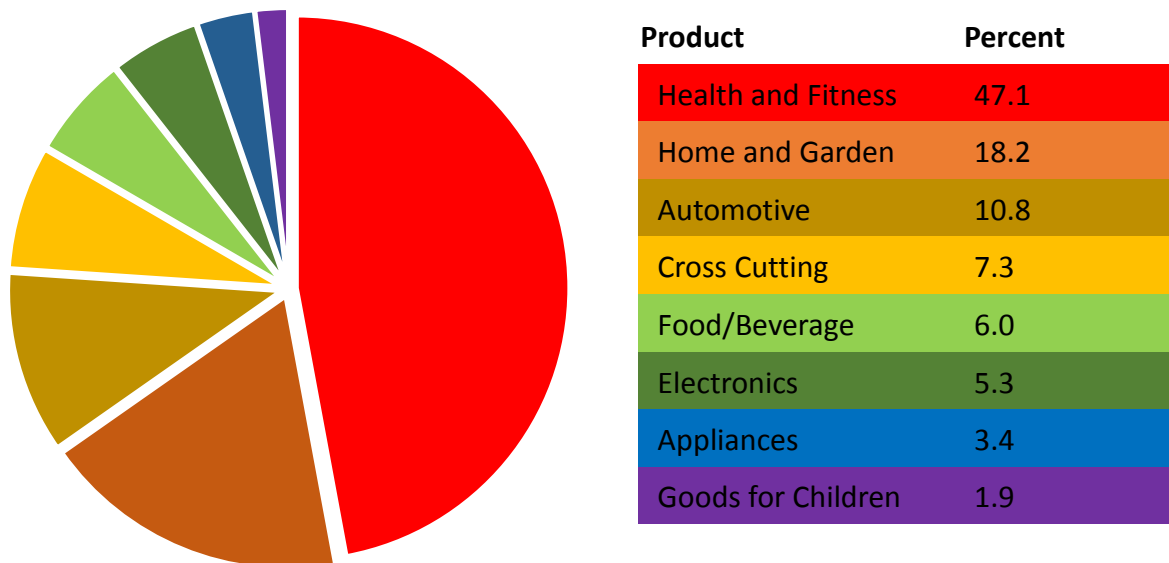


Figure 1.3 Subcategories of nanosilver applications¹⁶

CHEMISTRY

There are many options in nanotechnology, but nanosilver remains the most popular. Like all nanoparticles, AgNPs exhibit a high surface area to volume ratio. So why is silver used more than any other nanomaterial? Perhaps it is because the extensive versatility of nanosilver has been proven in antimicrobial, optical, and conductive applications. But why has silver succeeded with such versatility? This goes back to the unique electron configuration - the lone *s* electron that makes the silver ion very reactive. AgNPs exploit this property on a larger scale. Essentially, AgNPs are by definition, composed of zero-valent metallic Ag that act as a source of Ag⁺ ions¹⁷. Therefore, the high surface area is a particularly important property for nanosilver because it increases the rate at which silver ions are released. In fact, many silver nanoparticles are engineered to release

silver ions. This gives AgNPs their most desired characteristic – their antimicrobial activity.

Antimicrobial Properties: The broad spectrum of antimicrobial activities have made AgNPs desired in many personal care products and medical devices. Nanosilver can inhibit the growth of both gram-positive and gram-negative bacteria¹⁸. Viruses have also been shown to be susceptible to AgNPs. Nanosilver decreases HIV activity and also inhibits further replication¹⁹. The inhibition of hepatitis B virus²⁰ and herpes simplex virus²¹ was also assessed. Nanosilver is even an effective fungicide. AgNPs can kill a number of ordinary fungal strains including *Aspergillus fumigatus*²². It is reported AgNPs biocidal activity is attributable to the slow release of Ag⁺. Other mechanisms such as interaction with thiol groups in proteins and enzymes, inhibition of DNA replication, and induction of oxidative stress¹⁵ make it more difficult for bacteria to produce resistant strains. These antiviral and antimicrobial properties have been used in everything from water filtration²³ to coating socks^{24,25}. Other than direct applications, AgNPs have even been used as biosensors for quantitative detection²⁶.

Optical Properties: In addition to antimicrobial properties, AgNPs exhibit unique optical characteristics. Under irradiation of light, AgNPs display surface plasmon resonance (SPR). This is the same phenomena used to confirm nanoparticles' presence in ancient materials, like the Lycurgus cup. Essentially, the unique lone *s* electron creates an optical anomaly. The collective oscillations of columbic attractions between the negative electron cloud and the positive nuclei create the SPR²⁷. This phenomenon is visible with UV-Vis spectroscopy and is typically used to characterize AgNPs. Since the width and position of the SPR peaks are influenced by the size, shape, and dispersion of the

nanoparticles, UV-Vis offers quick estimates of these characteristics²⁸. The resultant absorbance peak within a spectrum directly relates to molecules absorbing electromagnetic radiation (ultraviolet and visible light) within a specific wavelength region. The optical properties of nanosilver also offer an enhancement to other spectroscopic techniques like surface enhanced Raman spectroscopy (SERS) and metal-enhanced fluorescence²⁹. Incident electromagnetic radiation is enhanced in the presence of nanosilver SPR and can consequently increase the detection limits of Raman techniques. Although not effective for all analytes, this enhancement does offer increased versatility.

Conductive and Thermal Properties: Conductive and thermal properties have opened the potential for printing circuit components. Nanoscale electronics open a whole realm of electronic possibilities. Not only can circuit components be made smaller, but they can offer mechanical flexibility. With this advancement, nanosilver films can be developed and used in flexible displays³⁰. Another benefit is that the melting point of silver is dramatically lowered at the nanoscale, thus, a lower heat treatment is required. This allows silver to be directly dispensed onto polymeric or temperature sensitive substrates without damaging them³¹. Research is still optimizing a compromise between the size of nanosilver wires and its conductive potential, but nanosilver has still made an appearance in computer components, but not for their conductive properties. Some keyboards and computer mice have already been manufactured with a nanosilver coating to exploit the more popular antimicrobial properties¹⁶.

Synthesis and Characterization: Whatever the desired function, nanosilver products generally utilize a colloid in at least one step of the production process. Most methods involve the reduction of a silver salt with a reducing agent³². For example, the

most widely used method, the Creighton synthesis, reduces silver nitrate with sodium borohydride. Often, a capping agent will be added to help stabilize or functionalize the colloid for a specific purpose. These commonly include polyvinyl alcohol (PVA), poly(vinylpyrrolidone) (PVP), citrate, bovine serum albumin (BSA), or cellulose¹⁵. In addition, the size, shape, concentration, and charge can be controlled by various synthesis details to generate ideal nanoparticles for a particular purpose^{33,34}. Once AgNPs are synthesized, they are much more than just nano-scaled clusters of silver - they are an entirely new entity. Likewise, there is a growing concern about the increased use of nanosilver as different physiochemical properties arise. In 2010 the USEPA came up a series of nine parameters that should be regularly characterized by the most advanced instrumentation available. Table 1.1 summarizes these criteria and appropriate characterization methods. Thus, as AgNPs' usage increase, they must be characterized accordingly, especially since there is a narrowing consensus on defining AgNPs' toxicity.

Table 1.1: Criteria and appropriate characterization methods proposed by the USEPA to appropriately characterize nanomaterials.³⁵

No.	U.S. EPA	Characterization Methods
1	Shape	Transmission and scanning electron microscopy (TEM and SEM)
2	Chemical composition	ICP-OES, Inductively coupled plasma – optical emission spectroscopy / mass spectroscopy. Fourier transform – infrared spectroscopy, Raman and SERS, X-Ray photoelectron spectroscopy (XPS), UV-Vis absorption spectrophotometry
3	Crystal structure	X-Ray Diffraction (XRD)
4	Average size	TEM, SEM, XRD, and dynamic light Scattering (DLS)
5	Size distribution	TEM, SEM, and atomic force microscopy (AFM)
6	Surface area	TEM, and Brunauer, Emmett and Teller (BET) measurements
7	Surface treatment	XPS, FT-IR, Raman, SERS, and scanning probe microscopy
8	Solubility	Solubility tests
9	Surface charge	Zeta potential measurements and SPM

TOXICITY

Argyria, the only confirmed symptom of silver exposure in humans, is considered only a cosmetic inconvenience as it merely adjusts skin pigments to a bluish gray³⁶. Essentially, silver is deposited in small blood vessels (capillaries) encased in a membranous vesicle (lysosomes) to prevent exposure to the more sensitive cell components. As the silver is exposed to light, it reduces to metallic silver⁸. However, research and reviews have suggested ionic silver has drastic impacts in numerous experimental models. Silver toxicity is well-documented and mostly depends on the concentration of free silver ions (Ag^+) while silver sulfide, silver chloride, and silver thiosulfate have not been shown to be toxic³⁷. The intent here is not to reproduce numerous biological reviews, but rather to acknowledge the variety of studies that has been conducted. In a literature assessment of peer-reviewed articles, it was reported 26% of the arguments that support evaluation of nanosilver make the claim that it is toxic to organisms³⁸. The concern is free silver ions that form from nanosilver. Again, most AgNPs are engineered to release Ag^+ ions, although inconclusive as a whole nanosilver has demonstrated histo-, cyto-, and geno-toxicity in multiple experimental organisms. All results are attributable to free Ag^+ ions. Histotoxicity examples include tissue deformities and silver accumulation. *In vivo* cytotoxicity has been demonstrated with the generation of ROS, inflammation, and cell death^{39,40,41}. Others claim nanosilver exhibits genotoxicity. Nanosilver has been shown to cross cell membranes by mimicking essential ion characteristic (*i.e.*, Na^+) and thus deliver free silver ions into the cellular nucleus⁴¹. This mechanism is often appropriately referred to as the “Trojan horse⁴¹”. Unfortunately, most of this research is focused on mammalian cells or bacteria^{8,37,41}. Although beneficial, these experiments are often designed around

anticipated results by simulating unrealistic concentrations of AgNPs. Research must go beyond concentration studies. Since most products will be discarded as aqueous waste down the drain either as colloidal silver or leached nanosilver, research must also focus on the realistic impact AgNPs will have once released into freshwater environments (Kim, 2005).

ENVIRONMENTAL CONCERNS

Nanosilver Regulation: As numerous products take advantage of AgNPs, desirable properties environmental and health concerns escalate. Although only 5% or 1,230 tons of the total silver is allocated to manufacturing AgNPs, there is still a concern in the role they may play, in the environment with their unique chemistry. Currently, nanosilver is considered safe for mammalian cells⁴² despite countless research that claims otherwise. As with most industries, there are larger factors at play and the Silver Nanoparticle Working Group strives to promote nanosilver's innocence. The USEPA has regulated some nanosilver products under FIFRA. Interestingly, it is not silver's size that leads to this decision, but rather, its bactericidal properties. A washing machine may not seem like a pesticide, but the antimicrobial properties have placed a few commercially sold appliances on FIFRA's list^{43,44,45}. However, nanosilver is still new enough for most industries to benefit from the knowledge gaps despite the fact nanosilver has been on the market longer than ionic silver¹³. The first non-nanosilver product was not registered until 1994, forty years after Algaedyn. Ionic silver is more toxic as seen in numerous reviews^{46,37,45} but nanosilver can release silver ions. The USEPA issued a report in 2011 with a demand to manage nanomaterial risks more effectively³⁵ and had updated it every year

since. Of course, as with any regulation, compliance only limits a facility's waste, and as the nanosilver industry grows as a whole, this may not be enough.

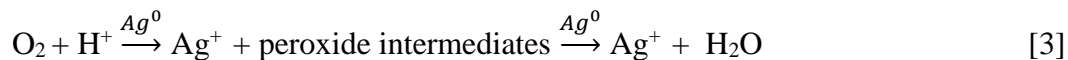
The toxicity of silver is known and is reported by multiple government agencies^{4,8,9}, but nanosilver is different, and correlation to existing regulations is difficult since most are based on concentrations. Although an adequate temporary solution this is not an effective solution for future regulations since it is unknown if AgNP toxicity is attributed directly to AgNPs or to the release of Ag⁺ ions. Thus, there is a need for risk assessment and environmental surveillance beyond concentration, but currently, few methodologies exist.

Nanosilver Release: The biggest gaps in silver nanotechnology exist in the distance between the most defined forms of silver. Just as metallic silver is not the same as a silver compound, AgNP's physiochemical properties are different, mainly due to large surface area to volume ratios. Additional variation in size, concentration, shape, charge, and functionality only make identifying their fate and transport more difficult. Extrapolations can be made – and they are – but almost always with assumptions. If any conclusions are to be made on nanosilver toxicity, research should also confirm the possibility of such exposure. In an ideal world, every form of nanosilver would be given individual focus, but the numerous varieties of AgNPs make it nearly impossible to consider every scenario. Nonetheless, it is sensible to infer possibilities. Generally, there are two broad categories to contemplate. Commonly referred to as *fate and transport* these words simply mean that released nanosilver may either 1) persist and accumulate as nanosilver in biological entities, or 2) it may change form and complex with soil components or other potential contaminants. A variety of research studies have proposed a few potential options, each is briefly discussed.

Aggregation – The simplest definition of aggregation refers to the collection of smaller units or parts into a larger mass or body⁴⁷. In nanotechnology this terminology is used to describe the flocculation of nanoparticles into larger particles or aggregates. By definition, once nanoparticles have aggregated into dimensions greater than 100 nm, they are no longer considered nanoparticles. Likewise, aggregates' surface area per volume ratio tends to be less compared to the individual nanoparticles. Since the size of nanoparticles relates so closely to their reactivity, aggregation greatly reduces the activity of nanoparticles. There are two possible forms: homoaggregates and heteroaggregates⁴⁸. Homoaggregates simply refers to AgNPs aggregating with other AgNPs. Heteroaggregates refer to AgNPs aggregating with other materials. In freshwater environments, this primarily includes natural organic matter (NOM) or minerals. There is a variety of water chemistries that can influence aggregation such as salinity, temperature, surrounding chemicals, but the final resultant particle is perhaps most influenced by AgNPs themselves. Before conclusions are made, other possible transformations must be discussed.

Soluble ions (Ag⁺) – Aggregation implies the formation of larger particles, which in its own regard is not very concerning as the reactivity will certainly be decreased. On the other hand, the more likely scenario is much less pleasant. The oxidative dissolution of AgNPs will essentially become a significant source of the highly reactive Ag⁺ ions. It has already been suggested Ag⁺ ions can complex with ligands, but what will happen with an excess of Ag⁺ ions? As ionic silver is one of the most toxic metals known to aquatic organisms⁸, oxidative dissolution of AgNPs raises toxicity concerns. Heavily influenced by pH and temperature, the release of Ag⁺ ions is the most environmentally concerning fate of AgNPs⁸.

Liu *et al.* predicted AgNPs would undergo complete oxidative dissolution with peroxide intermediates. The rate of ion released increased with temperature. The proposed pathway is shown below:



Ion release is therefore highly dependent on pH, (effectively, protons). Dissolution rate decreases with increasing pH. Dobias *et al.* concluded dissolution was faster at lower pH but never observed complete dissolution under anoxic or oxic conditions⁴⁹. This suggests that AgNPs are most stable at environmentally relevant pH values, but they also observed the most significant dependence on nanoparticle size - larger sized particles were more resistant to dissolution. He also demonstrated PVP- and Tan-AgNPs are more prone to Ag⁺ release than Cit-AgNPs⁴⁹. Hence research must not only look at both Ag⁺ and AgNPs but also capping agents, temperature, and pH.

Persist as AgNPs – Since AgNPs release Ag⁺ ions and AgNPs can also aggregate, the least likely possibility is for AgNPs to remain as AgNPs indefinitely. However, this cannot be entirely ruled out. Dobias's results showed that larger particles never completely dissolved. Therefore, even as they initially shrink, smaller nanoparticles will also be retained. As another example, Chinnapongse *et al.* showed that citrate-capped 20 nm AgNPs in environments with lower salinity and less NOM than average levels was stable enough to create a potential risk for accumulation⁵⁰. However, the potential influence of pH and temperature was not considered.

New AgNPs – Other research has even shown organic matter has reductive potential. This suggests that new nanoparticles can form from dissolved Ag⁺ ions. Akaighe *et al.*'s results suggest the potential for the formation of new AgNPs in the presence of

organic matter, namely, humic acids (HA)⁵¹. So even if research continues to support the dissolution of AgNPs the resulting Ag⁺ ions may also form new AgNPs, implying that not all AgNPs may be anthropogenic. It is worth mentioning Akaighe claimed the formation was most effective at higher temperatures, so although possible, this seems most likely in environments with elevated temperature (*i.e.*, hot-springs), where organic matter would be less than a river or lake. Furthermore, the experiments were sealed from atmospheric gases which could certainly impact solution pH and oxygen content⁵¹. In environmental research, experimental exposure to atmospheric gases is important when surface waters are exposed as this directly impacts the transformation of AgNPs, especially if AgNPs are easily oxidized.

Oxidation of AgNPs – Silver nanoparticles have also shown to partially oxidize (on the surface). Just as bulk silver can eventually tarnish, AgNPs can undergo a similar mechanism but on a much smaller scale. This oxidation of AgNPs effectively changes the surface, which also alters the reactivity of the nanoparticle. For example, Lok *et al.* confirmed oxidized AgNPs have more antimicrobial activities than zero-valent AgNPs⁵². However, it was suggested that the oxidation essentially precedes the dissolution of AgNPs. So, while dissolution affects the release of Ag⁺, it depends on oxidation. Dobias *et al.* also implied the same mechanism: partial surface oxidation followed by dissolution⁴⁹. Predictably, this is attributed to the available surface area, which is why smaller nanoparticles dissolved more readily.

The complexity of the environment and diversity of engineered AgNPs contribute to these multiple conclusions. Furthermore, not only is the specific form of nanosilver

relevant but also where and how it is released. Countless factors such as pH, temperature, oxygen, organic matter, etc. will all play a very important role in the fate of AgNPs.

GAPS OF KNOWLEDGE AND MAIN GOALS

As mentioned previously, this dissertation has approached the environmental concerns associated with silver nanoparticles from three different directions to help answer one question: What is the fate of silver nanoparticles in freshwater environments? Chapter 2 looks at the biological implications of released AgNPs and emphasizes the importance to distinguish Ag accumulation based on the different forms of Ag (*i.e.*, AgNPs vs. Ag⁺). This is accomplished by using different tissues within freshwater crayfish and variety of chemical and biological analytical techniques. Chapter 3 presents a method to characterize AgNP adsorption behavior and distribution to mineral components of soil. Briefly, it was understood that not all Ag would become bioavailable due to complexation schemes with soil components, and since there is limited data on the interaction with minerals, aluminum oxide was chosen as a model adsorbent because it may serve as a proxy for the alumina octahedra of the wide variety of aluminosilicates of its abundance in soils throughout the world. Lastly, Chapter 4 addresses the importance of educating future generations about nanomaterials and the importance in characterizing them in accordance with governmental regulations. This was accomplished by developing a laboratory module to introduce STEMM students to inductively coupled plasma optical emission spectroscopy (ICP-OES) as an analytical technique to measure total silver content within AgNPs and assess their interest and performance with questionnaires and evaluations.

REFERENCES

- (1) Huheey, J. E.; Keiter, E. A.; Keiter, R. L. *Inorganic Chemistry: Principles of Structure and Reactivity*, 4th ed.; 1997.
- (2) Parfitt, G. D.; Smith, A. L. *Trans. Faraday Soc.* **1963**, *59*, 257–267.
- (3) Rentz, E. J. *Silver Hydrosol Info* **2012**.
- (4) Purcell, T. W.; Peters, J. J. *Environ. Toxic. Chem* **1998**, *17* (4), 539–546.
- (5) Hayden, J. (2013) Silver. *Mineral Education Coalition*. doi: <http://www.mineralseducationcoalition.org/minerals/silver>
- (6) Dean, J. A. *Lange's Handbook of Chemistry*; McGraw-Hill: New York, 1999.
- (7) Staff, J. J. *Chem. Educ.* **2000**, *77* (3), 328A.
- (8) Luoma, S. N. **2008**, PEN15-Silver Nanotechnologies and the Environment: Old Problems of New Challenges? Woodrow Wilson International Center for Scholars. 2008; http://www.nanotechproject.org/process/assets/files/7036/nano_final.pdf.
- (9) Levard, C.; Reinsch, B. C.; Michel, F. M.; Oumahi, C.; Lowry, G. V.; Brown, G. E. *Environ. Sci. Technol.* **2011**, *45* (12), 5260–5266.
- (10) Freestone, I.; Meeks, N.; Sax, M.; Higgit, C. *Gold Bull.* **2007**, *40* (7), 270–277.
- (11) Chang, K. *The New York Times: Science*. 2005.
- (12) Padeletti, G.; Fermo, P. *Appl. Phys.* **2013**, *113*, 825–833.
- (13) Nowack, B.; Krug, H. F.; Height, M. *Environ. Sci. Technol.* **2010**, *45* (4), 1177–1183.
- (14) Lea, M. C. *Trans. Faraday Soc.* **1889**, 476–491.
- (15) Yu, S.; Yin, Y.; Liu, J. *Environ. Sci. Process.* **2013**, *15*, 78–92.
- (16) Wilson Ce. New Nanotechnology Consumer Products Inventory <https://www.wilsoncenter.org/article/new-nanotechnology-consumer-products-inventory> (accessed September 1, 2016).
- (17) Lok, C. N.; C.M., H.; Chen, R.; He, Q. Y.; Yu, W. Y.; Sun, H.; Tam, P. K.; Chiu, J.; Che,

- C. J. Biol. Inorg. Chem.* **2007**, *12*, 527–534.
- (18) Liu, J.; Hurt, R. H. *Environ. Sci. Technol.* **2010**, *44*, 2169–2175.
- (19) Lara, H. H.; Ayala-Nunez, N. V.; Turrent, L. D. I.; Padilla, C. R. *Microbiol. Biotechnol.* **2009**, No. 26, 615–621.
- (20) Lu, L.; Sun, R. W. Y.; Chen, R.; Hui, C. K.; Ho, C. M.; Luk, J. M.; Lau, G. K. K.; Che, C. M. *Antivir. Ther* **2008**, No. 13, 253–262.
- (21) Baram-Pinto, D.; Shukla, S.; Perkas, N.; Gernanken, A.; Sarid, R. *Bioconjugate Chem.* **2009**, *20*, 1497–1502.
- (22) Wright, J. B.; Lam, K.; Hansen, D.; Burrell, R. E. *Am. J. Infect. Control* **1999**, *27*, 344–350.
- (23) Order No. R1-2012-0031. *Efficient recovery justifies silver's use in solar cells*; City of Arcata, Municipal wastewater treatment facility., 2012; p NPDES: CA0022713.
- (24) Meyer, D. E.; Curran, M. A.; Gonzalez, M. A. *J. Nanopart. Res.* **2011**, No. 13, 147–156.
- (25) Foltynowicz, Z.; Gwiazdowska, D.; Rodewald, D.; Nowaczyk, A.; Filipiak, M. *Fibres Text.* **2013**, *5* (101), 91–96.
- (26) Oldenburg, S. J. Silver Nanoparticles: Properties and Applications. *SigmaAldrich* **2014**.
<http://www.sigmaaldrich.com/technical-documents/articles/materials-science/nanomaterials/silver-nanoparticles.html>
- (27) Pavel, I. E.; Alnajjar, K. S.; Monahan, J. L.; Stahler, A.; Hunter, N. E.; Weaver, K. M.; Baker, J. D.; Meyerhoefer, A. J.; Dolson, D. A. *J. Chem. Educ.* **2012**, *89* (2), 286–290.
- (28) Dorney, K. MA Chemical Free Approach for Increasing the Biochemical Surface-enhanced Raman Spectroscopy (SERS) Sensing Capabilities of Colloidal Silver Nanoparticles., Wright State University, 2013.
- (29) Deng, W.; Xie, F.; Baltar, H. T. M. C. M.; Goldys, E. M. *Phys. Chem. Chem. Phys.* **2013**, No. 15, 15695–15708.
- (30) Mo, L.; Liu, D.; Zhou, X. *Env. Sci Technol* **2009**.

- (31) Kim, D.; Moon, J. *Electrochem. Solid-State Lett.* **2005**, 8 (11), J30.
- (32) Tolaymat, T. M.; El Badawy, A. M.; Genaidy, A.; Scheckel, K. G.; Luxton, T. P.; Suidan, M. *Sci. Total Environ.* **2010**, 408 (5), 999–1006.
- (33) Sun, Y.; Xia, Y.; Fabrega, J.; Fawcett, S. R.; Renshaw, J. C.; Lead, J. R. *Science (80-.)*. **2002**, 298 (19), 2176–2178.
- (34) Fabrega, J.; Luoma, S. N.; Tyler, C. R.; Galloway, T. S.; Lead, J. R. *Environ. Int.* **2011**, 37 (2), 517–531.
- (35) Hanson, N.; Harris, J.; Joseph, L. A.; Ramakrishnan, K.; Thompson, T. *Off. Insp. Gen. Epa* **2011**, No. 12, 1–23.
- (36) James, W. D.; Berger, T. G.; Elston, D. M.; Odom, R. B. *Saunders Elsevier* **2006**, 858.
- (37) Ratte, H. A. N. S. T. O. N. I. R. **1999**, 18 (1), 89–108.
- (38) Boholm, M.; Arvidsson, R. *J. Clean. Prod.* **2014**, 68, 135–143.
- (39) Chen, X.; Schluesener, H. J. *Toxicol. Lett.* **2008**, No. 176, 1–12.
- (40) Lee, K. J.; Browning, L. M.; Nallathamby, P. D.; Desai, T.; Cherukuri, P. K.; Xu, X.-H. *N. Chem. Res. Toxicol.* **2012**, 25 (5), 1029–1046.
- (41) Lima, R. De; Seabra, B.; Durán, N. **2012**, No. January, 867–879.
- (42) Agno, K.; Braun, G.; Pavel, I.; Morrill, A. R.; Seferos, D. S.; Bazan, G. C.; Reich, N. O.; Moskovits, M.; Govindaraju, K.; Tamilselvan, S.; Kiruthiga, V.; Singaravelu, G.; Kim, J. S. J. H.; Kuk, E.; Yu, K. N.; Kim, J. S. J. H.; Park, S. J.; Lee, H. J.; Kim, S. H.; Park, Y. K. Y. H.; Park, Y. K. Y. H.; Hwang, C. Y.; Kim, Y. K.; Lee, Y. S.; Jeong, D. H.; Cho, M. H.; Bhati-kushwaha, H.; Malik, C. P.; Tamboli, D. P.; Lee, D. S.; Savithramma, N.; Rao, M. L.; Rukmini, K.; Suvarnalatha, P.; Esteban-Tejeda, L.; Malpartida, F.; Esteban-Cubillo, a; Pecharromán, C.; Moya, J. S.; Pal, S.; Tak, Y. K.; Song, J. M.; Fayaz, A. M.; Balaji, K.; Girilal, M.; Yadav, R.; Kalaichelvan, P. T.; Venketesan, R.; Patil, S. V.; Borase, H. P.; Patil, C. D.; Salunke, B. K.; Aguilar-Méndez, M. a.; Martín-Martínez, E. S.; *et al. Nanomedicine Nanotechnology, Biol. Med.*

2013, 3 (1), 2525–2532.

- (43) Briquet, L. G. V.; Catlow, C. R. A.; French, S. A. *J. Phys. Chem. C* **2009**, 113 (38), 16747–16756.
- (44) Hass, K. C.; Schneider, W. F.; Curioni, A.; Andreoni, W. *Science* (80-.). **1998**, 282 (5387), 265–268.
- (45) Herberts, C. A.; Hagens, W. I.; Oomen, A. G.; Heugens, E. H. W.; Roszek, B.; Bisschops, J.; Gosens, I.; Meent, D. I. K. V. A. N. D. E.; Dekkers, S.; Jong, W. I. M. H. D. E. **2009**, 3 (June).
- (46) Blasco, J.; Volland, M.; Pérez, S.; Negrete, C. G.; Otero, J.; Fernandez, A.; Garrido, I. M.; Hampel. In *Spanish National Research Plan*; 2008; p CTM2012-38720-C03-03.
- (47) Merriam-Webster. *Aggregate*; 2014.
- (48) Lau, B. L. T.; Hockaday, W. C.; Ikuma, K.; Furman, O.; Decho, A. W. *Colloids Surfaces A*. **2013**, 435 (20), 22–27.
- (49) Dobias, J.; Bernier-Latmani, R. *Environ. Sci. Technol.* **2013**, 47 (9), 4140–4146.
- (50) Chinnapongse, S. L.; MacCuspie, R. I.; Hackley, V. A. *Sci. Total Environ.* **2011**, 409 (12), 2443–2450.
- (51) Akaighe, N.; MacCuspie, R. I.; Navarro, D. A.; Aga, D. S.; Banerjee, S.; Sohn, M.; Sharma, V. K. *Environ. Sci. Technol.* **2011**, 45 (9), 3895–3901.
- (52) Lok, C.-N.; Ho, C.-M.; Chen, R.; He, Q.-Y.; Yu, W.-Y.; Sun, H.; Tam, P. K.-H.; Chiu, J.-F.; Che, C.-M. *J. Biol. Inorg. Chem.* **2007**, 12 (4), 527–534.

CHAPTER 2

FRESHWATER CRAYFISH: A POTENTIAL BENTHIC-ZONE INDICATOR OF NANOSILVER AND IONIC SILVER POLLUTION

*Seth W. Brittle¹, Sessa L. A. Paluri¹, Daniel P. Foose¹,
Matthew T. Ruis², Matthew T. Amato², Nhi H. Lam¹,
Bryan Buttigieg², Zofia E. Gagnon^{2*}, and Ioana E. Sizemore¹*

¹Department of Chemistry, Wright State University,
3640 Colonel Glenn Hwy., Dayton, OH, 45435

²Department of Environmental Science, Marist College,
3399 North Road, Poughkeepsie, NY, 12601

COPYRIGHT PERMISSION

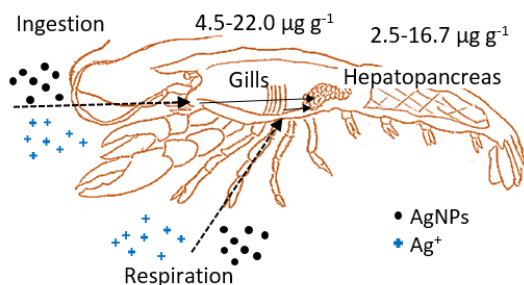
The following chapter is reproduced from a published *Environmental Science and Technology* manuscript authored by Seth W. Brittle. The article, “*Freshwater crayfish: a potential benthic-zone indicator of nanosilver and ionic silver pollution*” was accepted after a set of revisions. Permission to use this work in its entirety for this thesis/dissertation has been granted by the ES&T editorial staff. The full citation of the early access article is the following:

Brittle, S. W.; Paluri, S. L. A.; Foose, D. P.; Ruis, M. T.; Amato, M. T.; Lam, N. H.; Buttigieg, B.; Gagnon, Z. E.; Sizemore, I. E. Freshwater crayfish: a potential benthic-zone indicator of nanosilver and ionic silver pollution. *Enviro. Sci. Technol.* **2016**, *50*, 7056-7065. DOI: 10.1021/acs.est.6b00511

SUMMARY OF INVOLVEMENT

Seth Brittle was responsible for planning, developing, and implementing the experimental set-up, as well as collecting, managing, and analyzing the harvested samples. Although his primary focus was chemically digesting the tissues and measuring their total silver content ICP-OES, he also had a supportive role in all sample measurements and analysis. Furthermore, the colloidal AgNPs, ionic Ag and NaBH₄ solutions used in the experiment were synthesized and characterized by him. Lastly, drafting and editing of the manuscript, associated figures, tables, and supporting information were constructed by him.

GRAPHICAL ABSTRACT



ABSTRACT

Nowadays, silver nanoparticles (AgNPs) are utilized in numerous applications, raising justified concerns about their release into the environment. This study demonstrates the potential to use freshwater crayfish as a benthic-zone indicator of nanosilver and ionic silver pollution. Crayfish were acclimated to 20-L aquaria filled with Hudson River water (HRW) and exposed for 14 days to widely-used Creighton AgNPs and Ag⁺ at doses of up to 360 µg L⁻¹ to surpass regulated water concentrations. The uptake and distribution of Ag in over 650 exoskeletons, gills, hepatopancreas and muscles samples were determined by inductively coupled plasma optical emission spectroscopy (ICP-OES) in conjunction with two complementary U.S. EPA-endorsed methods: the external calibration and the standard additions. Reflecting the environmental plasticity of the two investigated species, *Orconectes virilis* accumulated in a dose-dependent manner more Ag than *Procambarus clarkii* (on average 31% more Ag). Both species showed DNA damage and severe histological changes in the presence of Ag. However, Ag⁺ generally led to higher Ag accumulations (28%) and was more toxic. By the harvest day, about 14 ± 9 % of the 360 µg L⁻¹ of AgNP exposure in the HRW oxidized to Ag⁺ and may have contributed to the observed toxicities and bioaccumulations. The hepatopancreas (1.5-17.4 µg of Ag g⁻¹ of tissue) was identified as the best tissue-indicator of AgNP pollution while the gills (4.5-22.0 µg g⁻¹) and hepatopancreas (2.5-16.7 µg g⁻¹) complementarily monitored the presence of Ag⁺.

KEYWORDS

freshwater crayfish • benthic zone-indicator • ICP-OES quantification • nanosilver and ionic silver bioaccumulation

INTRODUCTION

The risks associated with the increased propagation of nanomaterials has attracted significant attention from researchers and funding agencies.^{1,2} Silver nanoparticles (AgNPs) have been extensively used in many applications due to their unique antimicrobial², optical³, and electrochemical^{4,5} properties. Currently, it is estimated that about 25% of the nanomaterial-containing consumer products (*i.e.*, over 400 products) exploit the properties of AgNPs.⁶ For the past decade, the *in vitro* and *in vivo* toxicities of AgNPs have been extensively studied, and it was generally agreed that most of the adverse effects are caused by the release of Ag⁺ from AgNPs.^{1,7-10} In water, nanosilver has been demonstrated to act as a major reservoir of Ag⁺ ions,^{8,11,12} which can generate reactive oxygen species (ROS) and subsequently trigger oxidative stress in organisms.^{7,13} Although Ag⁺ at low-ppb levels was found to be toxic to various aquatic organisms¹⁴ such as fish (96-h LC₅₀ of 6.5-13.0 µg L⁻¹ and 22.0 µg L⁻¹ for rainbow trout¹⁵ and zebrafish, respectively^{16,17}) and aquatic crustacean (48-h LC₅₀ of 1.2 µg L⁻¹ for *Daphnia magna*¹⁸), nanosilver has also been shown to possess inherent toxicity.^{7,10,19,20} More recently, AgNPs were found to employ additional mechanisms in zebrafish^{10,21-23} and *Daphnia magna*^{19,24} by mutating DNA, disrupting cellular metabolism, and causing necrosis and/or apoptosis.^{7,9,19-28}

The U.S. Environmental Protection Agency (EPA) considers Ag in all soluble forms a priority surface water pollutant because of its persistence and overall environmental impact²⁹. Recently, officials from sewage industries³⁰ and other

organizations (*e.g.*, International Center for Technology Assessment³¹) have begun expressing concerns to EPA about the increased release of nanosilver in wastewater effluents and landfill runoff, ultimately increasing the total bioavailability of Ag in freshwater.^{2,7,11,26,32} Discharges of nanosilver have already been reported in multiple studies involving the washing of nanosilver-coated fabrics^{33,34} and the leaching of nanosilver from paints³⁵ or water filters¹. However, their environmental fate largely remains undetermined;^{2,36} nanosilver may convert to Ag⁺^{11,12}, form complexes with other ions, molecules, or molecular moieties^{2,12,36-38}, agglomerate upon interaction with natural organic matter^{36,39}, or remain in nano-form⁴⁰.

Irrespective of the fate of nanosilver, Ag toxicity in water is currently determined by the concentration of Ag⁺.^{2,29} However, only a few studies^{36,41} have undertaken the tasks of independently examining the uptake and biodistribution of the two silver forms (AgNPs and Ag⁺) in organisms primarily residing in freshwater benthic zones, despite available literature evidence^{2,7,14} suggesting anthropogenic Ag's fate resides at the sediment-water interface. Thus, the selective quantification of Ag pollution in all zones of the freshwater ecosystem still presents a challenge. To address this important knowledge gap, this study focused for the first time on quantifying the selective uptake and distribution of both AgNPs and Ag⁺ in a freshwater organism, which resides in the benthic zone, namely crayfish. This was achieved through inductively coupled plasma optical emission spectroscopy (ICP-OES) in conjunction with two complementary EPA-endorsed methods of calibration^{42,43} that heretofore have not been used together on aquatic models. In addition, a more diverse selection of tissue samples (exoskeletons, gills, hepatopancreas, and muscles) from each specimen was examined compared to previous environmental

studies.^{2,7,13-24,26-28} The uptake levels of Ag in crayfish tissues were further correlated with observed neurological and pathological changes for a better understanding of their toxicity.

Two species of crayfish, *Procambarus clarkii* and *Orconectes virilis*, were selected as biological models because of their previous use in quantifying other heavy metal pollutants in freshwater.⁴⁴⁻⁴⁶ The crayfish model offers several advantages in comparison to other organisms that have been proposed as potential nanosilver indicators including green algae^{20,47,48}, periphyton⁴⁹, *Daphnia magna*^{19,24,50}, zebrafish^{8,16,17,21-23}, and rainbow trout^{15,51,52}. As benthic detritivores, crayfish have a relatively simple anatomy and represent the largest mobile macroinvertebrate in the temperate freshwater ecosystem,⁵³⁻⁵⁵ where many pollutants including AgNPs and AgNP-aggregates may accumulate.^{2,11,36} These features make crayfish an attractive freshwater environmental/toxicological model. Crayfish are also frequently consumed by humans in the southern U.S. and in parts of Australia and Europe⁵⁵. Additionally, crayfish exhibit wide, stable populations^{53,54}, have a high tolerance to pollution^{44,45} and were assigned a high score in various biological water quality indices⁵⁶ (e.g., a score of 8 on a 10-scale of the Biological Monitoring Working Party⁵⁷). Hence, the study of crayfish may offer insight into the accumulation levels and toxicological effects of Ag even at high exposure levels.

In this work, doses of Creighton AgNPs and Ag⁺ as high as 360 $\mu\text{g L}^{-1}$ in Hudson River water (HRW) (Figure 2.S1) were chosen to correlate with previous studies and to surpass regulated water concentrations (i.e., EPA-permitted secondary drinking water maximum contaminant level of 100 $\mu\text{g L}^{-1}$)⁵⁸ (Figures 2.S2 and 2.S3). Situated in central New York State, the 315-mile long Hudson River ecosystem sustains a large population of flora, fauna and people that have historically offered a foundation for many freshwater

studies.⁵⁹ The Creighton reaction was employed for the aqueous synthesis of AgNPs because, as indicated by Tolaymat in his comprehensive review⁶⁰, it represents the most widely-used nano-fabrication approach due to its simplicity, low-cost and moderate size-distribution of AgNPs. The concentration of the AgNP- and Ag⁺-stock samples for crayfish exposure and the total amount of Ag accumulated in chemically digested tissues were accurately quantified through ICP-OES in conjunction with the external calibration and the standard addition methods. While the external calibration curve is the gold-standard for most metal accumulation studies with a large number of samples^{42,43,61}, the standard additions method is increasingly becoming important in the quantification of metallic NPs, where matrix effects may occur.⁶²⁻⁶⁴ ICP-OES was selected because it is a well-established EPA analytical method for the quantification of metals down to the ppb level within water⁴³ and tissues⁶⁵. External tissues that were collected for ICP-OES analysis due to their immediate contact with the environment included the epicuticle surface of the exoskeleton and the epithelial layers of the gills.^{53,66} Internal tissues that were examined by ICP-OES comprised the abdominal tail flexor due to its regular consumption by higher trophic organisms (including humans)⁵⁵ and hepatopancreas due to its primary role in digestion and detoxification.^{53,54,66} Overall, this work demonstrates the influence of AgNP- and Ag⁺-exposure on tissues of freshwater crayfish and presents the possibility of using crayfish tissues as indicators of AgNP- and Ag⁺-pollution.

MATERIALS AND METHODS

All materials were purchased from Fisher Scientific and used without further modification unless specified. High-quality water (18.2 MΩ•cm) was obtained from a LabConco system.

Synthesis and Characterization of AgNPs: A Creighton method⁶⁷ was chosen to fabricate negatively charged, unfunctionalized colloidal AgNPs. In this synthesis, a 2:1 mM ratio of sodium borohydride (NaBH₄) to silver nitrate (AgNO₃) was used to minimize the amount of excess reagents and byproducts.⁶⁷⁻⁶⁹ Ultraviolet-visible (UV-Vis) absorption spectroscopy was employed to confirm the formation of spherical AgNPs by the presence of a localized surface plasmon resonance (LSPR) peak.⁶⁹ In preparation for total Ag quantification by ICP-OES, colloidal samples were digested in 2 mL of OPTIMA grade nitric acid (67-70% HNO₃) at 225 °C. These samples (< 200 µL) were then diluted to 2% HNO₃ and analyzed by a Varian 710 ICP-OES unit equipped with an SPS 3 autosampler. A LabRam HR800 Raman system was utilized to verify colloidal purity (Supporting Information). The nanocolloid was used fresh in order to avoid the potential release of Ag⁺ cations from AgNPs. This redox reaction may occur with time (6-125 days) under favorable conditions such as the presence of H⁺, dissolved O₂, or increased temperature.¹²

Cloud Point Extraction of AgNPs and Ag⁺: In order to quantify the possible release of Ag⁺ ions from AgNPs within the water tank environment, a separate experiment was ulterior carried out in smaller aquaria filled with 1 L of HRW, to which either AgNPs or Ag⁺ in the highest exposure amount, *i.e.*, 360 µg L⁻¹, were added (*N* = 3 aquaria for each control or treatment). CPE controls included HRW alone and fresh Creighton AgNPs. All experimental tank conditions were recreated similar to the ones in the crayfish tanks at a later date. Aliquot samples were collected from the bottom of each tank, where the crayfish normally inhabit, on the first (day 1) and the last day of the experimental duration (day 14), and subjected to a cloud point extraction (CPE) procedure to separate AgNPs from Ag⁺. Recent CPE studies on AgNPs showed that the two Ag species may be isolated from

aqueous matrices by the addition of $\text{Na}_2\text{S}_2\text{O}_3$ and Triton X-114.⁷⁰⁻⁷² While $\text{Na}_2\text{S}_2\text{O}_3$ chelated Ag^+ , Triton X-114 formed micelles with AgNPs⁷⁰⁻⁷². The two phases resulting from CPE (Figure 2.1) were then separated by centrifugation and analyzed for the total Ag content by ICP-OES following the ICP-OES procedures for the colloidal AgNP controls. Experimental details for the CPE procedure are given in Supporting Information. For further analysis, UV-Vis absorption spectra were measured from HRW containing a higher concentration of AgNPs (1 mg L^{-1}). AgNPs could not be detected by absorption spectroscopy in the crayfish tanks due to the lower sensitivity of the method at these concentrations ($< 360 \text{ } \mu\text{g L}^{-1}$).

Crayfish Acclimation: Crayfish specimens of similar age (~2 years), length (7 ± 2 cm and 7 ± 3 cm), and weight (22.2 ± 8.7 g and 18.5 ± 9.4 g) were purchased from Carolina Biological Supplies (*P. clarkii*) and Northeastern Aquatics, Inc. (*O. virilis*). Upon arrival, crayfish were sexed, and three experimental organisms were randomly placed in each tank ($N = 2$ tanks for each control or treatment, at least one organism of each sex per tank), where they were allowed to acclimate to the laboratory and Hudson River conditions for three days. The preparation of the 20-L aquaria, the filtration of the Hudson River water (HRW)⁷³, and the water quality measurements are described in the Supporting Information. Crayfish were fed daily one-quarter of an H_2O Stable Wafer (New Life Spectrum).

Silver Dosing: Each organism was weighed before adding colloidal AgNPs and removing the equivalent amount of water. Crayfish were exposed for 14 days to either AgNPs or Ag^+ from AgNO_3 (30, 120, and $360 \text{ } \mu\text{g L}^{-1}$, Figure 2.S1). Control groups included cages submerged in the Hudson River and aquaria containing only HRW or concentrations of NaBH_4 stoichiometrically equivalent to those used in synthesis (20, 80,

and 240 $\mu\text{g L}^{-1}$). A laboratory control containing filtered HRW alone served as a water chemistry control. Details are provided in the Supporting Information (Figures 2.S1-2.S3).

Behavioral and Gross Pathology: Threat responsiveness⁷⁴⁻⁷⁷ and gross visual observations of animal health (*i.e.*, exoskeleton cleanliness, coloring consistency, bodily integrity, molting, and mortality – Table 2.S1)^{53,77,78} were recorded daily. Details are provided in the Supporting Information.

Tissue Sampling: On the morning of harvest, crayfish were again weighed and measured. Crayfish were then anesthetized with ice for 15 min in labeled bags following the DeForest Mellon procedure.⁷⁷ Upon removal from the anesthetic conditions, specimens were surgically decapitated within 5-10 s to avoid major stress. Encephalon, hepatopancreas, tail flexor, and a dorsal section of the exoskeleton (6x per treatment and species) were collected for histological analysis. Encephalon tissues (3x per treatment and species) were chosen at random and immediately analyzed for DNA damage.

ICP-OES Sample Preparation: Over 650 exoskeletons, gills, hepatopancreas, and muscles were oven dried for 72 hours at 80°C, weighed and digested in glass beakers following the U.S. EPA methods 200.11⁷⁹ and 3052⁶⁵. Briefly, samples were subjected to a 15-min “cold” digestion at room temperature using 5 mL of OPTIMA grade HNO₃ (67-70%). This was followed by a “hot” digestion at ~180 °C until all solid material was dissolved. Next, the temperature was reduced to 80 °C, and 2 mL of reagent grade hydrogen peroxide (30% H₂O₂) was slowly added to bleach samples. Sample beakers were removed from the hot-plate (when < 200 μL remained), cooled, rinsed five times with HQ water, and transferred to 10- or 25-mL volumetric flasks for dilutions to 2% HNO₃. Lastly, each

sample was split between two ICP-OES test tubes to allow for duplicate measurements to be independently performed.

ICP-OES Analysis: Digested tissues and colloidal samples were loaded into the autosampler, peristaltically pumped into a Meinhard nebulizer at a rate of 2 mL min^{-1} , and aspirated together with a 15.0 L min^{-1} argon gas flow. The samples were measured in triplicate using an axially positioned quartz torch, two wavelengths for Ag (328.068 nm and 338.289 nm), a read time of 15 s and a stabilization delay of 45 s. External Calibration Method: Ag^+ standards were prepared from a 10^3 mg L^{-1} of Ag^+ SPEX CertiPrep stock standard by quantitative dilutions to 2% OPTIMA grade HNO_3 and HQ water. An eleven-point external calibration curve was then constructed (0, 5, 10, 15, 20, 25, 50, 75, 100, 125, and $150 \text{ } \mu\text{g L}^{-1}$) and the total amount of Ag was determined by interpolation for each treatment and individual tissue. Standard Additions Calibration Method: Standard addition curves were also constructed for all tissue samples within each treatment to account for potential matrix interferences and to perform quality control. Equal volumes of digested samples (1.00 mL) and known concentrations of $10^3 \text{ } \mu\text{g L}^{-1}$ of Ag^+ standard were added in gradual volume increments of $25 \text{ } \mu\text{L}$, in the 0-100 μL range. The relative percent difference (RPD) and percent recovery (R) were obtained by comparing the Ag concentrations from both calibration methods in accordance with the U.S. EPA guidelines (Supporting Information).^{42,43}

DNA Analysis: Encephalon samples were processed for DNA damage with a Trevigen CometAssay kit.⁸⁰ Briefly, tissue was minced in 2 mL of 20 mM of EDTA in PBS solution, centrifuged, and $10 \text{ } \mu\text{L}$ of the supernatant was mixed with $90 \text{ } \mu\text{L}$ of low melt LMAgarose. The mixture was then immobilized on pre-treated CometAssay slides and

chilled at 4 °C. Sample-filled slides were treated with an alkaline solution (0.26 M of NaOH) for 30 min to unwind the DNA. Next, the slides were placed into the standardized Comet Assay[®] Electrophoresis System, filled with a buffer of pH > 13 (200 mM of NaOH and 1 mM of EDTA), and subjected to 21 V / 40 mA for 30 min. Afterward, the slides were rinsed with 95% ethanol (EtOH), allowed to air dry, and stained with SYBR-Green. An Olympus BX51 epifluorescent microscope coupled to a Magnafire SP digital camera was used to photograph fluorescent comets. DNA comet lengths (on average $N = \sim 40$ per slide for each Ag exposure or control) were measured using Image-Pro Plus software. Distribution of DNA between the tail and head of the comet was used to evaluate the degree of DNA damage with respect to controls.

Histopathological Analysis: Hepatopancreas and encephalons were rinsed in a saline solution and placed in a modified Demke's fixative for seven days (formalin, glacial acetic acid, 95% EtOH, and distilled water).⁸¹ Samples were then removed from the fixative and sequentially submerged in: 70% EtOH for 24 h, 95% EtOH for 30 min, twice with absolute EtOH for 30 min, and twice in clearing agent (SafeClear) for 30 min. The tissues were then positioned in plastic Peel-A-Way[®] disposable histology molds. Paraffin infiltration and embedding were done using a Leica EG 1160 Paraffin Embedding Center (Leica Microsystems, Wetzlar, Germany) in freshly-melted Type L paraffin for 30 min. The paraffin molds were sectioned with a Spencer microtome to 6- μ m thick; the slices were fixed with 50% albumin / 50% glycerol on glass slides and stained using the general *Up and Down* series with Hematoxylin-2 and Eosin-Y dyes. Prepared slides were examined using the same epifluorescent microscope.

Statistical Analysis: SigmaPlot 12.0 was used to examine statistical variation amongst treatments. One-way ANOVA was performed independently on all results and was followed by individualized *post-hoc* analysis for further statistical examination (two-way ANOVA was performed on water metrics). Student-Newman-Keuls (SNK) multiple comparison tests were independently performed on all water metrics and DNA comet lengths to identify values with $p > 0.950$ significance at the $\alpha=0.05$ probability level. The average of both scores from the behavioral analysis and the average from the duplicate ICP-OES measurements underwent a Holm-Šidák one-way adjustment at the probability level $\alpha \leq 0.05$ to investigate the variation in responses and Ag accumulation levels amongst all treatments and controls.

RESULTS AND DISCUSSION

Synthesis and Characterization of AgNPs: Synthesized AgNPs were characterized in accordance with EPA's recommendations.^{82,83} ICP-OES revealed an average Ag concentration of $15.4 \pm 0.8 \text{ mg L}^{-1}$, and Raman spectroscopy confirmed the absence of organic impurities and silver oxide peaks. In our previous TEM work, these AgNPs appeared spherical, had an average diameter of $14.1 \pm 13.4 \text{ nm}$ and a moderate size distribution in the 1-100 nm range.⁸⁴ The total AgNP surface area was roughly estimated to be $\sim 1500 \text{ nm}^2$ based off the average TEM diameter.⁸⁴ Previous Zeta-potential measurements demonstrated that these AgNPs are negatively charged and are stable at the experimental pH of this study (ζ -potential of -41.47 mV at $\text{pH} = 8.2$).^{84,85} Details are provided in the Supporting Information (Figure 2.S4).

Cloud Point Extraction of AgNPs and Ag⁺: In the control measurements, CPE demonstrated that the fresh Creighton colloid of AgNPs alone contained small amounts of Ag⁺ ions and small amounts of Ag⁺ converted to AgNPs in the HRW ($\leq 10 \%$ by day 14th).

In the sample measurements, CPE successfully verified the persistence of AgNPs at the bottom of the aquaria at day 14 after the exposure to $360 \mu\text{g L}^{-1}$ of AgNPs (Figure 2.1). More specifically, $35 \pm 6 \%$ of the total Ag was found to be in AgNP form, while $14 \pm 9 \%$ was in Ag^+ ionic form at day 14. It is assumed that the detected Ag^+ is the result of the AgNP oxidation in the water tank environment. As one can notice, there is no considerable difference between the Ag^+ content at day 1 and day 14 after the AgNP exposure (Figure 2.1) suggesting that the redox reactions may quickly reach a dynamic equilibrium within the aquarium environment. The remaining percentage of $\sim 51\%$ might have been adsorbed to the rock substrate, the walls, or the filtering material of aquaria. The change in the color of tank water from cloudy yellow-brownish at day 1 to clear light-yellow at day 14 seems to confirm the settling of AgNPs onto the mentioned solid components of the tank (Figure 2.S5). This observation is further supported by the UV-Vis absorption spectra that were collected from the AgNPs in HRW ($1 \mu\text{g L}^{-1}$). The absorption spectra (Figure 2.S6) suggest that at day 1, HRW induces the possible formation of larger or differently shaped AgNPs and/or AgNP-aggregates through the appearance of an additional LSPR peak at 516 nm. However, the new peak disappears at day 14, possibly due to their settling.

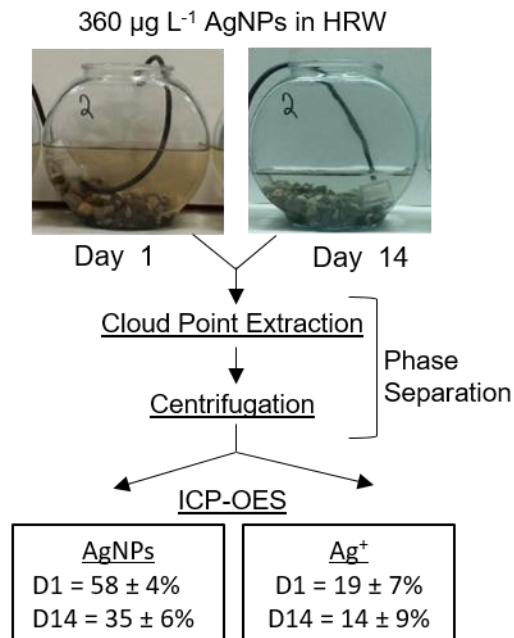


Figure 2.1. Schematic showing the separation of the two Ag species (AgNPs and Ag⁺) from the HRW in the aquaria at day 1 and day 14 after the AgNP exposure via CPE and centrifugation, and their subsequent quantification for total Ag by ICP-OES.

Water Metrics: No significant differences were observed amongst any aquaria or experimental data with respect to water metrics (Figures 2.S7 and 2.S8). The only exception was the river control due to the dynamic nature of the river ecosystem.

Anatomical and Behavioral Observations: There was no notable impact on the experimental results due to incidences of molting and/or loss of appendages (Table 2.S1). Only one specimen was harvested with gastroliths and therefore omitted from further analysis. All Ag-treated *P. clarkii* exhibited an increase in average weight between the start and the end of the experiment (3.0–7.4%), with the exception of the 120 $\mu\text{g L}^{-1}$ of AgNP exposure, where a small decrease (2.6 %) in weight was noticed (Figure 2.S9). In contrast, all Ag-treated *O. virilis* experienced weight loss (1.7–23.3%) (Figure 2.S9). Possible explanations for these weight trends may include differences in the source of the animals

and/or responses to an altered diet. The only significant behavioral observation was a decrease in fear responses in the Ag⁺-exposed specimens ($p < 0.05$, Figure 2.S10).

Silver Quantification: as revealed by the standard additions, matrix effects were negligible in all digested tissues (Supporting Information); the relative percent differences (RPD) were less than the EPA quality control guidelines ($< 10\%$). Thus, the external calibration method was deemed suitable for the quantification of total Ag in the digested samples. Sample calibration curves from both methods are given in Figure 2.S11. Overall, negligible Ag amounts ($< \text{minimum detection limit (MDL)} = 3.0 \mu\text{g L}^{-1}$, Supporting Information) were detected in all controls, suggesting that the water sourced from Hudson River contained undetectable levels of Ag. Figure 2.2 summarizes the total Ag accumulated within each harvested tissue.

External tissues:

A) *Exoskeleton*—the extremely-ordered chitin-calcium carbonate scaffolding of the exoskeleton acts to support the internal organs of a crayfish while simultaneously offering defense to the external environment.^{53,54,78} As seen in Figure 2.2A, small amounts of Ag accumulated in any exoskeleton of Ag-treated crayfish ($0.17\text{--}1.95 \mu\text{g g}^{-1}$); these values were approximately one order of magnitude lower than those corresponding to gills and hepatopancreas (Table 2.S2). It appears the highly calcified tissue had little interaction with either of the two Ag species. This is consistent with previous studies that have shown metal cations and metal nanoparticles accumulate more readily in soft tissues (*e.g.*, liver^{7,13,27,41,46}, gills^{7,13,41,46}, and muscles^{14,41,45,46}) (Figure 2.3). The accumulation that did occur in the Ag⁺ treatments ($0.64\text{--}1.95 \mu\text{g g}^{-1}$) was concentration-dependent in both species, and no significant difference was observed between the two species ($p > 0.05$). This accumulation

may be attributed to the electrostatic attractions between the primarily negatively charged exoskeleton and the positively charged Ag^+ ions.^{53,78,86} Despite the AgNP negative charge, Ag also accumulated in the AgNP treatments but in smaller amounts (0.17–1.49 $\mu\text{g g}^{-1}$). Previous research suggested that the AgNP adhesion to the epicuticle surface of other aquatic arthropods (*Daphnia magna* and *Thamnocephalus platyurus*) may be due to changes in Ag speciation during dissociation or aggregation.⁵⁰ In addition, AgNP adsorption may also occur at the sparse mineralized calcite (CaCO_3) sites on the epicuticle (amorphous CaCO_3 is more common in arthropod exoskeletons), which are protonated at pH values less than 8.5-9.0 (pH_{pzc})⁸⁷. *O. virilis* tanks containing AgNPs displayed a concentration-dependent accumulation with 31-44% higher levels of Ag than *P. clarkii*, which showed no concentration dependence. Although very structurally similar to *O. virilis*, *P. clarkii* are considered an invasive species in many parts of the world⁵³⁻⁵⁶ *P. clarkii* are highly adaptable and extremely resilient to pollution changes, which has been primarily attributed to their thicker exoskeletons and increased metabolism of non-biologically essential metals.^{44-46,78}

B) Gills—similar to fish, aquatic crustacean use gills to exchange dissolved oxygen into the circulatory system, mainly through the hemolymph.^{53,66} A closer examination of Figure 2.2B shows that gills are most susceptible to Ag^+ at the highest exposure concentration in both species (15.2 $\mu\text{g g}^{-1}$ for *P. clarkii* and 22.0 $\mu\text{g g}^{-1}$ for *O. virilis*). This is probably due to the increased availability of Ag^+ ions, which might interfere with the activity of the Na^+/K^+ -ATPase pump by mimicking Na^+ ions.^{2,14,26,52} In addition, gill tissue has also been shown to filter out toxic metal ions such as Zn^{2+} , Cd^{2+} , Pb^{2+} , and Hg^{2+} in crayfish.^{44,46,51,52,88,89} The inherently large surface area of the gill lamellae allows for

substantial exposure to environmental pollutants (Figure 2.3). A comparable sensitivity of gills to Ag⁺ ions at similar concentrations was reported by Farkas *et al.* for rainbow trout.⁵² Although the Ag accumulation levels at lower Ag⁺ doses are not as significant as those detected in the hepatopancreas of crayfish, a dose- dependent trend (2.50-22.00 µg g⁻¹) was seen at all concentrations. Statistical differences between the Ag content of gills in both species were observed in the highest AgNP and Ag⁺ doses; the highest Ag amounts were detected in *O. virilis* (15.2 µg g⁻¹ for *P. clarkii* and 22.0 µg g⁻¹ for *O. virilis*). Likewise, the higher Ag content of *O. virilis* may simply be due to *P. clarkii*'s increased resistance to pollutants.^{44-46,53,54} Although the overall Ag accumulation in the AgNP treatments was concentration dependent (1.8 – 8.8 µg g⁻¹), it was not as significant as that of Ag⁺ or those of the corresponding AgNP doses in hepatopancreas (Figure 2.2D); only the highest dose demonstrated a statistical difference (17.40 µg g⁻¹ for *P. clarkii* and 19.15 µg g⁻¹ for *O. virilis*). This accumulation may be explained by the presence of sulfhydryl-rich proteins in gills that can form complexes with AgNPs and Ag⁺ (*e.g.*, metallothionein-like proteins), thereby inhibiting Ag mobility.^{7,14,88-91} Other AgNP-environmental studies have also reported Ag concentration levels in fish livers higher than those seen in the gills.^{14,51,88} This preference was attributed to differences in the exposure routes of gill and liver,^{14,51,88} *i.e.*, respiration versus ingestion, respectively (Figure 2.3). Wu and Zhou also suggested that the primary exposure to nanosilver in fish results from drinking and ingestion of particles into the gastrointestinal tract, which subsequently end up in liver.⁹²

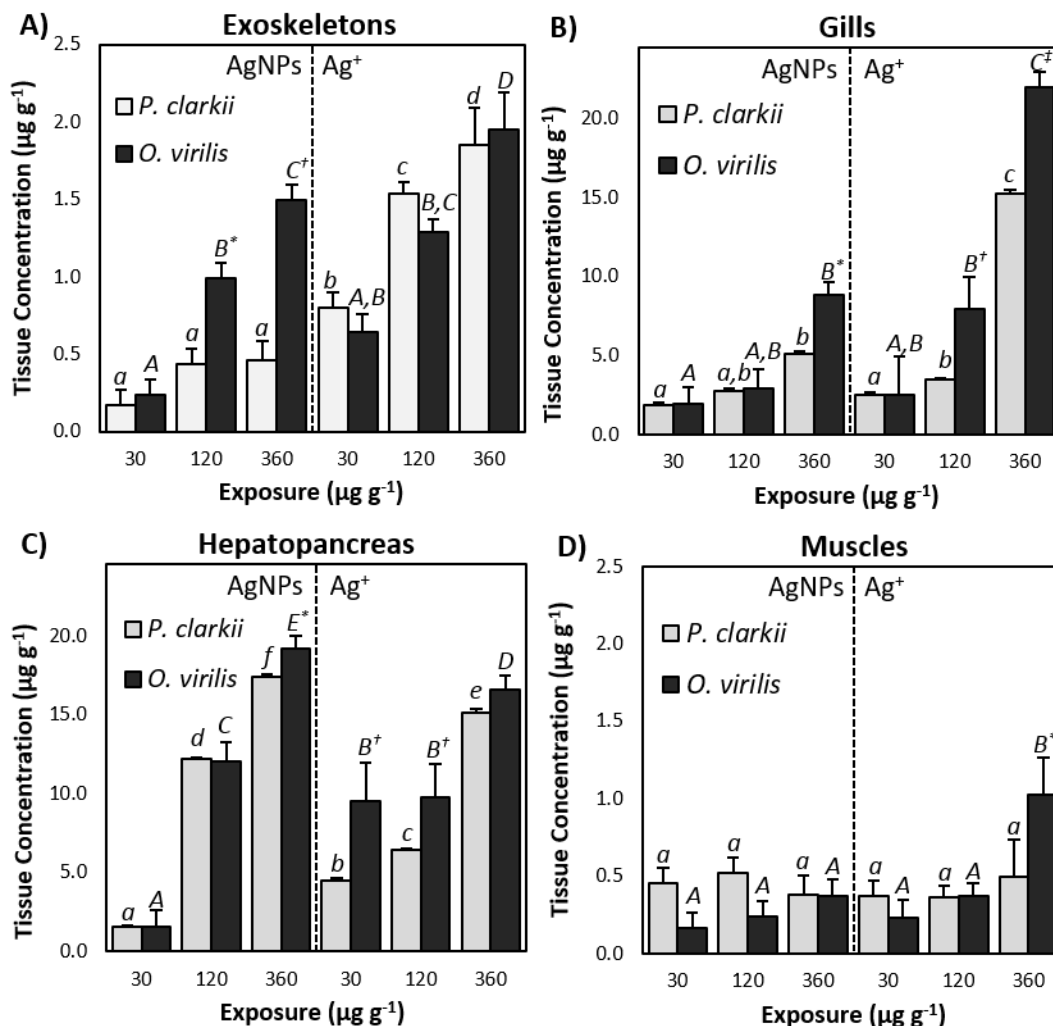


Figure 2.2. Total Ag accumulation (μg of Ag per g of dry tissue) within Ag-exposed tissues from *P. clarkii* and *O. virilis*. Error bars denote standard error from $N = 6$ organisms (except for the 120 and 360 $\mu\text{g L}^{-1}$ of Ag^+ treatment where $N = 4$ due to specimen mortality, see Supporting Information for details). Lower-cased italicized letters mark statistical differences between Ag-exposed *P. clarkii* at the $\alpha=0.05$ level within each tissue. Capitalized letters statistically compare Ag accumulation at the same level for the *O. virilis* species. Values with two letters are statistically the same to each individual letter. *, †, ‡ indicate statistical differences between both species within identical treatments at the $\alpha=0.05$ level. Table 2.S2 summarizes the specific Ag accumulation values.

Internal tissues:

A) *Hepatopancreas*—working as the digestive and metabolic gland, the hepatopancreas in crayfish functions similarly to the liver and the pancreas of higher trophic organisms.^{53,66} As shown in Figure 2.2C, the hepatopancreas may serve as an indicator for AgNP pollution in both species. This observation closely follows previous studies (*e.g.*, rainbow trout), where Ag accumulation from nanosilver was highest in livers.^{26,27,51,88} In this study, the hepatopancreas exhibited the highest dose-dependent Ag accumulation (1.54–19.15 $\mu\text{g g}^{-1}$, Figure 2.2C); at least twice as much Ag from AgNPs was present in the hepatopancreas when compared to all other tissues (*e.g.*, ~217.9% more than the gills). Hepatopancreas, being the major detoxifying organ and a soft internal tissue, is expected to be the primary reservoir of xenobiotics such as AgNPs and Ag^+ (Figure 2.3). Furthermore, as benthic detritivores, crayfish filter-feed on the substrate where many metal pollutants may deposit.^{2,7,13,53,54} Besides ingestion, Ag species may also enter the hepatopancreas via hemolymph oxygenated at the gills.^{53,54} Hence, Ag internal mobility may be significantly attenuated at the hepatopancreas (Figure 2.3). It has been previously demonstrated the hepatopancreas is the most susceptible tissue to metal accumulation.⁴⁴⁻⁴⁶ For instance, the hepatopancreas of *P. clarkii* exposed to heavy metal ions (*i.e.*, Cd, Cu, Zn, Pb, and As) was determined as one of the best freshwater bioindicators of these metal contaminants.⁴⁴⁻⁴⁶ Other environmental studies showed that AgNPs may enter the hepatocytes of zebrafish and rainbow trout by endocytosis and then act as sources of Ag^+ ions^{2,93}, or as Ag^+ ions resulting from their prior dissociation.^{2,11,12,16,28,94} Ag accumulation was on average 81.3% lower in the Ag^+ exposures than the corresponding AgNP exposures. The increased chemical reactivity of Ag^+ may contribute to the lower *in vivo* mobility of

Ag⁺ ^{9,10}. At the two lower Ag⁺ doses, the hepatopancreas accumulated more Ag than the gills (280% for the 30 µg L⁻¹ dose and 154% for the 120 µg L⁻¹ dose); the highest Ag⁺ exposure demonstrated higher Ag levels in the gills than the hepatopancreas (117% more for 360 µg L⁻¹). Thus, the hepatopancreas in conjunction with the gills should be considered tissue indicators in Ag⁺ pollution studies. Again, *O. virilis* proved to be in general more susceptible to AgNPs (*i.e.* on average, 8 % more Ag accumulation occurred in *O. virilis*) and Ag⁺ exposures (*i.e.*, on average, 68% in *O. virilis*) than *P. clarkii*.

B) Muscles—the tail flexor is the largest muscle of the crayfish, which allows the specimen to quickly propel backward and aids in mobility and steering during swimming or predatory escape.^{53,66,74} Overall, the tail muscles contained the least amount of Ag when compared to all other tissues (0.16–1.03 µg g⁻¹). In fact, the Ag levels of muscles were 24-68% and 23-271% smaller than those measured for the exoskeleton of *O. virilis* and *P. clarkii*, respectively (Table 2.S2). Figure 2.2D shows a concentration-independent trend in both species; the only significant difference was within the highest Ag⁺ treatment taken from *O. virilis* (1.03 µg g⁻¹). In crayfish, muscles are secondarily exposed to possible water pollutants that are first internalized by respiration or ingestion (Figure 2.3). Muscle tissues of *P. clarkii* have been previously shown to accumulate other heavy metals (*i.e.*, Pb, Cd, and As⁴⁴⁻⁴⁶), but in good agreement with our results, their levels were smaller than those recorded for gills, exoskeleton, or hepatopancreas. The same trend has been reported for nanosilver accumulation within fish muscles (*e.g.*, rainbow trout⁵¹), where the highest Ag contents were observed within the liver tissue, and the lowest ones were in the muscles.

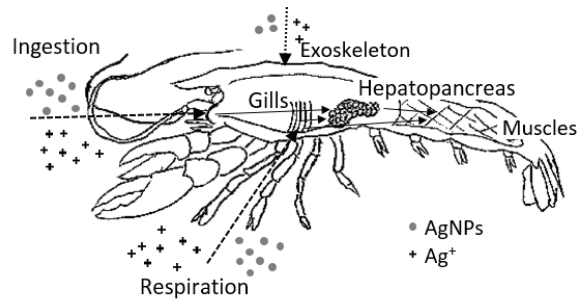


Figure 2.3. Schematic showing the possible exposure routes to environmental Ag pollution. Pathways of external exposure (dotted line) include exoskeleton and gills, while those of internal exposure (solid line) comprise hepatopancreas and muscle. Both AgNPs (gray circles) and Ag⁺ ions (black plus signs) are shown together for illustrative purposes and are out of scale.

Overall, less than 2.4% and 1% of the administered Ag⁺ and AgNPs, respectively, were assimilated within the crayfish tissues (Figure 2.S12). The remaining Ag was either retrieved in the tank water (13.8-73.3%) or was adsorbed onto the solid surfaces of aquaria and substrate. Previous research suggested that less than 25% of dissolved or colloidal Ag is biologically available¹⁴ or remains unchanged¹³. Furthermore, this is in good agreement with other freshwater benthic organisms such zebra mussels,¹⁴ which were reported to assimilate similar levels of dissolved Ag (up to 4%). However, in contrast to zebra mussels, crayfish tissues offer the advantage of individual analysis.

DNA Analysis: as DNA becomes damaged, it can travel further distances in an electrophoresis chamber.⁸⁰ Figure 2.4 summarizes the average DNA comet lengths. A tabulated summary of the DNA damage (Table 2.S3) and sample images of the DNA comets (Figure 2.S13) are given in the Supporting Information. Student-Newman-Keuls statistical tests revealed that all Ag exposures were statistically different from the lab controls ($\alpha = 0.05$ -level) and river controls (no comets). The degree of DNA damage was in general found to increase with the increase in the amount of Ag⁺ or AgNPs added to the

tanks. The most significant DNA changes were detected for the two highest Ag⁺- and AgNP-administered doses, for which the comets were found to be the longest, 24.4-27.8 μm and 21.7-23 μm, respectively. These comet lengths resulting from Ag⁺- and AgNP-exposure were 280% and 250% longer than those corresponding to the lab controls, respectively. These observations are in good agreement with other comet assay studies⁸⁰, which reported single and double DNA strand breakage for fish exposed to nanosilver. For example, Bothun *et al.* found that AgNPs could freely pass through the cellular membrane and induce DNA damage.⁹⁵ Crayfish in the NaBH₄ and lab control tanks also displayed DNA damage (7.8-19.5 μm), but it was significantly less than that corresponding to the Ag-containing tanks. This may be the result of stress from tank confinement. As expected, *O. virilis* displayed longer DNA comets than *P. clarkii* for the Ag⁺ (11%) and NaBH₄ exposures (26%). However, the differences between the two species (< 3%) were not statistically significant for the AgNP exposures ($p > 0.05$) possibly due to the better adaptation status of *P. clarkii*.^{53,54}

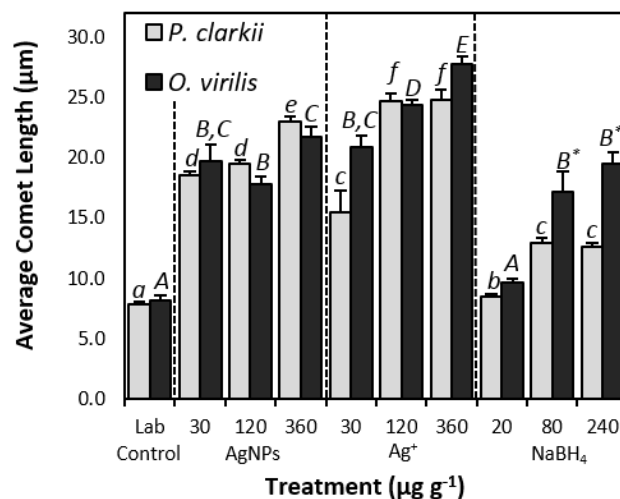


Figure 2.4. Degree of DNA damage quantified through comet lengths in *P. clarkii* and *O. virilis* (in average $N = 40$ DNA comets per each treatment). River control revealed no comets. Lower-cased italicized letters mark statistical differences between Ag-exposed *P. clarkii* species at the $\alpha=0.05$ level within each tissue. Capitalized letters statistically compare Ag accumulation at the same level for the *O. virilis* species. Values with two letters are statistically the same to each individual letter. * indicates statistical differences between both species within identical treatments at the $\alpha=0.05$ level. Table 2.S3 summarizes the specific DNA comet lengths in both species.

Histological Analysis: exposure to both forms of Ag had significant pathological effects on all examined samples. Such symptoms in aquatic organisms exposed to heavy metals suggest pathological physical stress.^{16,26,81,96,97} The most drastic changes were again noticed for the highest Ag-doses in both gills and hepatopancreas.

Encephalon—normal morphology was observed in all controls, while pyknotic cells indicative of cell necrosis were detected in all exposures, but occurred more frequently in the Ag⁺ treatments. The Ag⁺ treatment was found to cause the most physical damage to the neural tissue in both species (Figure 2.S14). In addition, necrosis was obvious in the crayfish that interacted with both Ag forms.

Gills—Cross sections of all control samples showed healthy gill structure (Figure 2.S15). The histological examination revealed changes in the basal epithelial membrane

for all Ag-exposures. For example, hyperplasia and loss or rupturing of pillar cells, a pathological change called clubbing, signaled permanent damage in gill architecture.⁹⁷

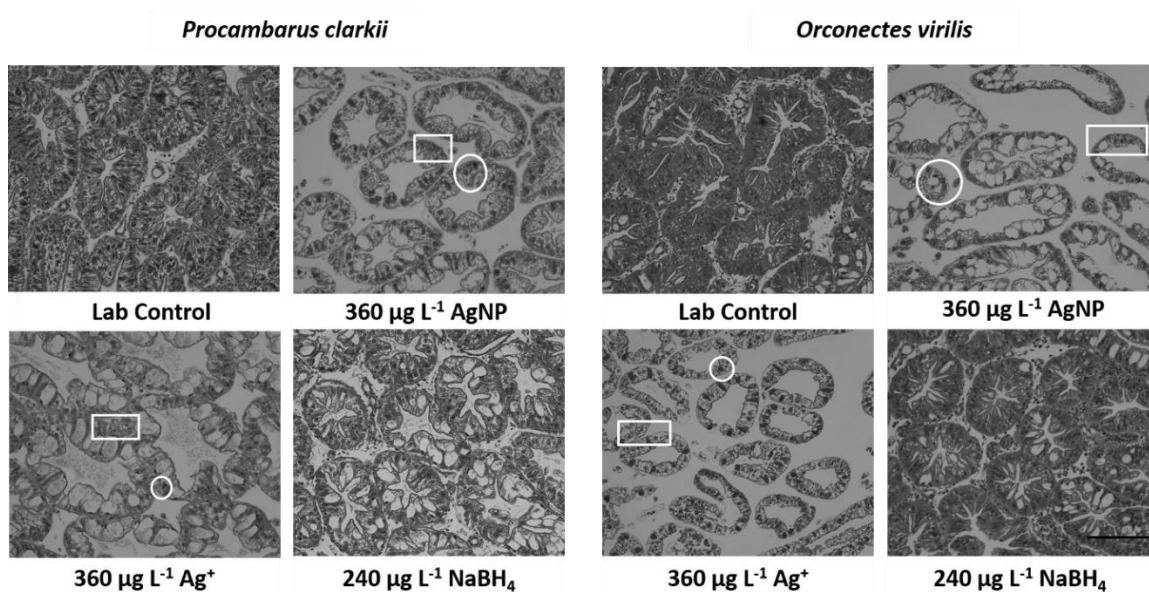


Figure 2.5. Histological cross sections of hepatopancreas tissue stained with hematoxylin and eosin in both crayfish species. River control exhibited intact cells. The highest AgNP and Ag⁺ exposures revealed pyknotic nuclei (enclosed by a circle), *i.e.*, the first step to cell necrosis. Eosinophilic inclusions were also observed (enclosed by a rectangle). No adverse effects were seen in any NaBH₄ treatment. Scale bar is 10 µm and applies to all images.

Hepatopancreas—Hepatocytes of both species exhibited larger vacuolization in all Ag-exposures when compared to controls (Figure 2.5). Observed broken cell membranes, damaged organelles, and darker nuclei were indicative of an overall decreased cellular integrity. It has been previously reported that as damaged chromatin condenses, cell nuclei absorb more stain and thus appear darker.^{16,96,97} These darker spots, known as eosinophilic inclusions, also appeared here as a result of the stress undergone by hepatocytes in the presence of Ag⁺ ions (either from the Ag⁺ exposure or the AgNPs' dissociation). The occurrence of Ag⁺ ions is routinely followed by intracellular accumulation by mimicking essential ions (*e.g.*, Na⁺ or K⁺) and thus, causing electrolytic imbalance.^{97,98} The observed

histopathological changes may also be due to AgNPs entering hepatocytes by endocytosis and then acting as a source of Ag⁺ ions.^{93,97,98} This was described as the “Trojan horse” mechanism and may be the most concerning possibility because the internal leaching of Ag⁺ ions from AgNPs may potentially be more toxic than Ag⁺ alone.^{2,93}

CONCLUSION

Several main observations can be drawn from this study: a) both crayfish species, *O. virilis* and *P. clarkii*, showed negative responses (DNA damage and severe histological changes) to the presence of AgNPs or Ag⁺ ions (30-360 µg L⁻¹) in their ambient environment. However, *O. virilis* was less tolerant to Ag exposure and experienced a dose-dependent association between metal accumulation and pathological responses. By the harvest day, about 14 ± 9 % of the 360 µg L⁻¹ of AgNP exposure in the HRW oxidized to Ag⁺ and may have contributed to the observed toxicities and bioaccumulations. b) The Ag⁺ exposure led to higher accumulation levels than the equivalent AgNP doses in all collected tissues except for the hepatopancreas. c) The hepatopancreas was identified as the best tissue indicator of AgNP pollution in crayfish (accumulation levels of 1.5-17.4 µg g⁻¹). d) The gills (4.5-22.0 µg g⁻¹) and hepatopancreas of crayfish (2.5-16.7 µg g⁻¹) should be considered as complementary tissues for monitoring the freshwater pollution with Ag⁺ ions. e) Overall, this study demonstrates the *O. virilis* species of crayfish as a potential benthic-zone indicator of freshwater pollution with Ag in either ionic or nano form.

ACKNOWLEDGEMENTS

The NSF-nanoEHS Award #14383405 is highly acknowledged. Garrett VanNess and Joseph Solch are thanked for their assistance in the maintenance and operation of the ICP-OES system at WSU. Biology undergraduates at Marist College, Alexandra McCahill, and Nicole Pagones, are acknowledged for their assistance in the behavioral analysis.

REFERENCES

- 1) Nowack, B.; Krug, H. F.; Height, M. 120 Years of Nanosilver History: Implications for Policy Makers. *Environ. Sci. Technol.* 2010, 4, 1177–1183; dx.doi.org/10.1021/es103316q.
- 2) Luoma, S. N. PEN15-Silver Nanotechnologies and the Environment: Old Problems of New Challenges? *Woodrow Wilson International Center for Scholars*. 2008; http://www.nanotechproject.org/process/assets/files/7036/nano_pen_15_final.pdf.
- 3) Evanoff, D. D.; Chumanov, G. Synthesis and Optical Properties of Silver Nanoparticles and Arrays. *ChemPhysChem*. 2005, 6, 1221 – 1231; DOI 10.1002/cphc.200500113.
- 4) Kim, D.; Moon, J. Highly Conductive Ink Jet Printed Films of Nanosilver Particles for Printable Electronics. *Electrochem. Solid. St.* 2005, 8 (11), J30-J 33; DOI 10.1149/1.2073670.
- 5) Li, Y.; Wu, Y.; Ong, B. S. Facile Synthesis of Silver Nanoparticles Useful for Fabrication of High-Conductivity Elements for Printed Electronics. *J. Am. Chem. Soc.* 2005, 127, 3266-3267; DOI 10.1021/ja043425k.
- 6) The Project on Emerging Nanotechnologies. Consumer Products Inventory-Silver Database. Washington, DC; <http://www.nanotechproject.org/cpi/browse/nanomaterials/silver-nanoparticle/>.
- 7) Fabrega, J.; Luoma, S. N.; Tyler, C. R.; Galloway, T. S.; Lead, J. R. Silver nanoparticles: Behaviour and effects in the aquatic environment. *Environ. Int.* 2011, 37, 517–531; DOI 10.1016/j.envint.2010.10.012.
- 8) Asharami, P. V.; Wu, Y. L.; Gong, Z.; Valiyaveetil, S. Toxicity of silver nanoparticles in zebrafish models. *Nanotechnology*. 2008, 19, 255102; DOI 10.1088/0957-4484/19/25/255102.
- 9) Mchshan, D.; Ray, P. C.; Yu, H. Molecular toxicity mechanism of nanosilver. *J. Food Drug Anal.* 2014, 22, 116-127; DOI 10.1016/j.jfda.2014.01.010.

- 10) Johnston, H. J.; Hutchison, G.; Christensen, S. P.; Hankin, S.; Stone, V. A review of the *in vivo* and *in-vitro* toxicity of silver and gold particulates: Particle attributes and biological mechanisms responsible for the observed toxicity. *Crit. Rev. Toxicol.* 2010, 40 (4), 328-346; **DOI** 10.3109/10408440903453074.
- 11) Dobias, J.; Bernier-Latmani, R. Silver Release from Silver Nanoparticles in Natural Waters. *Environ. Sci. Technol.* 2013, 47, 4140–4146; DOI 10.1021/es304023p.
- 12) Liu, J.; Hurt, R. H. Ion Release Kinetics and Particle Persistence in Aqueous Nano-Silver Colloids. *Environ. Sci. Technol.* 2010, 44 (6), 2169-2175; **DOI** 10.1021/es9035557.
- 13) Massarsky, A.; Trudeau, V. L.; Moon, T. W. Predicting the environmental impact of nanosilver. *Environ. Toxicol. Phar.* 2014, 38, 861–873; DOI 10.1016/j.etap.2014.10.006.
- 14) Ratte, H. T. Bioaccumulation and Toxicity of Silver Compounds. *Environ. Toxic. Chem.* 1999, 18 (1), 89-108; **DOI** 10.1002/etc.5620180112.
- 15) Davies, P. H.; Goettl, J. P.; Sinley, J. R. Toxicity of Silver to Rainbow Trout (*Salmo Gairdneri*). *Water Res.* 1978, 12, 113-117; DOI 10.1016/0043-1354(78)90014-3.
- 16) Choi, J. E.; Kim, S.; Ahn, J. H.; Youn, P.; Kang, J. S.; Park, K.; Yi, J.; Ryu, D. Induction of oxidative stress and apoptosis by silver nanoparticles in the liver of adult zebrafish. *Aquat. Toxicol.* 2010, 100, 151–159. DOI 10.1016/j.aquatox.2009.12.012.
- 17) Griffitt, R. J., Luo, J., Gao, J., Bonzongo, J. C., Barber, D. S. Effects of particle composition and species on toxicity of metallic nanomaterials in aquatic organisms. *Environ. Toxicol. Chem.* 2008, 27, 1972–1978. DOI 10.1897/08-002.1.
- 18) Kennedy, A. J.; Hull, M. S.; Bednar, A. J.; Goss, J. D.; Gunter, J. C.; Bouldin, J. L.; Vikesland, P. J.; Steevens, J. A. Fractionating Nanosilver: Importance for Determining Toxicity to Aquatic. *Environ. Sci. Technol.* 2010, 44 (24), 9571-9577; DOI 10.1021/es1025382.

- 19) Zhao, C.; Wang, W. Comparison of Acute and Chronic Silver Nanoparticles and Silver Nitrate to *Daphnia Magna*. *Environ. Toxicol. Chem.* 2011, 30 (4), 885-892; DOI 10.1002/etc.451.
- 20) Navarro, E.; Piccapietra, F.; Wagner, B.; Marconi, F.; Kaegi, R.; Odzak, N.; Sigg, L.; Behra, R. Toxicity of Silver Nanoparticles to *Chlamydomonas reinhardtii*. *Environ. Sci. Technol.* 2008, 42 (23), 8959–8964; DOI 10.1021/es801785m.
- 21) Lee, K. J.; Browning, L. B.; Nallanthamby, P. D.; Desai, T.; Cherukuri, P. K.; Xu, X. N. *In Vivo* Quantitative Study of Sized-Dependent Transport and Toxicity of Single AgNPs Using Zebrafish Embryos. *Chem. Res. Toxicol.* 2012, 25, 1029–1046. DOI 10.1021/tx300021u.
- 22) Lee, K. J.; Browning, L. B.; Nallanthamby, P. D.; X. N. Study of Charge-Dependent Transport and Toxicity of Peptide-Functionalized Silver Nanoparticles Using Zebrafish Embryos and Single Nanoparticle Plasmonic Spectroscopy. *Chem. Res. Toxicol.* 2013, 26, 904-917; DOI 10.1021/tx400087d.
- 23) Browning, L. M.; Kerry, J. L.; Nallanthamby, P. D.; Xu, X. N. Silver Nanoparticles Incite Size- and Dose-Dependent Developmental Phenotypes and Nanotoxicity in Zebrafish Embryos. *Chem. Res. Toxicol.* 2013, 26, 1503–1513; DOI 10.1021/tx400228p.
- 24) Poynton, H. C.; Lazorchak, J. M.; Impellitteri, C. A.; Blalock, B. J.; Rogers, K.; Allen, H. J.; Loguinov, A.; Heckman, J. L.; Govindasmawy, S. Toxicogenomic Responses of Nanotoxicity in *Daphnia magna* Exposed to Silver Nitrate and Coated Silver Nanoparticles. *Environ. Sci. Technol.* 2012, 46, 6288–6296; DOI 10.1021/es3001618
- 25) Heshmati, M.; ArbabiBidgoli, S.; Khoei, S.; Rezayat, S. M.; Parivar, K. Mutagenic Effects of Nanosilver Consumer Products: a new Approach to Physicochemical Properties. *Iran J. Pharmaceutical Res.* 2015, 14 (4), 1171-1180; PMID 26664384, PMCID PMC4673945.

- 26) Winjhoven, S.; Peijnenburg, W. J. G. M.; Herberts, C. A.; Hagens, W. I.; Oomen, A. G.; Heugens, E. H. W.; Roszek, B.; Bisschops, J.; Gosens, I.; Meent, D. V.; Dekkers, S.; De Jong, W. H.; Zijverden, M.; Sips, A. D.; Geertsma, R. E. Nano-silver - a review of available data and knowledge gaps in human and environmental risk assessment. *Nanotoxicology*, 2009, 3(2), 109-138; DOI 10.1080/17435390902725914.
- 27) Reidy, B.; Haase, A.; Luch, A.; Dawson, K. A.; Lynch, I. Mechanisms of Silver Nanoparticle Release, Transformation and Toxicity: A Critical Review of Current Knowledge and Recommendations for Future Studies and Applications. *Materials*. 2013, 6, 2295-2350; DOI 10.3390/ma6062295.
- 28) Lima, R.; Seabra, A. B.; Dúran, N. Silver nanoparticles: a brief review of cytotoxicity and genotoxicity of chemically and biogenically synthesized nanoparticles *J. Appl. Toxicol.* 2012, 32: 867–879. DOI 10.1002/jat.2780.
- 29) 40 CFR Part 423, Appendix A; <https://www.gpo.gov/fdsys/pkg/CFR-2014-title40-vol29/pdf/CFR-2014-title40-vol29-part423-appA.pdf>.
- 30) Horenstein, B. Tri-TAC response to “Silver and Compounds Registration Review” (Docket Number EPA–HQ–OPP–2009–0334). September 22, 2009; http://www.scap1.org/SCAP%20Alerts/TriTAC%20Letter_EPA_Silver_Registration_Review_092209.pdf
- 31) Housenger, J. E. EPA Response to "Petition for Rulemaking Requesting EPA Regulate Nano-Silver Products as Pesticides" US EPA, Office of Chemical Safety and Pollution Prevention. March 19, 2015; EPA-HQ-OPP-2008-0650_
- 32) Seltenrich, N. Spheres of Influence-Nanosilver: Weighing the Risks and Benefits. *Environ. Health Persp.* 2013, 121 (7), a220-a225; DOI 10.1289/ehp.121-a220.
- 33) Benn, T.; Cavanagh, B.; Hristovski, K.; Posener, J. D.; Westerhoff, P. The Release of Nanosilver from Consumer Products Used in the Home. *J. Environ. Qual.* 2010, 39, 1875-1882; DOI 10.2134/jeq2009.0363.

- 34) Lorenz, C.; Windler, L.; von Goetz, N.; Lehmann, R. P.; Schuppler, M.; Hungerbrühler, K.; Heuberger, M.; Nowack, B. Characterization of silver release from commercially available functional (nano)textiles. *Chemosphere*. 2012, 89, 817–824; DOI 10.1016/j.chemosphere.2012.04.063.
- 35) Kaegi, R.; Sinnet, B.; Zuleeg, S.; Hagendorfer, H.; Mueller, E.; Vonbank, R.; Boller, M.; Burkhardt, M. Release of silver nanoparticles from outdoor facades. *Environ. Pollut.* 2012, 158, 2900-2905; DOI 10.1016/j.envpol.2010.06.009.
- 36) Batley, G. E.; Kirby, J. K., McLaughlin, M. J. Fate and Risks of Nanomaterials in Aquatic and Terrestrial Environments. *Accounts of Chem. Res.* 2012, 46 (3), 854-862; DOI 10.1021/ar2003368.
- 37) Lok, C. N.; Ho, C. M.; Chen, R.; He, Q. Y.; Yu, W. Y.; Sun, H.; Tam, P. K.; Chiu, J.; Che, C. Silver nanoparticles: partial oxidation and antibacterial activities. *J. Biol. Inorg. Chem.* 2007, 12, 527–534; DOI 10.1007/s00775-007-0208-z.
- 38) Levard, C.; Reinsch, B. C.; Michel, F. M.; Oumahi, C.; Lowry, G. V.; Brown, G. E. Sulfidation Processes of PVP-Coated Silver Nanoparticles in Aqueous Solution: Impact on Dissolution Rate *Environ. Sci. Technol.* 2011, 45, 5260–5266; DOI 10.1021/ar2003368.
- 39) Lau, B. L. T.; Hockaday, W. C. Ikuma, K.; Furman, O.; Decho, A. W. A preliminary assessment of the interactions between the capping agents of silver nanoparticles and environmental organics. *Colloids Surface A*. 2013, 435 (20), 22–27; DOI 10.1016/j.colsurfa.2012.11.065.
- 40) Chinnapongse, S. L.; MacCusprie, R. I.; Hackley, V. A. Persistence of singly dispersed silver nanoparticles in natural freshwaters, synthetic seawater, and simulated estuarine waters. *Sci. Total Environ.* 2011, 409, 2443-2450; DOI 10.1016/j.scitotenv.2011.03.020.

- 41) Baun, A.; Hartmann, N. B.; Grieger, K.; Kusk, K. O. Ecotoxicity of engineered nanoparticles to aquatic invertebrates: a brief review and recommendations for future toxicity testing. *Ecotoxicology*. 2008, 17, 387–395; DOI 10.1007/s10646-008-0208-y.
- 42) U.S. Environmental Protection Agency. Inductively Coupled Plasma–Atomic Emission Spectrometry; Method 6010C, Revision 3; U.S. EPA: Washington, DC, 2007; <http://www3.epa.gov/epawaste/hazard/testmethods/sw846/pdfs/3050b.pdf>.
- 43) U.S. Environmental Protection Agency. Determination of Metals and Trace Elements in Water and Wastes by Inductively Coupled Plasma–Atomic Emission Spectrometry; Method 200.7, Revision 4.4; U.S. EPA: Washington, DC, 1991; http://www.epa.gov/sites/production/files/2015-08/documents/method_200-7_rev_4-4_1994.pdf
- 44) Alcorlo, P.; Otero, M.; Crehuet, M.; Baltanas, A.; Montes, C. The use of the red swamp crayfish (*Procambarus clarkii*, Girard) as an indicator of the bioavailability of heavy metals in environmental monitoring in the River Guadiamar (SW, Spain). *Sci. Total Environ.* 2006, 366 (1), 380–390; DOI 10.1016/j.scitotenv.2006.02.023.
- 45) Suárez-Serrano, A.; Alcaraz, C.; Ibáñez, C.; Trobajo, C. *Procambarus clarkii* as a bioindicator of heavy metal pollution sources in the lower Ebro River and Delta. *Ecotox. Environ. Safe.* 2010, 73(3), 280-6; DOI 10.1016/j.ecoenv.2009.11.001.
- 46) Kouba, A.; Buřič, M.; Kozák, P. Bioaccumulation and Effects of Heavy Metals in Crayfish: A Review *Water Air Soil Pollut.* 2010, 211, 5–16; DOI 10.1007/s11270-009-0273-8.
- 47) Stevenson, L. M.; Dickson, H.; Klanjscek, T.; Keller, A. A.; McCauley, E.; Nisbet, R. M. Environmental Feedbacks and Engineered Nanoparticles: Mitigation of Silver Nanoparticle Toxicity to *Chlamydomonas reinhardtii* by Algal-Produced Organic Compounds. *PLOS One*. 2013, 8 (9), 1-7; DOI 10.1371/journal.pone.0074456.

- 48) Oukarroum, A.; Samadami, M. Influence of pH on the Toxicity of AgNPs in the Green Alga *Chlamydomonas acidophila*. *Water Air Soil Pollut.*, 2014, 225, 2038-2045; DOI 10.1007/s11270-014-2038-2.
- 49) Matzke, M.; Gallego, J.; Hasselov, M.; Jurkschat, K.; Backhaus, T. Effects of Silver Nanoparticles of Freshwater Microbial Communities. 2012; URI <http://nora.nerc.ac.uk/21263/1/N021263PO.pdf>.
- 50) Blinova, I.; Niskanen, J.; Kajankari, P.; Kanarbik, L.; Kälndnen, A.; Tenhu, H.; Penttinen, O.; Kahru, A. Toxicity of two types of AgNPs to aquatic crustaceans *Daphnia magna* and *Thamnocephalus platyurus*. *Environ. Sci. Pollut. Res.* 2013, 20, 3456–3463; DOI 10.1007/s11356-012-1290-5.
- 51) Salari Joo, H.; Kalbassi, M. R.; Yu, I. J.; Lee, J. H. Bioaccumulation of silver nanoparticles in rainbow trout (*Oncorhynchus mykiss*): Influence of concentration and salinity. *Aquat. Toxicol.* 2013, 140-141, 398-406; DOI /10.1016/j.aquatox.2013.07.003
- 52) Farkas, J.; Christian, P.; Urrea, J. A. G.; Roos, N.; Hassellöv, M.; Tollefsen, K. E.; Thomas, K. V. Effects of silver and gold nanoparticles on rainbow trout (*Oncorhynchus mykiss*) hepatocytes. *Aquat. Toxicol.* 2010, 96, 44–52; DOI 10.1016/j.aquatox.2009.09.016
- 53) Holdich, D. M.; Lowery, R. S. *Biology of Freshwater Crayfish*. Timber Press: Portland, Oregon. 1988, pp.12, 83-91,155-160;
[https://gl.yorku.ca/GIProfProfiles.nsf/PublicationsAttachments/11F4D52E63F7BE51852574C2000C84AE/\\$File/Chapter%2016%20Cambarus.pdf](https://gl.yorku.ca/GIProfProfiles.nsf/PublicationsAttachments/11F4D52E63F7BE51852574C2000C84AE/$File/Chapter%2016%20Cambarus.pdf)
- 54) Holdich, D. M.; Sibley, P. J. Eds. *Management & Conservation of Crayfish*. Proceedings of a conference held on 7th November 2003, Environment Agency, Bristol. pp 217.
- 55) Holdich, D. M. A review of astaciculture: freshwater crayfish farming. *Aquat. Living Resour.* 1993, 6, 307-317.

- 56) *Management of Freshwater Biodiversity: Crayfish as Bioindicators*. Reynolds, J.; Souty-Grosset, C. Cambridge University Press: Cambridge, UK. 2012, pp. 81.
- 57) Chapman, D.; Jackson, J.; Krebs, F. Edited by: Bartram, J.; Balance, R. *Water Quality Monitoring - A Practical Guide to the Design and Implementation of Freshwater Quality Studies and Monitoring Programmes*. 1996, *Table 11.2*.
- 58) *Secondary Drinking Water Regulations: Guidance for Nuisance Chemicals*. US EPA; <http://www.epa.gov/dwstandardsregulations/secondary-drinking-water-regulations-guidance-nuisance-chemicals>.
- 59) Hudson River Estuary Program. New York State, Department of Environmental Conservation. <http://www.dec.ny.gov/lands/4920.html>. (accessed May 23, 2016)
- 60) Tolaymat, T. M.; Badawy, A. M.; Genaidy, A.; Scheckel, K. G.; Luxton, T. P.; Suidan, M. An evidence-based environmental perspective of manufactured silver nanoparticle in syntheses and applications: A systematic review and critical appraisal of peer-reviewed scientific papers. *Sci. Total Environ.* 2010, *408*, 999-1006; DOI 10.1016/j.scitotenv.2009.11.003.
- 61) Robinson, J. W.; Frame, E. M. S.; Frame, G. M., II *Undergraduate Instrumental Analysis*, 6th ed.; Marcel Dekker: New York, 2005; pp 391, 483–505.
- 62) Winchester, M. R. Method for Determination of the Mass Fraction of Particle-Bound Gold in Suspensions of Gold Nanoparticles. *NIST – NCL*. 2010, *Method PCC-11*; Version 1.1.
- 63) Hoque, M. E.; Khosravi, K.; Newman, K.; Metcalfe, C. D. Detection and characterization of silver nanoparticles in aqueous matrices using asymmetric-flow field flow fractionation with inductively coupled plasma mass spectrometry. *J. Chromatogr. A*. 2012, *1233*, 109– 115; DOI 10.1016/j.chroma.2012.02.011.
- 64) Brittle, S. W.; Baker, J. D.; Dorney, K. M.; Dagher, J. M.; Ebrahimian, T.; Higgins, S. R.; Pavel-Sizemore, I. E. *J. Chem. Educ.* 2015, *92*, 1061–1065; DOI 10.1021/ed500707k.

- 65) U.S. Environmental Protection Agency. Inductively Coupled Plasma–Atomic Emission Spectrometry; Method 3052, Revision 3; U.S. EPA: Washington, DC, 2007.
- 66) Huxley, T.H. *The Crayfish: An Introduction to the Study of Zoology*. v. XXVIII of the Inter-national Scientific Series. D. Appleton, New York. 1879.
- 67) Creighton, J. A.; Blatchford, C. G.; Albrecht, M. G., Plasma Resonance Enhancement of Raman-Scattering by Pyridine Adsorbed on Silver or Gold Sol Particles of Size Comparable to the Excitation Wavelength. *J Chem. Soc. Farad T 2*. 1979, 75, 790–798; DOI 10.1039/F29797500790.
- 68) Solomon, S. D.; Bahadory, M.; Jeyarajasingam, A. V.; Rutkowsky, S. A.; Boritz, C. Synthesis and Study of Silver Nanoparticles. *J. Chem. Educ.* 2007, 84, 322; DOI 10.1021/ed084p322.
- 69) Pavel, I. E.; Alnajjar, K. S.; Monahan, J. L.; Stahler, A.; Hunter, N. E.; Weaver, K. M.; Baker, J. D.; Meyerhoefer, A. J.; Dolson, D. A., Estimating the Analytical and Surface Enhancement Factors in Surface-Enhanced Raman Scattering (SERS): A Novel Physical Chemistry and Nanotechnology Laboratory Experiment. *J. Chem. Educ.* 2011, 89 (2), 286–290; DOI 10.1021/ed200156n.
- 70) Liu, J.; Chao, J.; Liu, R.; Tan, Z.; Yin, Y.; Wu, Y.; Jiang, G. Cloud Point Extraction as an Advantageous Preconcentration Approach for Analysis of Trace Silver Nanoparticles in Environmental Waters. *Anal. Chem.* **2009**, 81, 6496–6502. DOI 10.1021/ac900918e.
- 71) Yu, S.; Chao, J.; Sun, J.; Yin, Y.; Liu, J.; Jiang, G. Quantification of the Uptake of Silver Nanoparticles and Ions to HepG2 Cells. *Environ. Sci. Technol.* **2013**, 47, 3268–3274. DOI 10.1021/es304346p.
- 72) Mortada, W.; Hassanien, M. M.; El-Asmy, A. A. Cloud point extraction of some precious metals using Triton X-114 and a thioamide derivative with a salting-out effect. *Egypt J. App. Sci. I.* **2014**, 184-191.

- 73) Bansal, R. C.; Goyal, M. Activated Carbon Adsorption. 2005. CRC Press, Boca Raton, FL, USA.
- 74) Stankowich, T.; Blumstein, D. Fear in animals: a meta-analysis and review of risk assessment. *Proc. R. Soc. B.* 2005, 272, 2627–2634; DOI 10.1098/rspb.2005.3251.
- 75) Bergman, D. A.; Moore, P. A. Field Observations of Intraspecific Agonistic Behavior of Two Crayfish Species, *Orconectes rusticus* and *Orconectes virilis*, in Different Habitats. *Biol. Bull.* 2003, 205, 26–35.
- 76) Moore, P. A. Edited by Duffy, J. E.; Thiel, M. Agonistic Behavior in Freshwater Crayfish: The Influence of Intrinsic and Extrinsic Factors on Aggressive Encounters and Dominance. Oxford University Press, Inc., NY, NY. 2007, pp. 93; DOI 10.1093/acprof:oso/9780195179927.001.0001.
- 77) Wren, M.; Gagnon, Z. E. A histopathological study of Hudson River crayfish, *Orconectes virilis*, exposed to platinum group metals. *J. Environ. Sci. Health: A.* 2014, 49 (2), 135-145; DOI 10.1080/10934529.2013.838836.
- 78) Horne, F.; Tarsitano, S.; Lavalli, K. Aspects of Mineralization of the Cuticle of the Crayfish *Procambarus clarkii* (Decapoda, Cambaridae). *Crustaceana.* 2009, 82 (8), 1057-1065; DOI 0.1163/156854009X452740.
- 79) U.S. Environmental Protection Agency. Methods for the Determination of Metals in Environmental Samples. *U.S. EPA*: Washington, DC, 1991; www.epa.gov/method200.1.
- 80) Trevigen's CometAssay Procedure/Manual. Catalog # 4250-050-K. Purchased 2012, 2014.
- 81) Demke, D. D. A brief histology of the intestine of the turkey poult. *Am. J. Vet. Res.* 1954, 15 (56), 447-449; PMID 13171507.
- 82) *Detection and Characterization of Engineered Nanomaterials in the Environment: Current State-of-the-Art and Future Directions.* US EPA, Office of Research and Development: Washington, DC, 2014; http://cfpub.epa.gov/si/si_public_file_download.cfm?p_download_id=520064.

- 83) EPA Needs to Manage Nanomaterial Risks More Effectively. *US EPA RCRA*. 2011, 40
C.F.R. § 261.2; <http://www.epa.gov/sites/production/files/2015-10/documents/20121229-12-p-0162.pdf> .
- 84) Dorney, K. M.; Baker, J. D.; Edwards, M. L.; Kanel, S. R.; O'Malley, M.; Pavel-Sizemore, I. E.
Tangential Flow Filtration of Colloidal Silver Nanoparticles: A “Green” Laboratory
Experiment for Chemistry and Engineering Students. *J. Chem. Ed.* 2014, 91, 1044–1049;
DOI 10.1021/ed400686
- 85) Badawy, A. M.; Luxton, T. P.; Silva, R. G.; Scheckel, K. G. Suidan, M. T.; Tolaymat, T.
M. Impact of Environmental Conditions (pH, Ionic Strength, and Electrolyte Type) on
the Surface Charge and Aggregation of Silver Nanoparticles Suspensions. *Environ. Sci.
Technol.* 2010, 44, 1260–1266; DOI 10.1021/es902240k.
- 86) O'Brien, J. J.; Kumari, S.; Skinner, D. M. Proteins of Crustacean Exoskeletons: I.
Similarities and Differences among Proteins of the Four Exoskeletal Layers of Four
Brachyurans. *Biol. Bull.* 1991, 181, 427-441.
- 87) Moulin, P.; Roques, H. Zeta potential measurement of calcium carbonate. *J. Colloid Interf.
Sci* 2003, 261, 115–12; DOI 10.1016/S0021-9797(03)00057-2.
- 88) Bruneau, A.; Pilote, T. P.; Gagne, F.; Gagnon, C. Fate and Immunotoxic Effects of Silver
Nanoparticles on Rainbow Trout in Natural Waters. *J. Nanomed. Nanotechnol.* 2015, 6,
3; DOI 10.4172/2157-7439.1000290.
- 89) Scown, T.; Santos, E.; Johnston, B.; Gaiser, B.; Baalousha, M.; Mitov, S.; Lead, J. R.;
Stone, V.; Fernandes, T. F.; Jepson, M.; van Aerle, R.; Tyler, C. R.. Effects of aqueous
exposure to silver nanoparticles of different sizes in rainbow trout. *Toxicol. Sci.* 2010,
115, 521–34; DOI 10.1093/toxsci/kfq076.
- 90) Wood, C.M., Hogstrand, C., Galvez, F., Munger, R.S. The physiology of waterborne silver
toxicity in freshwater rainbow trout (*Oncorhynchus mykiss*) 2. The effects of silver

- thiosulfate. The effects of ionic Ag⁺. *Aquat. Toxicol.* 1996, 35, 111-125; DOI 10.1016/0166-445X(96)00004-5.
- 91) Morgan, I. J.; Henry, R. P.; Wood, C.M. The mechanism of acute silver nitrate toxicity in freshwater rainbow trout (*Oncorhynchus mykiss*) is inhibition of gill Na⁺ and Cl⁻ transport. *Aquat. Toxicol.* 1997, 38, 145–163; DOI 10.1016/S0166-445X(96)00835-1.
- 92) Wu, Y.; Zhou, Q.; Li, H.; Liu, W.; Jiang, G. Effects of silver nanoparticles on the development and histopathology biomarkers of Japanese medaka (*Oryzias latipes*) using the partial-life test. *Aquat. Toxicol.* 2010, 100, 160–167; DOI 10.1016/j.aquatox.2009.11.014.
- 93) Moore, M. N. Do nanoparticles present ecotoxicological risks for the health of the aquatic environment? *Environ. Internat.* 2006, 32, 967–976; DOI 10.1016/j.envint.2006.06.014.
- 94) Shahriar, S.; Behzadi, S.; Laurent, S.; Forrest, M. L.; Stroeve, P.; Mahmoudi, M. Toxicity of nanomaterials. *Chem. Soc. Rev.* 2012, 41, 2323–2343; DOI 10.1039/c1cs15188f.
- 95) Bothun, G. D. Hydrophobic silver nanoparticles trapped in lipid bilayers: size distribution, bilayer phase behavior, and optical properties. *J. Nanobiotechnology.* 2008, 6 (13), 10. DOI 10.1186/1477-3155-6-13.
- 96) Krishnaraj, C.; Harper, S. L.; Yun, S. *In Vivo* toxicological assessment of biologically synthesized silver nanoparticles in adult Zebrafish (*Danio rerio*). *J. Hazard. Mater.* 2016, 301, 480–491; DOI 10.1016/j.jhazmat.2015.09.022.
- 97) Seyed, J. Mohammad, K. Il, Y.; Lee, Ji. Chronic effect of waterborne silver nanoparticles on rainbow trout (*Oncorhynchus mykiss*): histopathology and bioaccumulation. *Comparative Clinical Pathology.* 2015, 24 (5), 995-1007; DOI 10.1007/s00580-014-2019-2.
- 98) Piccapietra, F.; Allué, C. G.; Sigg, L.; Behra, R. Intracellular Silver Accumulation in *Chlamydomonas reinhardtii* upon Exposure to Carbonate Coated Silver Nanoparticles and Silver Nitrate. *Environ. Sci. Technol.* 2012, 46, 7390–7397; DOI 10.1021/es300734m.

ASSOCIATED CONTENT

SUPPORTING INFORMATION

Supplementary information includes: justification of the concentrations used, additional details about the characterization of the AgNPs, water quality metrics, gross pathological changes, behavioral observations, Ag content of water tanks, tabulated ICP-OES results, and comet assay images with tabulated results.

MATERIALS AND METHODS

Aquaria preparation: Aqueon aquaria (26 cm × 32 cm × 51 cm) were washed with nitric acid (5% HNO₃ v/v) and deionized water (5× washes) to remove potential residual metals or other contaminants. Quarter inch diameter aquarium stones were pressure-washed extensively with tap water and three cups of the substrate stone were placed on the bottom of each tank (an average depth of ~3 cm). A gravel substrate of primarily quartz-based stones was chosen to avoid possible effects on water chemistry and nanosilver. All other submerged materials (*e.g.*, polyester filter and PVC shelters) were chosen for their chemical inertness. Crayfish shelters were prepared by cutting 2-in diameter PVC tubes into ~10 cm lengths, which were then halved lengthwise. Three of those shelters were placed on the substrate of each tank.

Hudson River water (HRW) filtration: One week prior to crayfish arrival, aquaria were prepared for crayfish acclimation. The tanks were filled with 20 L of raw HRW, and the contents were filtered for particulates for one week with Lee's Economy Corner Filters (polypropylene) filled with polyester filter floss (Acurel, Petco). Due to its highly absorptive nature and ability to remove metals, activated charcoal filters were not

used for this experiment¹. The filters were powered by Tetra Whisper Aquarium air pumps. A separate tank was completely filled with filtered HRW and served as a water supply to maintain the water level in each tank.

Silver Dosing: The experimental set-up is abbreviated in Figure 2.S1. The experimental concentrations (30, 120, and 360 $\mu\text{g Ag L}^{-1}$) were selected to encompass previous freshwater AgNP and Ag^+ pollution studies (Figure 2.S2) as well as different regulated levels (Figure 2.S3).

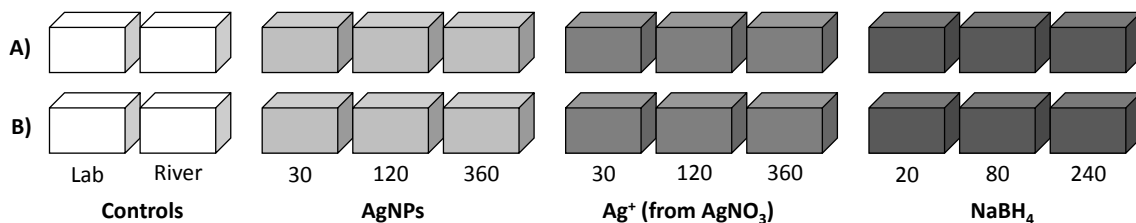


Figure 2.S1. Schematic of the experimental design. Each box represents one 20-L aquarium. All treatments and controls were duplicated to generate a larger N without overcrowding each tank. The only difference was one tank housed **A**) 2 females and one male, and the other housed **B**) the opposite, namely two males and one female. Crayfish sexes were varied between duplicate tanks to observe the sex' potential of influencing behavioral results; however, no statistical interaction of sex was revealed at the $p < 0.001$ level using a two-way ANOVA multiple comparisons with a Holm-Šidák adjustment. All concentrations are in $\mu\text{g L}^{-1}$.

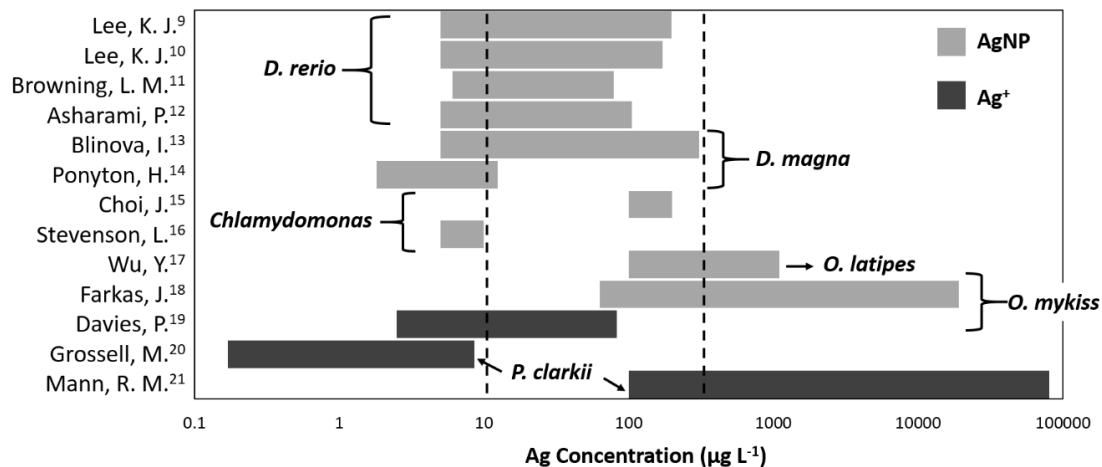


Figure 2.S2. Summary of previous research on the biological impact of nanosilver and ionic Ag⁺ in freshwater organisms. Dashed vertical lines denote the Ag concentration range utilized in this experiment. All concentrations have been converted into µg L⁻¹ for comparison purposes on the X-axis. Experimental species are provided in italics. References are given on the Y-axis.

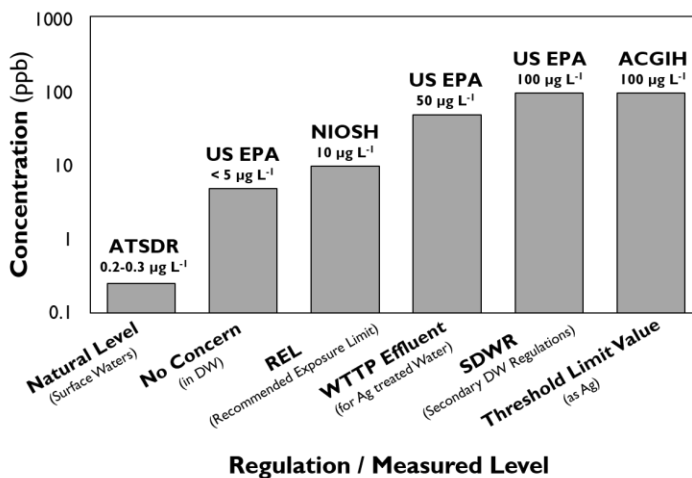


Figure 2.S3. Summary of current (2015) silver regulations within various government agencies. Concentrations have been converted into µg L⁻¹ for comparative purposes. Acronyms are defined as follows: ATSDR = Agency for Toxic Substances and Disease Registry, US EPA = United States Environmental Protection Agency, NIOSH = National Institute for Occupational Safety and Health, and DW = drinking water.

AgNP characterization: A LabRam HR800 Raman spectrophotometer equipped with a high-resolution confocal microscope (BX41, Olympus 50 X objective) was employed to verify colloidal purity of small aliquots of the colloidal AgNPs (2 mL) at two excitation wavelengths, namely 532.134 nm (Nd:YAG laser) and 632.817 nm (He-Ne laser). The following components and acquisition parameters were selected for the acquisition of single point spectra with a spectral resolution of $\sim 1 \text{ cm}^{-1}$: a holographic grating of $600 \text{ grooves mm}^{-1}$, a confocal hole of $300 \mu\text{m}$, a thermoelectrically cooled Andor CCD camera of 1024×256 pixels, an acquisition time of 30 s, and 5 cycles. Spectra were then processed in Origin 8 software.

Cloud Point Extraction of AgNPs and Ag^+ : Triplicate aquaria were set up in the same manner as for the crayfish experiment. Colloidal AgNPs or Ag^+ were diluted ($360 \mu\text{g L}^{-1}$) in Hudson River Water (HRW), and aliquots were collected on day 1 and 14. One milliliter was immediately digested by the same procedure outlined in the manuscript (diluted 1:10 to 2% HNO_3) and analyzed on ICP-OES to quantify total Ag. Another 9.5 mL was utilized for the CPE procedure (Figure 2.1). First, the pH was adjusted to the pH_{pzc} (pH at point zero charges) to allow for better separation of the two Ag species. To do this, 0.002 mL of HNO_3 (2%) was added to bring the pH to $\sim 3 - 3.5$. Next, 0.2 mL of Triton X-114 was poured to form AgNP micelles and then 0.1 mL of $\text{Na}_2\text{S}_2\text{O}_3$ to chelate Ag^+ ions. The mixture was then centrifuged for 5 min at $\sim 2 \times 10^3 \text{ g}$ to further separate the two phases. Upon centrifugation, the denser surfactant-AgNP mixture collected on the bottom pellet, while the supernatant contained mostly Ag^+ chelated to $\text{Na}_2\text{S}_2\text{O}_3$. One milliliter of the supernatant and 0.2 mL of the pellet were chemically digested and

analyzed for total Ag via ICP-OES. From these results, an average percent of AgNPs was determined with respect to the Ag measured in the pellet.

Water Metrics: Water quality metrics (*i.e.*, temperature, pH, dissolved oxygen, and conductivity) were recorded daily for each tank using a YSI Professional Plus coupled with a Quatro 4-port cable multisensor. The lab temperature was kept constant at 20°C.

Behavioral and gross pathology: gross visual observations of animal health (*e.g.*, exoskeleton cleanliness, coloring consistency, and bodily integrity) were also taken daily. Lab specimens were checked every day for threat responsiveness; fear responses were gauged by approaching crayfish with a glass stirring rod and were registered as positive if a specimen flipped its tail quickly in a manner similar to escape (“initiating flight” as defined by Stankowich and Blumstein²). Responses were recorded twice by two individuals similarly to Bergman³, Moore⁴, and Wren⁵ utilizing a ranking scale of 1 to 7. The average of both scores was then used for statistical analysis, which was blindly conducted by a third individual. Organisms that died during the experiment were subsequently removed from the tank and recorded as mortality. The experiment proceeded without interruption if any specimen molted as molting is a natural cycle of all arthropods^{6,7}. However, if gastroliths were observed during dissection, the specimen was eliminated from further analysis because this is a sign of pre-molting and hence increased vulnerability to environmental threats⁶⁻⁸.

RESULTS AND DISCUSSION

Characterization of AgNPs:

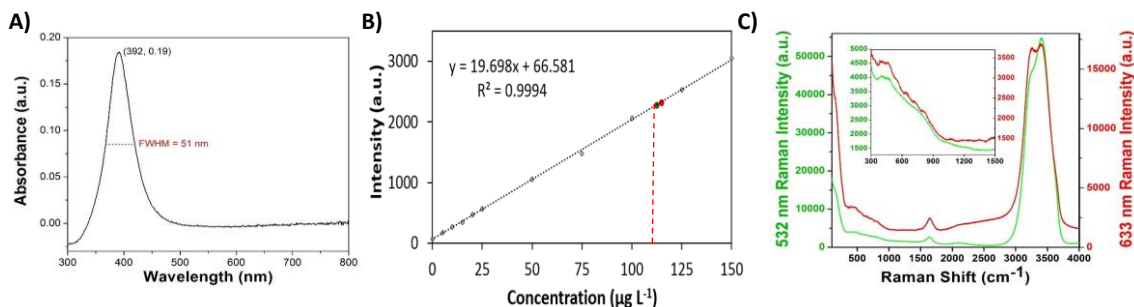


Figure 2.S4. Spectroscopic characterization of AgNPs. A) UV-Vis Absorption spectroscopy confirmed the formation of spherical AgNPs through a single, LSPR at 392 nm. B) The ICP-OES external calibration method was prepared to quantify total Ag concentration. The dashed red vertical line denotes the raw intensity observed for the digested and water diluted (1:100 v:v) AgNP colloid. The black line is the calibration curve constructed from nine Ag standards. C) Raman spectroscopy verified the purity of the Ag colloid with two excitation wavelengths at 532 nm and 633 nm; inset shows fingerprint region void of contaminants. The spectra were characteristic to the solvent utilized throughout the synthesis procedure: high-quality water. Water characteristic vibrational modes were observed at 1640 cm^{-1} (ν_2 H-H scissoring bend), 3241 cm^{-1} and 3394 cm^{-1} (symmetric ν_1 and asymmetric ν_3 O-H stretching).

CPE:

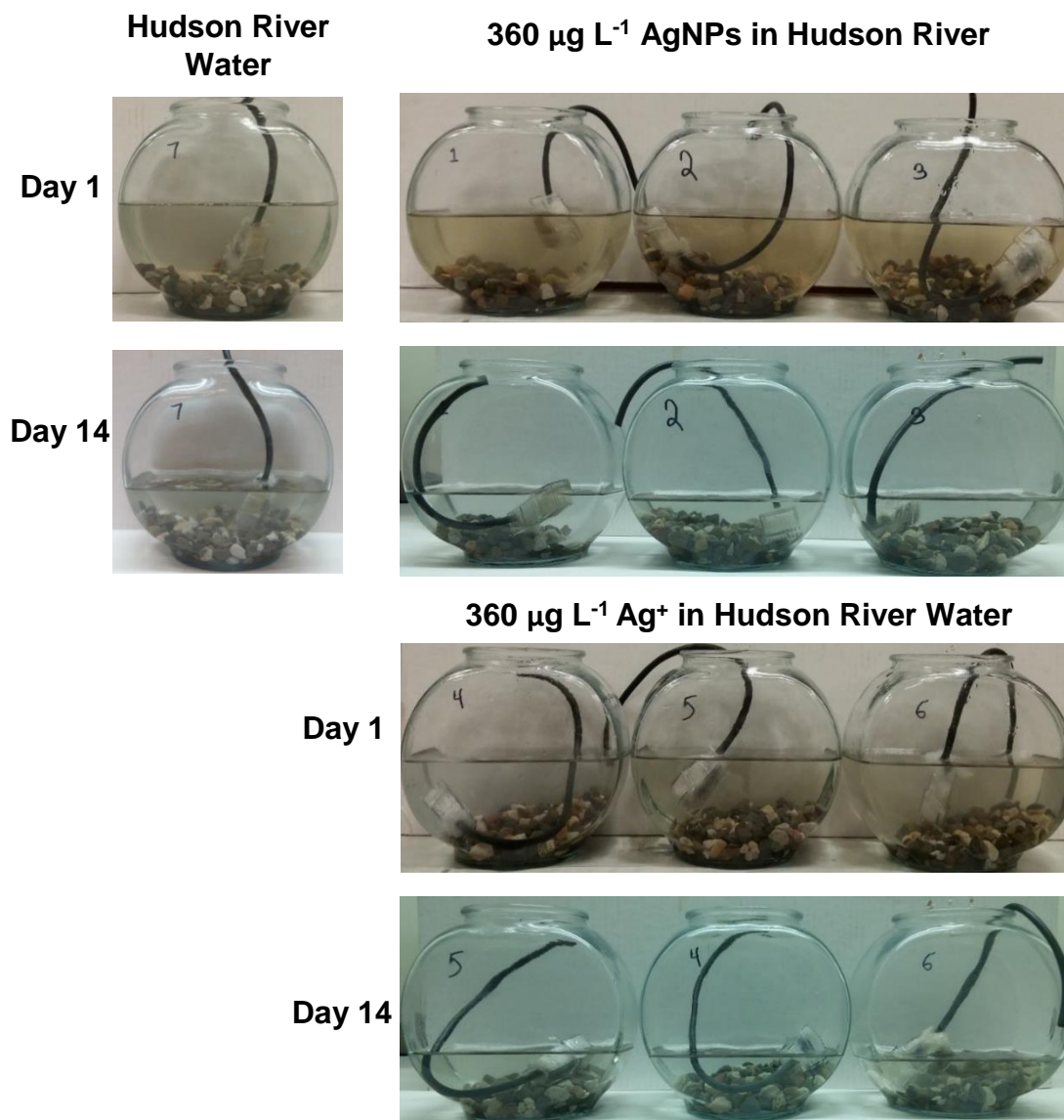


Figure 2.S5. Pictures of the CPE experimental set-up. Aquaria were filled with 1 L of Hudson River Water (HRW, no biological crayfish) and set up similarly to the aquaria in the crayfish experiment (same substrate, filters, and tubing). AgNPs ($360 \mu\text{g L}^{-1}$) or Ag⁺ ($360 \mu\text{g L}^{-1}$) were added at day 1, and aliquot samples were collected from the bottom of the tanks, where crayfish reside, at both day 1 and 14 (9.5 mL). Afterward, the water samples including HRW controls were processed by CPE, centrifugation, and ICP-OES in order to quantify the amount of AgNPs and Ag⁺.

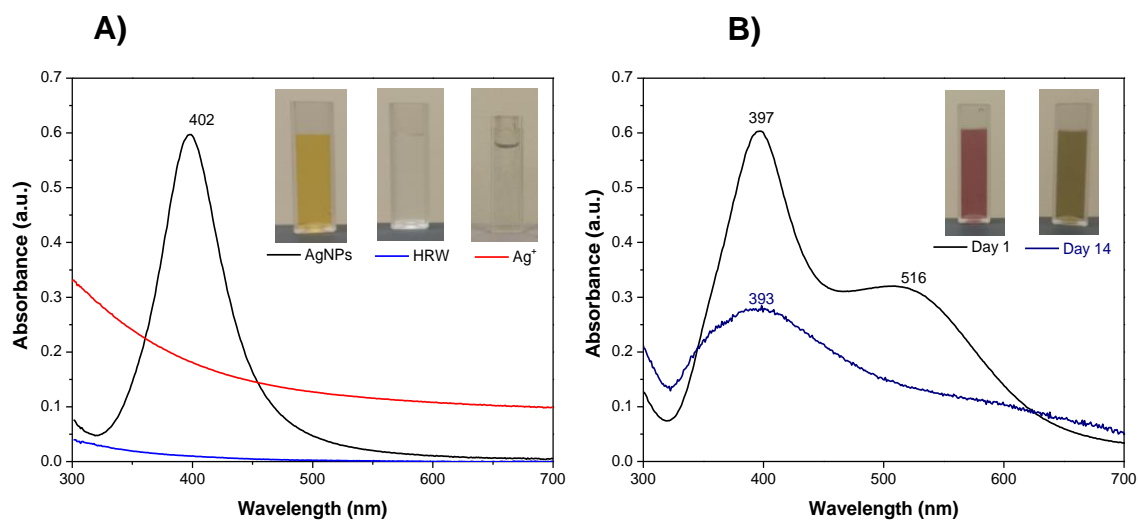


Figure 2.S6. UV-Vis Absorbance Spectra of A) the original colloidal Creighton AgNPs that exhibit a characteristic LSPR absorbance band at ~ 400 nm and have a transparent yellow color (inset). Hudson River Water (HRW) and an Ag^+ control displayed no apparent color and no absorbance. **B)** the AgNPs in HRW (1 mg L^{-1}) at day 1 and 14 showing significant changes in the LSPR peak and color.

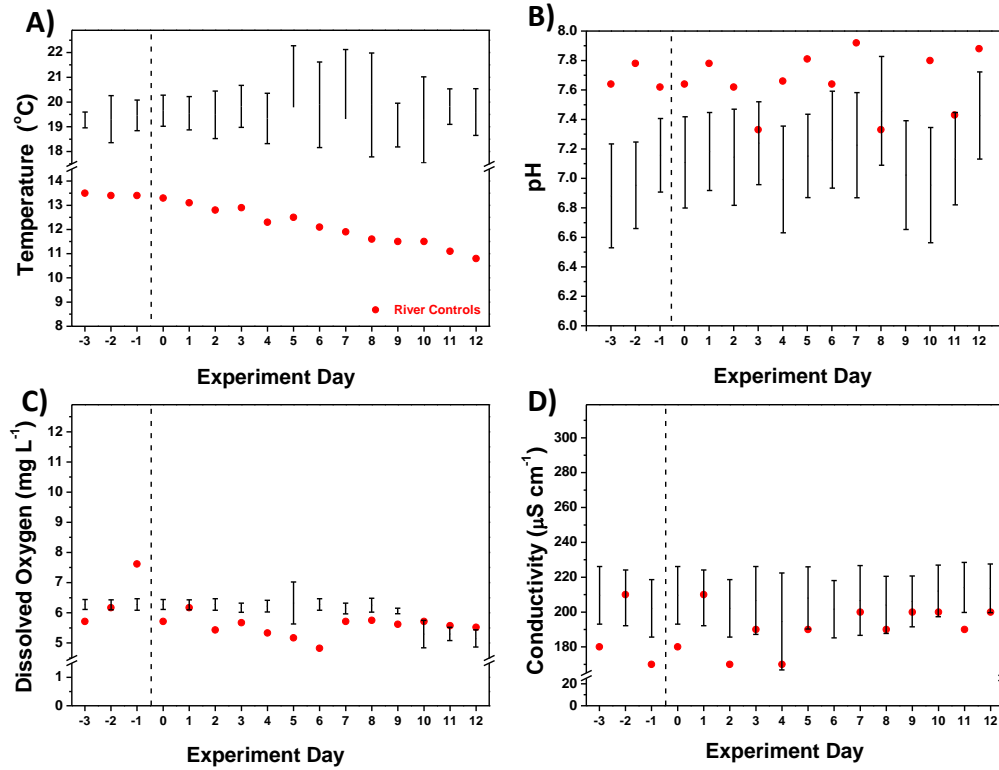


Figure 2.S7. Water metrics measured daily before and during the *P. clarkii* experiment: A) temperature, B) pH, C) dissolved oxygen, and D) conductivity. Only the river control (red) exhibited significant variation compared to the rest of the aquaria and day to day values. All other measurements are reported as a bracketed range of all 20 tanks measured daily. Metrics were not measured on harvest day.

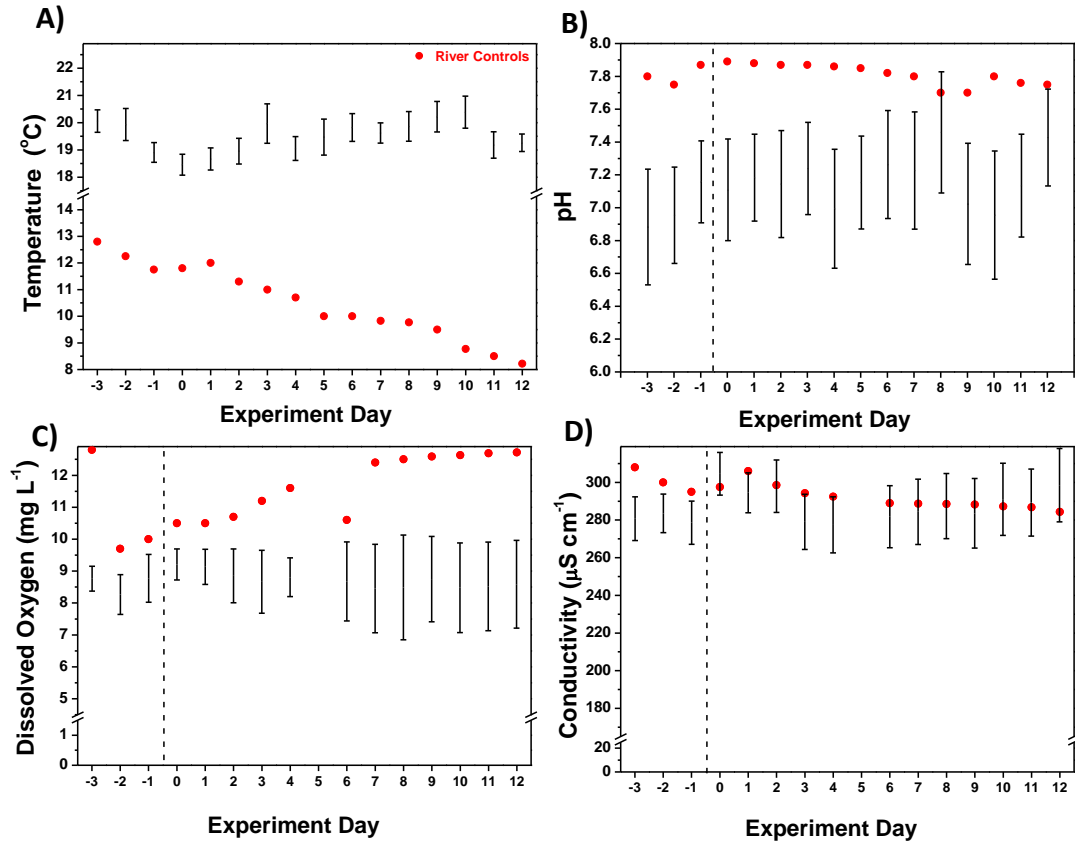


Figure 2.S8. Water metrics measured daily before and during the *O. virilis* experiment: A) temperature, B) pH, C) dissolved oxygen, and D) conductivity. Only the river control (red) exhibited significant variation compared to the rest of the aquaria and day to day values. All other measurements are reported as a bracketed range of all 20 tanks measured daily. Metrics were not measured on harvest day.

Anatomical and behavioral observation: On average (Figure 2.S9), only the lowest AgNP dose led to a small loss weight in *O. virilis*. The weight decrease could be attributed to numerous factors such as neurological damage or pathological changes. In contrast, *P. clarkii* experienced a decreased in weight at all Ag exposures. This may be due to the change in the feeding habits of the two species before their purchase; *P. clarkii* was raised in a lab controlled environment before purchase (Carolina Biological Supplies), while *O. virilis* was directly collected from Northeastern Aquatics fish hatchery (Rhinebeck, NY), where they probably foraged for food more than they would in a controlled aquaria. *P. clarkii* was also found to exhibit behavioral changes. Decreased fear responses were observed in both species as a result of AgNP and Ag⁺ stimuli (α -0.05 level); but no specific trends could be established (Figure 2.S10). This increased lethargy is in agreement with the DNA damage associated with the exposure to Ag.

Table 2.S1. Summary of physical changes observed throughout experiments. Ecdysis was documented when molt was present in a tank during daily observations. Presence of gastroliths was only recorded during dissection. Missing appendages were logged during harvest days. If a specimen died during the experiment or was pregnant during the harvest, it was marked and noted accordingly. “D” denotes the Day of the experiment.

		Controls		AgNPs			Ag⁺ from AgNO₃			NaBH₄		
		Lab	River	30	120	360	30	120	360	20	80	240
<i>P. clarkii</i>	Ecdysis	D 7		D 6			D 7			D10		
	Gastroliths									Harvest		
	Lost Appendages	1 claw, 1 leg		1 leg			2 legs			1 claw	1 leg	
	Death			1			1	2				
	Pregnant						1			1		
<i>O. virilis</i>	Ecdysis	3		D 6, D 10			D4					
	Gastroliths											
	Lost Appendages	2 legs, 1 claw		1 leg			2 legs			1 claw	1 leg	
	Death	1		1			1	1		.		
	Pregnant	1		1						1	1	

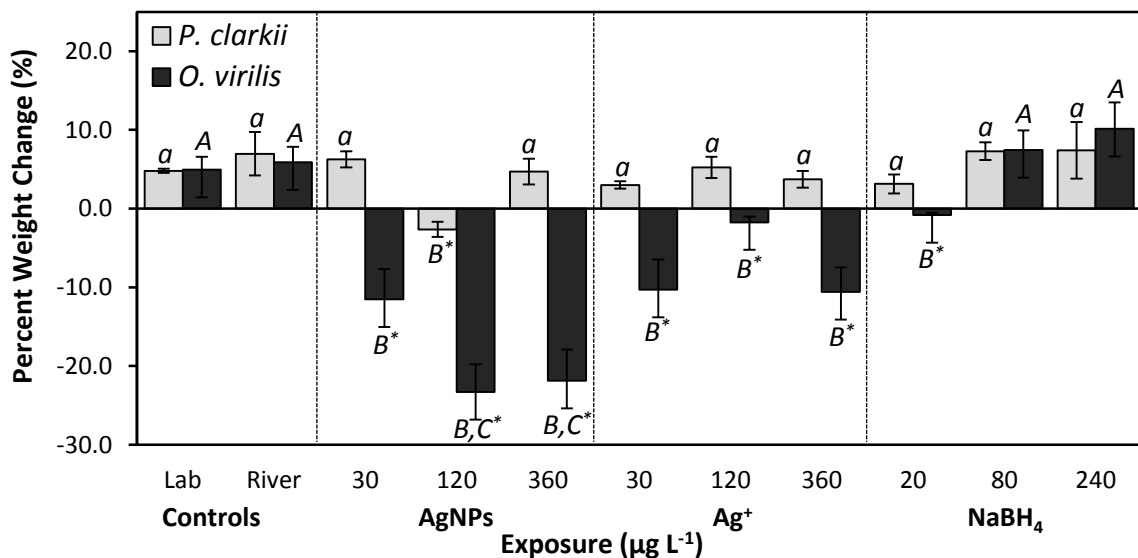


Figure 2.S9. Average percent weight change for A) *P. clarkii* and B) *O. virilis*. Treatment or control values denoted with the same letter and case were not statistically different as determined by one-way ANOVA ($p \leq 0.001$) and Holm-Šidák multiple comparison tests ($p \leq 0.05$). * marks differences between the two species. Bars represent the standard error.

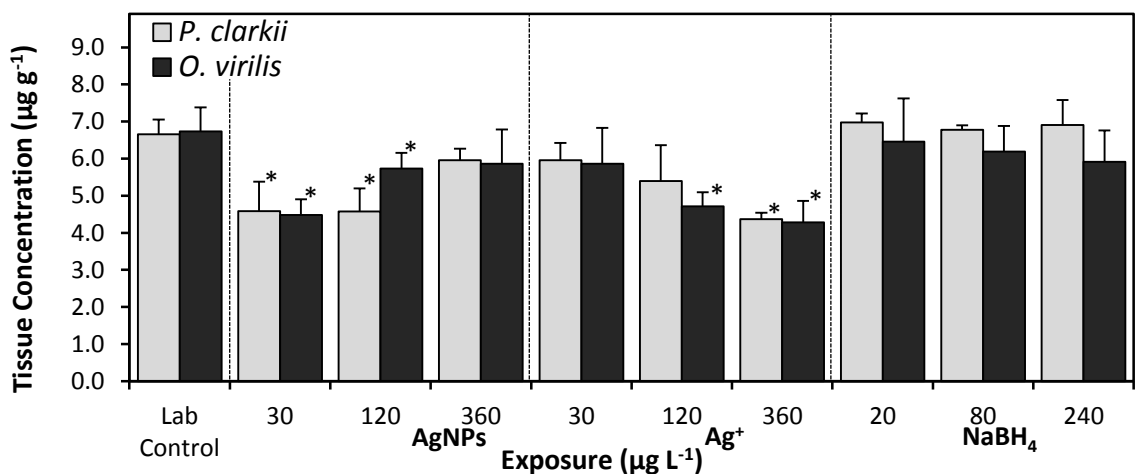


Figure 2.S10. Average fear response assigned using a ranking scale of 1 to 7 similarly to Bergman³, Moore⁴ and Wren⁵. Scores were assigned as follows: 7 = fast retreat (rapid tail flip), no hesitation; 6 = retreat, little hesitation; 5 = slower retreat, slight hesitation; 4 = quick backward movement, no tail flip; 3 = slower backward walk; 2 = slight response, only appendages moved; 1 = no response. Most scores assigned were 5 or above (> 90%). Any specimen mortality was excluded from the averaged scores.* denotes statistical differences at the $\alpha = 0.05$ -level.

Silver quantification: As mentioned in the manuscript, the standard addition calibration method indicated matrix effects were negligible in all digested tissues. The relative percent differences (RPD) were less than the EPA quality control guidelines (<10%). Thus, the external calibration method was deemed suitable for the quantification of total Ag in the digested samples. A sample calibration curve is provided for both methods in Figure 2.S11. RPD was calculated by taking the absolute value of the difference between the external calibration value and the standard addition value, which was then divided by the average Ag content obtained with the two methods (eq. 1).

$$RPD = \left| \frac{Ext. Cal. Value - Std. Add. Value}{((Ext. Cal. Value + Std. Add. Value)/2)} \right| \times 100\% \quad (1)$$

In addition, the percent recovery (R) can help determine the accuracy of the standard addition method²⁶. This may be estimated by the difference between a spiked sample and an unspiked sample, which is then divided by the concentration of the spike used in the addition (eq. 2). It is important to note that the concentrations before the consideration of the dilution factor were utilized here. Furthermore, it does not matter which spiked sample is used as long as the correct concentration of the spike is calculated and the respective spiked sample concentration is used. The concentration of the spike added was estimated from the dilution formula. According to the U.S. EPA Method 200.7²⁶, an optimal control limit exists within the 85 – 115% range. Because no recoveries below 85% or above 115% were observed, the method was deemed accurate, and matrix effects were considered minimal or nonexistent.

$$R = \frac{Spiked Sample - Unspiked Sample}{Spike Added} \times 100\% \quad (2)$$

A method detection limit (MDL) was determined by analyzing the lowest Ag standard ($5 \mu\text{g L}^{-1}$) seven separate times and using the equation below (eq. 3). Agilent Technologies claims a NIST certified detection limit of $1.062 \mu\text{g L}^{-1}$ for the primary emission wavelength of silver (328.068 nm) measured by a Varian 710-ES²⁷; however, the MDL determined here with 99% confidence by using (eq. 3) was $2.6 \mu\text{g L}^{-1}$ (eq. 4). *SD* refers to the standard deviation of the seven measurements ($0.823 \mu\text{g L}^{-1}$) and *T* is student's *t* value at a 99% confidence level for seven degrees of freedom (3.14).

$$MDL = T_{(n-1, 1-\alpha=0.99)} \times SD \quad (3)$$

$$MDL = 3.142 \times 0.823 = 2.594 \quad (4)$$

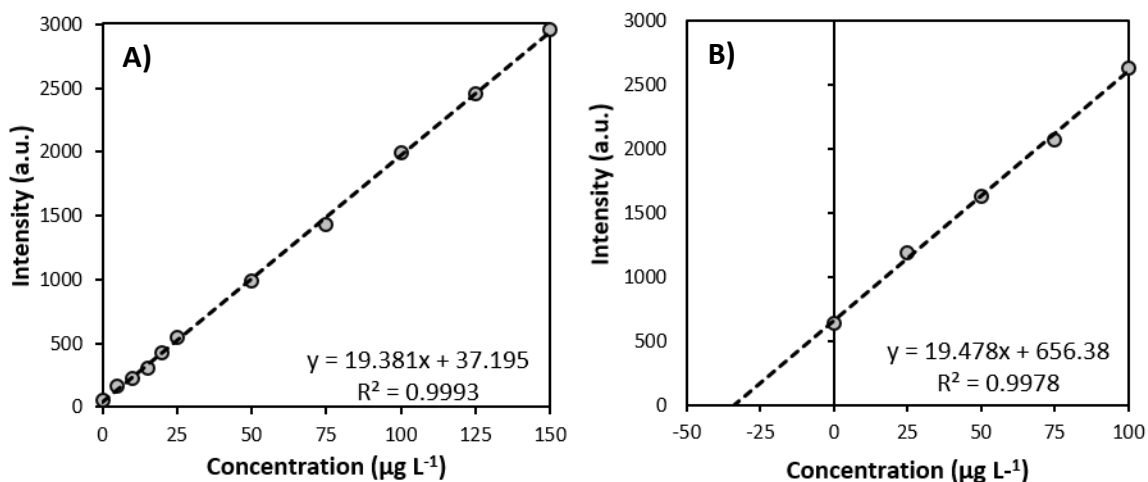


Figure 2.S11. External calibration curve (A) and standard addition curve (B) for the gills of *P. clarkii*. Standard addition sample is from the $360 \mu\text{g L}^{-1}$ of AgNP treatment with spikes of $10^3 \mu\text{g L}^{-1}$ of Ag standard in $25 \mu\text{L}$ increments and diluted to a final volume of 10 mL.

Table 2.S2. Total Ag detected in digested tissue samples. Values reported below the MDL of 3.0 $\mu\text{g L}^{-1}$ are estimated from extrapolation. Standard error is reported parenthetically below each value ($N = 6$ organisms on average).

		Controls		AgNP			Ag ⁺ from AgNO ₃			NaBH ₄		
		Lab	River	30	120	360	30	120	360	20	80	240
<i>P. clarkii</i>	Exoskeletons	0.04 (0.10)	0.04 (0.10)	0.17 (0.13)	0.44 (0.10)	0.46 (0.08)	0.80 (0.24)	1.54 (0.21)	1.85 (0.09)	0.04 (0.10)	0.00 (0.12)	0.10 (0.08)
	Muscles	0.07 (0.15)	0.01 (0.25)	0.45 (0.13)	0.52 (0.19)	0.37 (0.14)	0.37 (0.11)	0.36 (0.15)	0.49 (0.13)	0.12 (0.12)	0.04 (0.08)	0.05 (0.07)
	Gills	0.84 (0.73)	0.73 (0.32)	1.88 (0.24)	2.77 (0.22)	5.10 (0.32)	2.52 (0.18)	3.49 (0.56)	15.20 (0.22)	0.21 (0.47)	0.24 (0.15)	0.90 (0.10)
	Hepatopancreas	0.72 (0.56)	0.80 (0.36)	1.54 (0.74)	12.17 (0.62)	17.40 (0.22)	4.50 (0.61)	6.44 (0.61)	15.12 (0.83)	0.80 (0.21)	0.71 (0.89)	1.26 (0.19)
<i>O. virilis</i>	Exoskeletons	0.00 (0.10)	0.00 (0.10)	0.24 (0.13)	0.99 (0.10)	1.49 (0.08)	0.64 (0.24)	1.29 (0.21)	1.95 (0.09)	0.00 (0.10)	0.00 (0.12)	0.00 (0.08)
	Muscles	0.00 (0.10)	0.00 (0.10)	0.16 (0.10)	0.23 (0.12)	0.37 (0.08)	0.22 (0.24)	0.37 (0.21)	1.03 (0.09)	0.00 (0.13)	0.00 (0.10)	0.00 (0.08)
	Gills	0.00 (0.40)	0.71 (0.40)	1.95 (1.01)	2.93 (1.16)	8.83 (0.81)	2.50 (2.41)	7.91 (2.05)	22.00 (0.91)	0.00 (0.50)	0.00 (0.40)	0.00 (0.30)
	Hepatopancreas	0.84 (0.70)	1.40 (0.92)	1.58 (0.51)	12.05 (0.58)	19.15 (0.41)	9.51 (1.20)	9.77 (1.03)	16.56 (0.45)	0.76 (1.03)	0.56 (0.48)	1.11 (0.68)

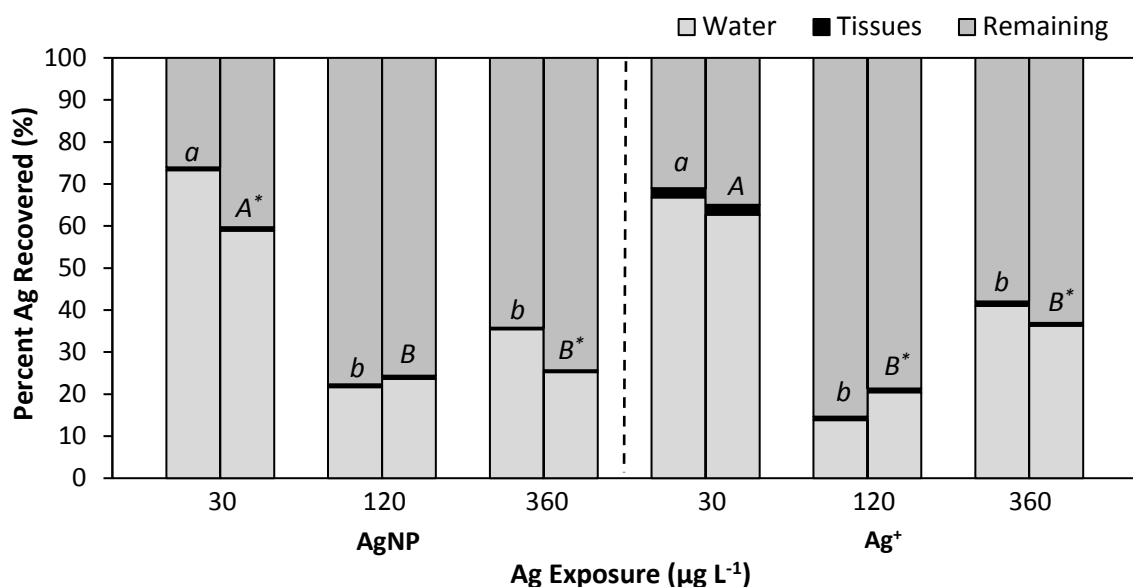


Figure 2.S12. Percent of Ag distribution. Total Ag accumulated within tissues ranged from 0.4-2.5% of the total amount available, while the Ag recovered from the tank water after exposure ranged from 20.4-73.3%. All other remaining Ag may have adsorbed onto the aquarium glass and/or the substrate. *P. clarkii* is represented on the left of each cluster; *O. virilis* is on the right. The same letters and case denote no statistical difference in remaining Ag at $\alpha = 0.05$ -level. *signifies a difference between species. The Ag species seemed to have no effect on total Ag present in water because similar Ag percentages were determined for both AgNPs- and Ag⁺-exposures in the tank water (66% vs. 64%, 22% vs. 17%, and 30% vs. 38% for the 30, 120, and 360 µg L⁻¹ of AgNP vs. Ag⁺ exposures, respectively).

DNA analysis:

Table 2.S3. Summary of all measured DNA comets for both species and amongst all treatments. Average number of comets examined per treatment was $N = \sim 40$. Standard error is provided parenthetically.

	Treatment	N	Average (μm)	
<i>P. clarkii</i>	Lab Control	78	7.85 (0.17)	
	30	56	18.60 (0.23)	
	AgNPs	80	19.51 (0.35)	
	360	78	22.96 (0.42)	
	Ag⁺ from	30	15	15.49 (1.79)
	80*	8	24.74 (0.58)	
	AgNO₃	360*	6	24.78 (0.84)
	20	80	9.66 (0.20)	
	NaBH₄	80	86	17.20 (0.41)
	240	83	19.51 (0.29)	
	<i>O. virilis</i>	Lab Control	25	8.17 (0.43)
		30	16	19.69 (1.43)
AgNP		80	17.81 (0.63)	
360		24	21.69 (0.90)	
Ag⁺ from		30	42	20.83 (0.96)
80*		10	24.38 (0.46)	
AgNO₃		360*	6	27.78 (0.60)
20		24	8.48 (0.33)	
NaBH₄		80	12	12.97 (1.66)
240		27	12.67 (2.96)	

* $N = < 10$ for Ag⁺ exposures due to immeasurable comet lengths attributed to DNA damage or specimen mortality.

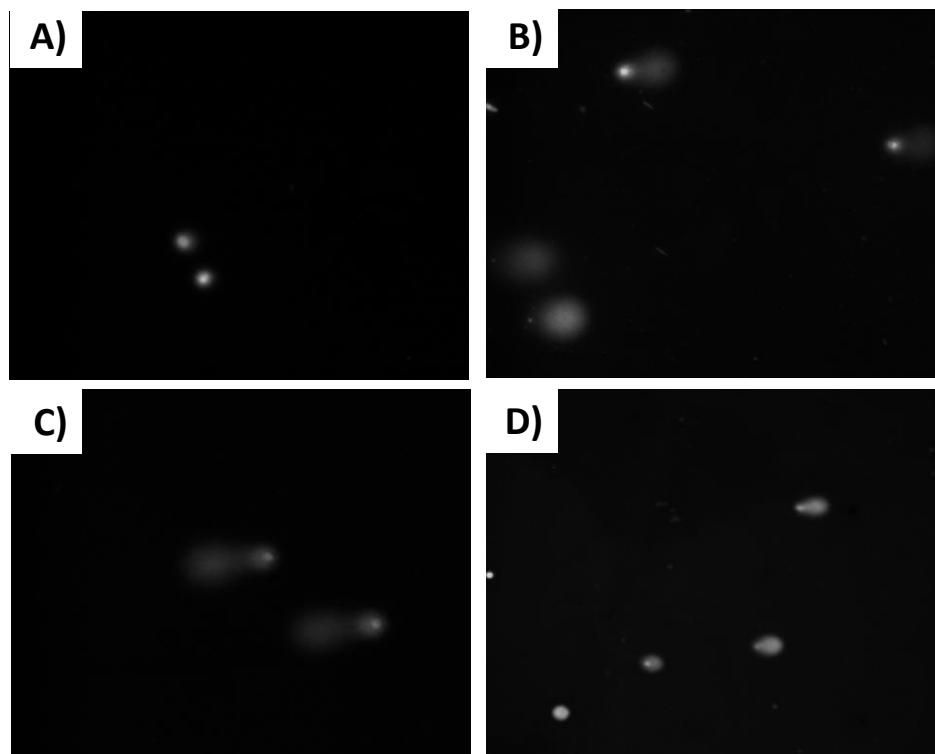


Figure 2.S13. Sample epifluorescent images from Single-Cell Gel Electrophoresis comet assays on neural complex tissue (encephalon and ganglion) from *P. clarkii*. A) River control exhibited no comets. The largest **B)** AgNP and **C)** Ag⁺ dose (360 µg L⁻¹) led to the longest comets, which is indicative of significant DNA damage. Comets were also observed in the **D)** NaBH₄ treatments, but of much shorter lengths. Image scale varies but comets seen are generally between 8 – 28 µm in length.

Histological analysis:

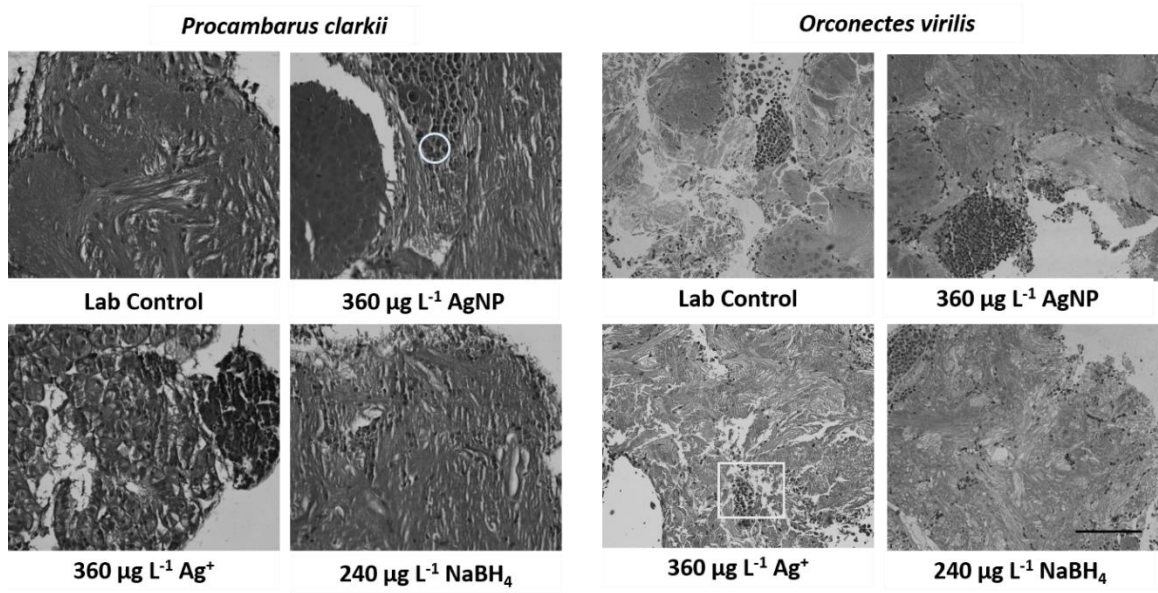


Figure 2.S14. Histological cross sections of the encephalon tissue stained with hematoxylin and eosin in both crayfish species. River control exhibited intact tissue with little fragmentation. The highest AgNP dose led to necrotic tissue (enclosed by a white circle). The corresponding Ag⁺ from AgNO₃ exposure also showed necrosis in addition to significant vacuolization and hypertrophy (enclosed by a white rectangle). No adverse effects were observed in any of the NaBH₄ treatments. Scale bar is 10 μm and applies to all images.

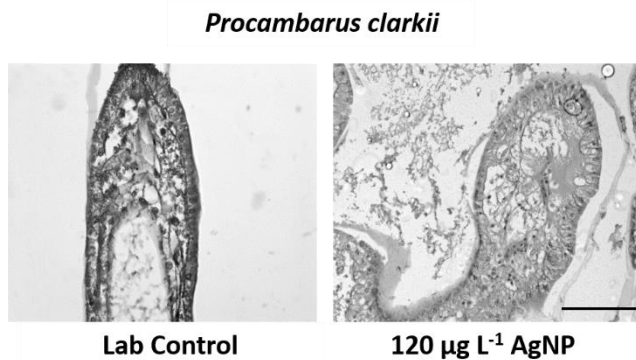


Figure 2.S15. Comparison of crayfish gill architecture in *P. clarkii*. Normal gill architecture was observed in the lab control. The gills of crayfish exposed to 80 $\mu\text{g L}^{-1}$ of AgNPs showed evidence of clubbing (swelling of second lamellae). Scale bar of 5 μm applies to both panels.

SUPPORTING INFORMATION REFERENCES

- 1) Bansal, R. C.; Goyal, M. Activated Carbon Adsorption. **2005**. CRC Press, Boca Raton, FL. USA.
- 2) Stankowich, T.; Blumstein, D. Fear in animals: a meta-analysis and review of risk assessment. *Proc. R. Soc. B.* **2005**, *272*, 2627–2634; DOI 10.1098/rspb.2005.3251.
- 3) Bergman, D. A.; Moore, P. A. Field Observations of Intraspecific Agonistic Behavior of Two Crayfish Species, *Orconectes rusticus* and *Orconectes virilis*, in Different Habitats. *Biol. Bull.* **2003**, *205*: 26–35.
- 4) Moore, P. A. Edited by Duffy, J. E.; Thiel, M. Agonistic Behavior in Freshwater Crayfish: The Influence of Intrinsic and Extrinsic Factors on Aggressive Encounters and Dominance. Oxford University Press, Inc., NY, NY. **2007**, pp. 93; DOI 10.1093/acprof:oso/9780195179927.001.0001.
- 5) Wren, M.; Gagnon, Z. E. A histopathological study of Hudson River crayfish, *Orconectes virilis*, exposed to platinum group metals. *J. Environ. Sci. Health: A.* **2014**, *49* (2), 135-145; DOI 10.1080/10934529.2013.838836.
- 6) Holdrich, D. M.; Lowery, R. S. *Freshwater Crayfish*. Timber Press: Portland, Oregon. **1988**, pp.12, 83-91,155-160.
- 7) Huxley, T.H. *The Crayfish: An Introduction to the Study of Zoology*. v. XXVIII of the Inter-national Scientific Series. D. Appleton, New York. 1879.
- 8) Horne, F.; Tarsitano, S.; Lavalli, K. Aspects of Mineralization of the Cuticle of the Crayfish *Procambarus clarkii* (Decapoda, Cambaridae). *Crustaceana.* **2009**, *82* (8), 1057-1065; DOI 0.1163/156854009X452740.

- 9) Lee, K. J.; Browning, L. B.; Nallanthamby, P. D.; Desai, T.; Cherukuri, P. K.; Xu, X. N. *In Vivo* Quantitative Study of Sized-Dependent Transport and Toxicity of Single AgNPs Using Zebrafish Embryos. *Chem. Res. Toxicol.* **2012**, *25*, 1029–1046.
- 10) Lee, K. J.; Browning, L. B.; Nallanthamby, P. D.; X. N. Study of Charge-Dependent Transport and Toxicity of Peptide-Functionalized Silver Nanoparticles Using Zebrafish Embryos and Single Nanoparticle Plasmonic Spectroscopy. *Chem. Res. Toxicol.* **2013**, *26*, 904-917; DOI dx.doi.org/10.1021/tx400087d.
- 11) Browning, L. M.; Kerry, J. L.; Nallanthamby, P. D.; Xu, X. N. Silver Nanoparticles Incite Size- and Dose-Dependent Developmental Phenotypes and Nanotoxicity in Zebrafish Embryos. *Chem. Res. Toxicol.* **2013**, *26*, 1503–1513, DOI dx.doi.org/10.1021/tx400228p.
- 12) Asharami, P. V.; Wu, Y. L.; Gong, Z.; Valiyaveetil, S. Toxicity of silver nanoparticles in zebrafish models. *Nanotechnology.* **2008**, *19*, 255102 (8pp); DOI 10.1088/0957-4484/19/25/255102.
- 13) Blinova, I.; Niskanen, J.; Kajankari, P.; Kanarbik, L.; Käländnen, A.; Tenhu, H.; Penttinen, O.; Kahru, A. Toxicity of two types of AgNPs to aquatic crustaceans *Daphnia magna* and *Thamnocephalus platyurus*. *Environ. Sci. Pollut. Res.* **2013**, *20*, 3456–3463; DOI 10.1007/s11356-012-1290-5.
- 14) Ponyton, H. C.; Lazorchak, J. M.; Impellitteri, C. A.; Blalock, B. J.; Rogers, K.; Allen, H. J.; Loguinov, A.; Heckman, J. L.; Govindasmawly, S. Toxicogenomic Responses of Nanotoxicity in *Daphnia magna* Exposed to Silver Nitrate and Coated Silver Nanoparticles. *Environ. Sci. Technol.* **2012**, *46*, 6288–6296 ; DOI dx.doi.org/10.1021/es3001618.

- 15) Choi, J. E.; Kim, S.; Ahn, J. H.; Youn, P.; Kang, J. S.; Park, K.; Yi, J.; Ryu, D. Induction of oxidative stress and apoptosis by silver nanoparticles in the liver of adult zebrafish. *Aquatic Toxicology*. **2010**, *100* 151–159; DOI 10.1016/j.aquatox.2009.12.012.
- 16) Stevenson, L. M.; Dickson, H.; Klanjscek, T.; Keller, A. A.; McCauley, E.; Nisber, R. M. Environmental Feedbacks and Engineered Nanoparticles: Mitigation of Silver Nanoparticle Toxicity to *Chlamydomonas reinhardtii* by Algal-Produced Organic Compounds. *PLOS One*. **2013**, *8* (9); DOI 10.1371/journal.pone.0074456.
- 17) Wu, Y.; Zhou, Q.; Li, H.; Liu, W.; Wang, T.; Jian, G. Effects of silver nanoparticles on the development and histopathology biomarkers of Japanese medaka (*Oryzias latipes*) using the partial-life test. *Aquat. Toxicol.* **2010**, *100*, 160-167, DOI 10.1016/j.aquatox.2009.11.014.
- 18) Farkas, J.; Christian, P.; Urrea, J. A. G.; Roos, N.; Hassellöv, M.; Tollefsen, K. E.; Thomas, K. V. Effects of silver and gold nanoparticles on rainbow trout (*Oncorhynchus mykiss*) hepatocytes. *Aquat. Toxicol.* **2010**, *96*, 44–52; DOI 10.1016/j.aquatox.2009.09.016.
- 19) Davies, P. H.; Goetti, J. P.; Sinley, J. R. Toxicity of Rainbow Trout. *Water Res.* **1978**, *12*, 113-117.
- 20) Grosell, M.; Brauner, C. J.; Kelly, S. P.; McGeer, J. C.; Bianchini, A.; Woods, C. M. Physiological Responses to Acute Silver Exposure in the Freshwater Crayfish (*Cambarus Diogenes Diogenes*)-A Model Invertebrate. *Environ. Toxicol. Chem.* **2002**, *21* (2), 369-374.

- 21) Mann, Reinier M.; Grosell, M.; Bianchini, A.; Wood, C. M. Biologically Incorporated Dietary Silver has no Ionoregulatory Effects in American Crayfish (*Procambarus Clarkii*). *Environ. Toxicol. Chem.* **2004**, *213* (2), 388-395.
- 22) Agency for Toxic Substances and Disease Registry (ASTDR). Silver. **1999**;
<http://www.atsdr.cdc.gov/toxfaqs/tfacts146.pdf>.
- 23) Secondary Drinking Water Regulations: Guidance for Nuisance Chemicals. *US EPA*; <http://www.epa.gov/dwstandardsregulations/secondary-drinking-water-regulations-guidance-nuisance-chemicals>.
- 24) US FDA. Q3D Elemental Impurities. U. S. Department of Health and Human Services. **2015**;
<http://www.fda.gov/downloads/drugs/guidancecomplianceregulatoryinformation/guidances/ucm371025.pdf>
- 25) World Health Organization (WHO). Silver in Drinking Water. **2014**, originally published in Guidelines for drinking-water quality, 2nd ed. Vol. 2. Health criteria and other supporting information. World Health Organization, Geneva, 1996.
- 26) U.S. Environmental Protection Agency. Methods for the Determination of Metals in Environmental Samples. *U.S. EPA*: Washington, DC, 1991;
www.epa.gov/method200.1.
- 27) "The Measure of Confidence" Agilent Technologies. 2010;
<https://www.chem.agilent.com/Library/brochures/5990-6496EN.pdf>.
- 28) EPA 40 CFR Part 136, APPENDEX B Revision 1.11;
http://www.epa.gov/region9/qa/pdfs/40cfr136_03.pdf.

CHAPTER 3

A RAMAN-BASED MOLECULAR IMAGING METHODOLOGY FOR CHARACTERIZING THE ADSORPTION BEHAVIOR AND DISTRIBUTION OF SILVER NANOPARTICLES TO HYDRATED MINERAL SURFACES

*Seth W. Brittle, Kevin A. O'Neil, Daniel P. Foose, Janice M. Sikon,
Kelsey L. Hood, Jasmine K. Johnson, Adam C. Stahler,
Steven R. Higgins, and Ioana E. Sizemore**

Department of Chemistry, Wright State University,
3640 Colonel Glenn Hwy., Dayton, OH, 45435

COPYRIGHT PERMISSION

The following chapter is reproduced from a drafted manuscript in preparation for submission to the journal of *Environmental Science and Technology* authored by Seth W. Brittle. Therefore, the article, “*A Raman-Based Molecular Imaging Methodology for Characterizing the Adsorption Behavior and Distribution of Silver Nanoparticles to Hydrated Mineral Surfaces*”, does not yet require copyright permission for reproduction in this dissertation.

SUMMARY OF INVOLVEMENT

Seth Brittle’s primary involvement was experimental contributions to each of the experiments and drafting the manuscript. He and the second co-author, Kevin O’Neil, worked closely on planning, developing, and implementing the experiment involving the micro-sized corundum samples and analyzing them with both with ICP-OES and Raman. He then expanded his involvement to include the larger single-crystal corundum samples and acquiring AFM and Raman images for comparative purposes. Furthermore, he helped with the sample preparations involving the muscovite samples. For all experiments, he also synthesized and characterized the colloidal AgNPs. Images constructed from AgNP exposed corundum and muscovite were constructed by Seth using the open source software, Vespucci, created by Daniel Foose, and the MATLAB code created by Adam Stahler, respectively.

ABSTRACT

The increased use of silver nanoparticles (AgNPs) in consumer products has created a growing need to monitor their release into the environment. Although minerals are known to affect the mobility and transformation of heavy metals within geochemical and aquatic systems, little is known about the interaction between AgNPs and minerals. Both label-free and label-enhanced Raman-based methods were constructed to characterize the adsorption behavior and distribution of Creighton AgNPs ($\sim 1 \mu\text{g mL}^{-1}$, $\sim 10 \text{ nm}$ in average diameter), on the surface of two minerals: 1) corundum ($\alpha\text{-Al}_2\text{O}_3$), both as large, single-crystal flat samples (*i.e.*, sapphire windows) and as fused micro-sized particles, and 2) freshly cleaved sheets of muscovite ($\text{KA}_2(\text{AlSi}_3\text{O}_{10})(\text{OH})_2$), all in the presence of an ionic strength adjuster (0.005 M of NaNO_3). Raman data was then analyzed using either Vespucci (a free open-source software) or a home-built MATLAB code. Label-free Raman revealed Ag adsorption to corundum occurred through silver oxidation (AgO), indicated by the appearance of an Ag-O stretching mode at $225\text{-}255 \text{ cm}^{-1}$. In addition, the adsorption process of AgNPs to corundum was supported with inductively coupled plasma optical emission spectroscopy (ICP-OES) and atomic force microscopy (AFM). ICP-OES indicated Ag did adsorb to $\alpha\text{-Al}_2\text{O}_3$ micro-particles, while AFM indicated increased presence of nano-sized features on topographic maps collected from the single crystal $\alpha\text{-Al}_2\text{O}_3$ samples. Labeled-enhanced Raman results suggest that AgNPs directly adsorb to the muscovite surface as intact AgNPs as revealed through surface enhanced Raman spectra of rhodamine 6G (a Raman label) tagged to adsorbed AgNPs. Overall, the results of this study demonstrate that physisorption and chemisorption mechanisms both play a role in the significant adsorption of Creighton AgNPs to corundum and muscovite and, thus reducing AgNP mobility in some soil environments.

Keywords

Raman spectroscopy, silver nanoparticles (AgNPs), hydrated minerals, corundum, muscovite, atomic force microscopy, adsorption.

INTRODUCTION

The remarkable expansion of nano-based technologies and products in the past few decades have raised considerable concern about their potential impact on human and environmental health. Special emphasis was placed on silver nanoparticles (AgNPs), the most commonly utilized nanomaterial in consumer products (*i.e.*, 54% of the total products)^{1,2} due to their unique antimicrobial³, optical⁴, and electrochemical properties⁵. About 1,230 tons of the total silver produced worldwide is allocated to the fabrication of AgNPs⁶. A major implication of the increased use of AgNPs stems from the high Ag content of the biosolids produced by wastewater treatment facilities. For example, a 2010 study reported that the release of silver nanoparticles (AgNPs) from washing of AgNP-containing athletic socks was significant², but the models of wastewater treatment facilities predicted the plants had more than adequate capacities to remove AgNPs from the waste stream. The resulting biosolids may then be sold as fertilizer, thus providing a pathway for these engineered nanomaterials to be introduced into soils through irrigation and rainfall. Numerous studies and reviews have already examined the health effects of AgNPs on both aquatic and terrestrial organisms including humans, and primarily attributed their toxicity responses to the release of Ag⁺ ions under favorable redox conditions^{3,7}. However, the impact AgNPs have on environmental health remains under investigation⁷⁻⁹ in view of their possible transformations⁹⁻¹⁴, the complex nature of their interaction with diverse soil components¹³⁻¹⁶, and the lack of rapid, cost and time efficient methodologies for studying these aspects^{8,15}.

Current research suggests that released AgNPs are most likely to be immobilized in soils due to the adsorption to natural organic matter (NOM) and minerals, respectively^{15,17-19}. Most of these studies focus on AgNPs adsorption to NOM because of the high affinity of AgNPs to sulfhydryl-rich functional groups, which are commonly present in NOM^{15,16,19}. However, NOM only makes up ~ 5 % of soil on average²⁰; therefore it is also important to examine the interaction of AgNPs with the main component of soils: minerals. Minerals make up ~ 45 % of most soils, while water and air account for the rest²⁰. Although there is extensive research available on the interactions between metal ions and soil minerals, only a few studies were reported on nanometals.²¹⁻²³ The research that does exist on AgNPs is generally focused on speculative modeling²⁴⁻²⁶ and ideal scenarios and/or utilizes advanced instrumentation techniques and methods (*i.e.*, X-ray absorbance spectroscopy (XAS), electron microscopy, atomic force microscopy) that usually require extensive sample preparation and expensive resources^{3,15,27}. Proposed here is a combination of previously used Raman-based mapping and chemometric methods²⁸⁻³⁰ (called Raman-based imaging methodology) for the simple and cost effective imaging of the distribution of AgNPs to various mineral surfaces and their molecular interaction mechanisms using two different types of software.

It was suggested that AgNPs released into the environment through wastewater, fertilizers or landfill runoff might exist in multiple forms¹⁵. Namely, AgNPs may persist in their nanoform, oxidize into Ag⁺ ions, aggregate into larger particles, or even form silver sulfide (Ag₂S), silver chloride (AgCl), silver sulfate (Ag₂SO₄), silver hydroxide (AgOH), silver carbonate (Ag₂CO₃), or silver oxide (Ag₂O)^{3,31}. Thus, any methodology capable of observing the molecular interaction mechanisms between AgNPs and minerals is essential

to the determination of AgNPs fate and transport. Raman spectroscopy offers a unique angle because it has molecular fingerprinting and multiplex detection capabilities, is non-destructive and aqueous compatible, and requires little to no sample preparation. Moreover, a Raman system equipped with a motorized stage can collect multiple point spectra in a raster x,y pattern (*i.e.*, Raman maps) to effectively investigate and map molecular interactions across large surfaces at both micro and nanoscale. Furthermore, the proposed molecular imaging approach is novel in that it offers the possibility of performing either label-free or label-enhanced SERS measurements. While others have already reported studying the molecular interactions between environmental minerals (*e.g.*, quartz, calcite, corundum) and AgNPs³²⁻³⁵ through the acquisition of label-free point Raman spectra, and SERS spectra, no approaches were yet proposed for the rigorous mapping of the adsorption and distribution behavior of AgNPs onto mineral surfaces. Herein, it is demonstrated the proposed Raman-based imaging methodology can achieve these goals for different types of minerals. However, if no direct molecular interaction occurs between minerals and AgNPs, a Raman active label of large scattering cross-section (*e.g.*, rhodamine 6G (R6G) dye) and high affinity toward AgNPs may be utilized to make the AgNPs “Raman-visible” and to indirectly image their distribution on mineral surfaces with increased sensitivity. Our group has already reported single-molecule SERS detection events of R6G (10^{-15} M) adsorbed onto Creighton AgNPs³⁶. When a target species is located in the immediate vicinity of a single AgNP or at the nano-sized interstitial site of aggregated AgNPs, the so-called surface enhanced Raman spectroscopy (SERS) effect occurs and further boosts the sensitivity of the Raman-based detection method down to the single-molecule level³⁷⁻⁴⁰. The SERS enhancement is largely due to the increase in the magnitude of both the incident

and the scattered electromagnetic fields resulting from the excitation of localized surface plasmon resonances (LSPR) present in AgNPs.^{39,41-43} Thus, the Raman-mapping of mineral surfaces exposed to AgNPs results in the collection of a large number of SERS spectra characteristic to the interaction of the two systems. An additional element of novelty is the coupling of SERS measurements with chemometric methods employed using two types of software: 1) Vespucci, a free, open-source, and stand-alone hyperspectral analysis software written in C++ API, and 2) a home-built MATLAB code.

The characterization potential of the proposed Raman-based imaging methodology was demonstrated on two representative minerals in bulk form: corundum ($\alpha\text{-Al}_2\text{O}_3$) and muscovite ($\text{KA}_2(\text{AlSi}_3\text{O}_{10})(\text{OH})_2$). Most current research that does exist on AgNPs is generally focused on the interactions with silicate minerals^{9,31}. Thus, both a silicate and a non-silicate mineral were selected as mineral models. Furthermore, both minerals contain aluminum, which is the third most abundant element in the earth's crust, after oxygen and silicon.⁴⁴ corundum is a rock-forming mineral encountered in streams and beach sands, while muscovite is the most common mica-group mineral⁴⁵.

The Creighton synthesis is one of the most widely-used bottom-up fabrication approaches of colloidal AgNPs due to its simplicity, time and cost efficiency⁴⁶. A concentration of 1 mg L^{-1} was used in order to ensure sub-monolayer coverage at the mineral surface and to surpass the maximum contaminant level (MCL) set by the U.S. Environmental Agency (EPA) for Ag^+ in drinking water caused by both natural and anthropogenic sources (0.1 mg L^{-1}).⁴⁷ Because both minerals have a pH pristine point of zero charge (pH_{ppzc} of 7.5 for muscovite^{48,49} and 9.1 for corundum⁴⁹) close to the pH (= 8.2) of as-prepared Creighton AgNPs solutions (Zeta potential of -44.7 mV^{27}), a strong

interaction between the two is expected at typical pH values of soils (3.5-9)⁵⁰. For illustrative purposes, the interaction mechanism between micro-sized, spherical corundum particles (average diameter of 1 μm) and AgNPs was also interrogated by the proposed Raman-based imaging methodology in the pH range from 6 to 11. Aggregation of Creighton AgNPs in the corundum mixtures were noticed at smaller (< 6) or larger pH values (> 11). In addition, two other widely-used analytical and microscopic techniques, namely inductively coupled plasma optical emission spectroscopy (ICP-OES) and atomic force microscopy (AFM), were employed to confirm the Raman imaging results and to compare the proposed method to popular alternatives that offer only information related to the interaction or distribution, but not both. Specifically, ICP-OES quantified the total amount of AgNPs adsorbed onto the mineral surface, *i.e.*, the total surface coverage. Atomic force microscopy (AFM) in intermittent contact mode mapped the AgNPs adsorption and physical distribution on single crystal corundum surfaces.

MATERIALS AND METHODS

Single-crystal corundum and muscovite samples were purchased from Marketech International. Fused corundum beads were purchased from Alfa Aesar. High-quality (HQ) water (18.2 $\text{M}\Omega\cdot\text{cm}$) was obtained from a LabConco system and utilized throughout the course of all experiments. All other materials were purchased from Fisher Scientific and used without further modification unless specified.

Synthesis and Characterization of AgNPs: A modified Creighton method²¹ was chosen to fabricate negatively charged, colloidal AgNPs in water. Specifically, a 2:1 molar ratio of sodium borohydride (NaBH_4) to silver nitrate (AgNO_3) solutions was used to minimize the amount of excess reagents and byproducts.^{37,51,52} Similar to chapter 2 Raman

spectroscopy, ICP-OES, and ultraviolet-visible (UV-Vis) absorption spectroscopy were employed to verify colloidal purity, quantify total Ag content, and confirm the formation of spherical AgNPs by the presence of a LSPR peak, respectively.³⁷

Sample Preparation: A summary of the controls and samples for each mineral and AgNPs interaction is presented in Table 3.S1 ('S' denotes tables/figures in Supporting Information). Two sets of mineral samples were prepared for the characterization of AgNPs adsorption to minerals: 1) corundum (α -Al₂O₃) and 2) muscovite (KAl₂(AlSi₃O₁₀)(OH)₂). For corundum, two different materials were used: 1) cylindrical single α -phase crystal samples measuring 25 mm in diameter and 5 mm thick (marketed as sapphire windows by Marketech International) used for their flat surface and single (11 $\bar{2}$ 0) crystal structure facilitating sample preparation in Raman and AFM analysis, and 2) fused micro-sized particles offering a large polydispersed surface area for interaction. Freshly cleaved muscovite samples were cut into 10×10 mm squares and used as is. *Flat mineral surfaces*—the corundum single-crystal samples were sequentially washed with acetone (HPLC grade), methanol (HPLC grade), and nitric acid (70% OPTIMA grade) in a sonic bath for 10 min each. Next, the samples were annealed at 1250°C for 12 h to provide a “clean” terraced surface. Ten muscovite sheets and one corundum sample (one crystal) were then submerged in colloidal AgNPs (10 mL of 1 mg mL⁻¹ of AgNPs) with 100 μ L of 5 M of sodium nitrate (used as an ionic strength adjuster (ISA) similarly to other environmental studies with AgNPs¹⁹). Additional preparation was performed on the muscovite samples by utilizing a fluorescent cationic dye, rhodamine 6G (*i.e.*, a SERS probe). Control groups included bare unreacted mineral surfaces with 1) no solution exposure, 2) exposure only to HQ water, 3) exposure only to AgNPs solution, and 4) exposure only to the R6G for the

muscovite (10^{-3} M). *Micro-sized spherical particles of mineral*—additional experiments were performed using corundum as a model. Corundum particles (99 % fused α -Al₂O₃, $\overline{SSA}=7 \mu\text{m}^2 \text{g}^{-1}$) were purchased from Alfa Aesar and ~1.2 g was used for each control or sample similarly to the bulk samples. This amount was determined to yield a submonolayer coverage, assuming 100% AgNP adsorption. Next the weighed amount was mixed with colloidal AgNPs (100 mL of 1 mg mL⁻¹ of AgNPs), sodium nitrate as an ionic strength adjuster (ISA) (100 μ L of 5 M of NaNO₃), and pH adjusters (5-100 μ L of 0.1 M of HNO₃ or 0.1 M of sodium hydroxide (NaOH)). A SevenGo Duo pro model pH meter was calibrated daily with four pH buffers (4.0, 7.0 10.0, and 12.0) and used to measure the pH. After stirring for 30 min, the liquid samples were centrifuged for 2 min at 5000 Gs in an AccuSpin Micro 17/17R model centrifuge. The centrifuge supernatants containing free, unbound AgNPs were saved for ICP-OES analysis, while the centrifuge pellets consisting of corundum particles with bound AgNPs (denoted AgNP-corundum) were collected for Raman imaging. Control groups included corundum particles alone, AgNPs alone, similar mixtures without AgNPs or without corundum particles at each pH.

Raman Spectroscopy Analysis: A LabRam HR800 Raman system was utilized to verify colloidal purity, to examine possible molecular interactions between AgNPs and the two minerals, and to image AgNP distribution on mineral surfaces. *Sample Measurements*—spectra were acquired either with a 532.134 nm Nd:YAG (corundum samples) or a 632.8 nm HeNe (muscovite samples) laser both set to an output of 17mW and backscattered photons were measured using a thermoelectrically cooled Andor CCD camera of 1024 \times 256 pixels. The following parameters were selected for the acquisition of the Raman data: confocal hole of 300 μ m, a holographic grating of 600 grooves mm⁻¹,

acquisition times ranging between 1-3 s, and averaged over 2-3 cycles. Under these conditions, the spectral resolution was $\sim 1.18 \text{ cm}^{-1}$. *Large flat mineral surfaces*—the flat corundum windows and muscovite sheets allowed for relatively easy optical focusing of the samples before and after experimental exposures. These samples were simply placed flat on a glass slide and then focused on with the aid of an optical camera coupled to the microscope. For each large corundum sample, 961 spectra were measured in a map size of $31 \times 31 \text{ }\mu\text{m}$ grid in $1 \text{ }\mu\text{m}$ increments. Acquisition time was one second averaged over two cycles and the spectral range measured was 100-1700 wavenumbers (cm^{-1}). For each muscovite control and sample, 900 spectra were measured in a $150 \times 150 \text{ }\mu\text{m}$ grid in $5 \text{ }\mu\text{m}$ increments. Larger increments were used here to avoid double detection of label-enhanced areas. Acquisition and cycle times were the same as the muscovite. *Micro-sized spherical particles of mineral*—aliquots of the resulting centrifuged pellets were smeared onto new glass microscope slides and $11 \times 11 \text{ }\mu\text{m}$ areas were mapped for each sample in order to obtain a representative molecular picture of the interaction between AgNPs and corundum particles. Since increased dispersity was anticipated with these non-flat samples, statistical confidence was strengthened by measuring three maps from three individually prepared samples, making nine maps in total for each pH (i.e., $n = 1089$ spectra for each pH). The Raman images were collected by scanning with a $1 \text{ }\mu\text{m}$ spatial resolution the surface of each sample in two dimensions with a motorized stage. *Data Analysis*—Raman point and averaged spectra were evaluated in Origin 8.5 software and a one-way ANOVA was performed followed by a Student-Newman-Keuls (SNK) multiple comparison tests independently on each pH $p > 0.950$ significance at the $\alpha=0.05$ probability level. While large Raman maps were processed either in Vespucci or a home-built MATLAB code, both

constructed independently by two of the co-authors for these exact types of analysis involving larger spectroscopic datasets. Essentially, the Vespucci code is aimed to be sourced freely to anyone without the need of additional costly software, such as MATLAB.⁵³ Muscovite samples were analyzed in MATLAB while all corundum samples were analyzed in Vespucci. Spectra from the micro-sized corundum particles were first median filtered (window size 7) and normalized to the 2-norm so that each spectrum vector had unit length. Peak centers and integrated areas were found for the Ag-O stretching mode (indicating AgNP oxidation) at 225-255 cm^{-1} using Vespucci^{40,54,55}. A linear baseline was drawn between the two abscissa values closest to the specified range. The area of the region was taken to be the trapezoidal numerical integral of the specified region. Peak centers were taken to be the abscissa value of the highest intensity point in the range after baseline subtraction. Maps from the bulk corundum were median filtered (window size 7), min-max normalized, and area integrated under the Ag-O stretch at 225-255 cm^{-1} also in Vespucci⁵⁴. Spectral data from the muscovite samples were first min-max normalized and derived with a second-degree polynomial. Next, a principle component analysis (PCA) was applied to the derived normalized data where each spectrum was correlated to one of two principally selected spectra. Briefly, a PCA isolates representative data patterns within the data matrix by generating new variables called principal components (PC) that are linear combinations of the original variables and act to explain as much variance in the data as possible.

ICP-OES Analysis: Quantitative characterization of the change in total Ag content reacted with the micro-sized corundum was measured with a Varian 710 ICP-OES system. Briefly, original colloids and supernatant samples containing free, unbound AgNPs were chemically digested and diluted in trace metal grade nitric acid (HNO_3) following the U.S.

EPA methods 200.11^{56,57} as described in chapter 2. An eleven-point external calibration curve (0, 5, 10, 15, 20, 25, 50, 75, 100, 125, and 150 $\mu\text{g L}^{-1}$) was then constructed, and the Ag concentrations of each sample were determined by interpolation from the calibration curve.

AFM analysis: An Agilent AFM operated in intermittent contact mode imaging (*i.e.*, AC Mode or Tapping Mode) was employed to examine the mineral surface features (*i.e.*, step edges) and the spatial distribution of AgNPs on the flat surfaces of the larger corundum. Cantilevers were obtained from Nanoworld (NCHR, Pointprobe, non-contact mode) and were fabricated from single-crystal Si and coated with Al, with nominal resonance frequency of 320 kHz and a nominal force constant of 42 N/m. Scanning speeds were typically set to 1-2 Hz and image sizes varied for each sample but at least one $2 \times 2 \mu\text{m}$ image with 256×256 pixels was recorded as this was deemed an appropriate size to detect and display features between 1-100 nm (*i.e.*, nanoparticles). AgNP adsorption was then interpreted by differentiating topographic profiles from the controls and the samples.

RESULTS AND DISCUSSION

Synthesis and Characterization of AgNPs: synthesized AgNPs were characterized in accordance with EPA's recommendations.^{58,59} ICP-OES revealed an average Ag concentration in the as-prepared colloidal suspension of $15.4 \pm 0.8 \text{ mg L}^{-1}$, and Raman spectroscopy confirmed the absence of organic impurities and silver oxide peaks. In previous TEM work, these AgNPs appeared spherical, had an average diameter of $14.1 \pm 13.4 \text{ nm}$ and a moderate size distribution in the 1-100 nm range.³⁶ The specific AgNP surface area was then estimated to be 20.9- 814.8 $\text{m}^2 \text{ g}^{-1}$ based on this size range (and assuming all nanoparticles are spherical).⁶⁰ Previous Zeta-potential measurements (see

chapter 2) demonstrated that these AgNPs are negatively charged and are stable at the experimental pH of this study (ζ -potential of -41.47 mV at pH = 8.2).^{60,61}

Label-Free Raman. *Large corundum*—The vibrational modes associated with corundum are identified and labeled in the supporting information (Table 3.S2⁶²⁻⁶⁵) As seen in Figure 3.1, the corundum window control appears only as corundum and matches literature assignments (Table 3.S2), while corundum exposed to AgNPs exhibit an additional peak. In fact, in all AgNP-treated corundum samples, additional molecular vibrations were observed in the range 225-255 cm^{-1} , which matches literature references for Ag-O stretches^{40,54,55} (Figure 3.1 and 3.2). Silver oxidation appears to be the driving mechanism of AgNPs adsorption to corundum. Therefore, Raman has potential to observe AgNPs interaction with corundum without labeling (no SERS probe). In Figure 3.1B the white and gray areas are attributable to a larger integrated area under 225-255 cm^{-1} where Ag-O is present. The spectrum with the most intense Ag-O peak seen (red line in Figure 3.1B) in 961 spectra is represented by the whitest pixel in the chemical image. Despite only a few Ag-O vibrations, a molecular interaction is still observed and is attributable to the oxidation of AgNPs. However, it should be noted this experiment was conducted only at pH = 9, but in natural aquatic systems, a wide range of pH values are possible, and since mineral surface charge and particle oxidation depend on pH, this helped justify the next phase of the experiment. Essentially, is AgNP adsorption to corundum pH dependent?

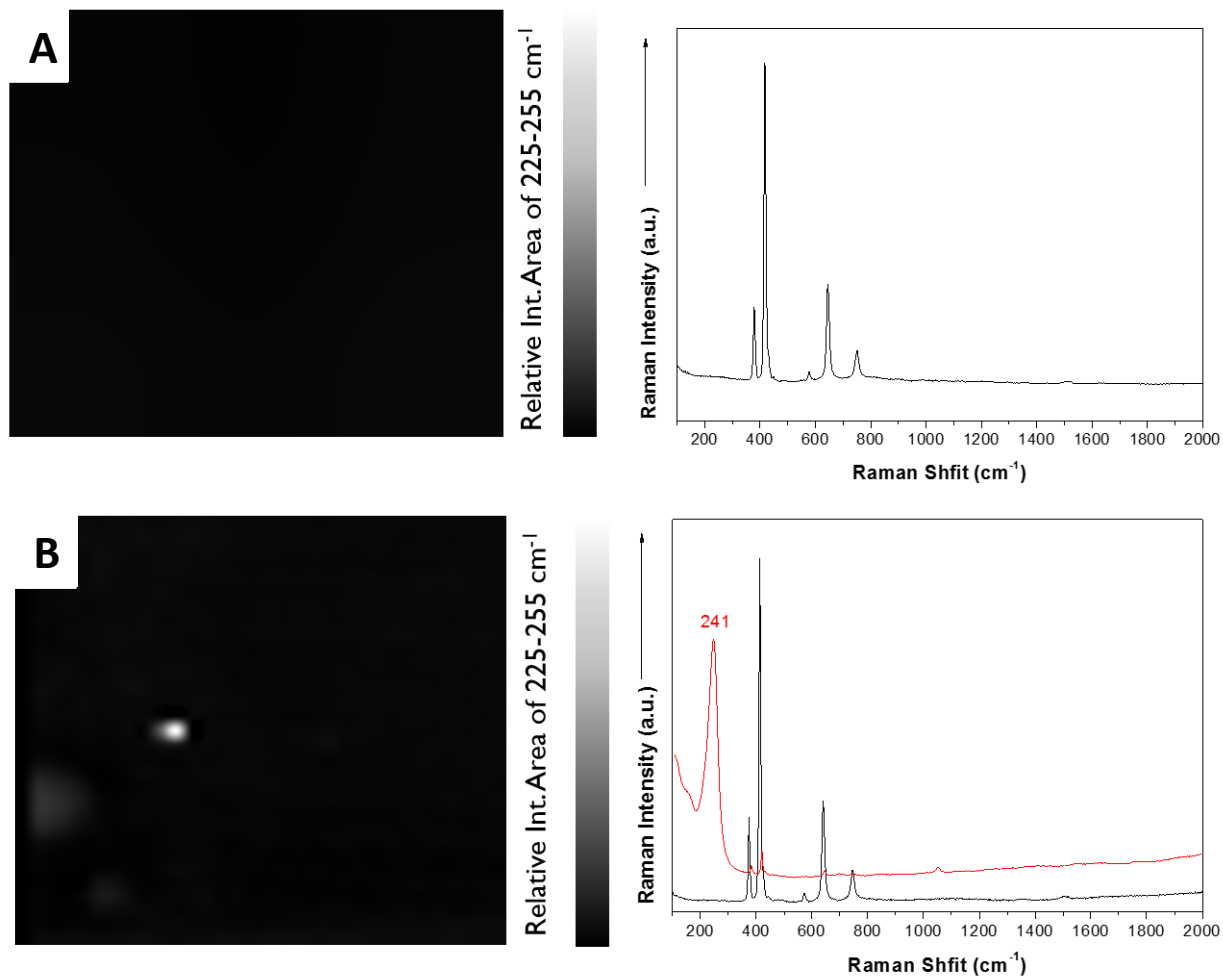


Figure 3.1. Chemical images of corundum windows before (A) and after (B) AgNP exposure (1 mg L⁻¹ for 30 min) and accompany average spectra. Spectra were first min-max normalized, then smoothed with a median filter with a window size of 7, and lastly, area was integrated under 225-255 cm⁻¹ (where the Ag-O stretch appears) and assigned a scalar color where Ag-O stretches are represented as white. Lack of visual variation confirms chemical surface uniformity in A, while white spot B suggests Ag-O is present in one pixel (1 μm²). Black spectra are averaged from the accompanying map on the left (both are 31x31 μm for a total number of spectra in each is 961). Red spectrum with stretch at 241 cm⁻¹ in B is from the white pixel and signifies the presence of Ag-O.

Micro-corundum particles—As expected, and seen in Figure 3.2, the control maps yielded no Ag-O peak, while at every experimental pH the Ag-O stretching mode at ~ 230 cm^{-1} was observed (Figure 3.2B). Overall, more Ag-O vibrations were recorded here than with the single crystal samples, possibly an artifact of random crystal structures versus an ordered lattice in the a -plane ($11\bar{2}0$)⁶⁶, thereby altering electronic densities on the surface. To analyze this further, the total number of Raman spectra exhibiting Ag-O stretching modes at each pH value was plotted as a function of pH (Figure 3.2C). With this analysis, AgNPs were found to exhibit more interactions with α - Al_2O_3 at $\text{pH} \geq 9$ ($n = 901$ - 1015 spectra) in comparison with all other examined pH values ($n = 796$ - 814) indicating a possible change in the interaction. However, the difference is not statistically significant ($p > 0.05$), so the adsorption process is pH independent. As another approach the integrated area under each Ag-O peak was measured since the intensity of the peak depends on the concentration of AgO which offers a semi-quantitative measurement of AgO and not just whether a peak is present or not (Figure 3.2D). Again, the differences amongst all pH values were not statistically significant ($p > 0.05$), despite pH 9 yielding the largest average area.

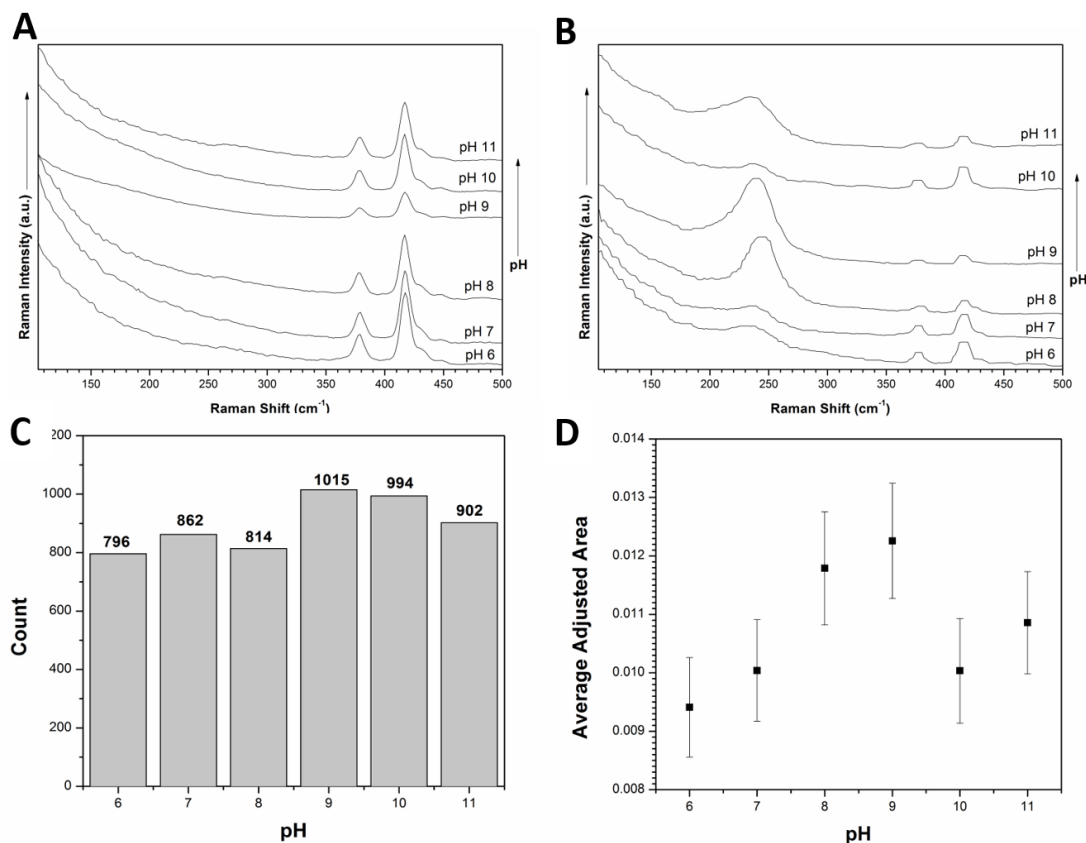


Figure 3.2 Raman spectra and statistical analysis of micro-sized corundum at all experimental pH values (6 – 11). **A)** Average spectra of corundum controls at each pH. **B)** Average spectra of corundum exposed to 1 mg L⁻¹ for 30 min at each pH. **C)** The total number of Raman spectra exhibiting Ag-O stretching modes at each pH value. **D)** Mean of the integrated area of the Ag-O stretching mode at each examined pH value with 95% confidence intervals. The values obtained at each pH represent an average of 1089 spectra from 3 separate trials.

Since both single crystal and micro-sized corundum experiments revealed the Ag-O stretches, indicated by the appearance the peak at 225-255 cm⁻¹, this helps confirm surface complexation of AgNPs to the terminus oxygen atoms (Ag-O-Al-). Again, the highest chemisorption levels were reported at pH ~ 9, when α -Al₂O₃ has zero net surface charge and is more readily available for direct molecular interactions with AgNPs. To help explain these mechanisms, Figure 3.3 was created to offer a visual complexation

scheme. At pH ~ 9, more mechanisms are occurring due to the lack of net surface charge as well as the presence of both positive and negative moieties (Figure 3.3B). Previously cited literature has shown the hydration of α -Al₂O₃ yields OH groups at the Al₂O₃ surface. The interaction between AgNPs and α -Al₂O₃ is expected to involve hydroxyl groups.⁶⁷ Due to the variety of surface sites that may exist on the corundum surface, multiple hydroxyl terminations may exist. Some hydroxyl groups will undergo deprotonation above the pH_{pzc} (pH = 9.1) of α -Al₂O₃ to create an overall negative charge above the pH_{pzc}. Less overall AgNP adsorption is expected at pH values > 9.1 than at all other investigated pH values. As seen in Figure 3.3, AgNPs can still bind to surface moieties that are not negatively charged due to the other possible mechanisms (e.g., surface complexation or hydrogen bonding⁶⁸ interactions).

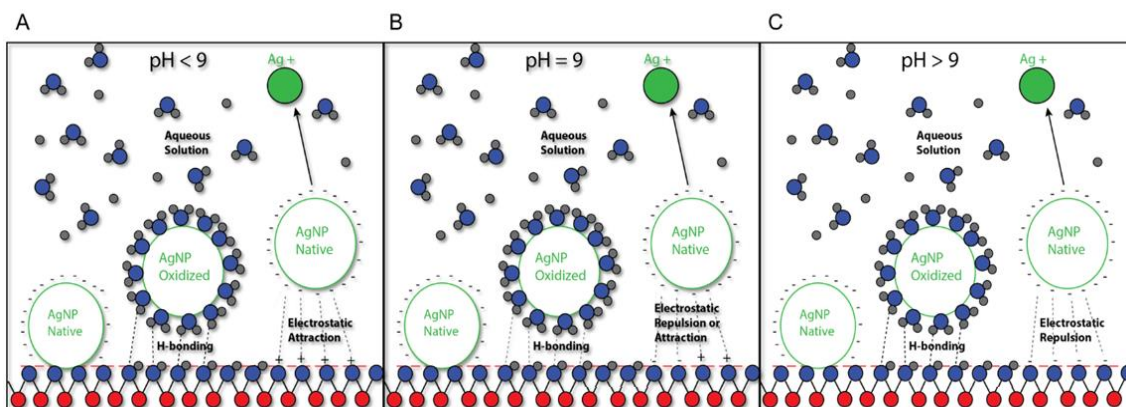


Figure 3.3. Complexation scheme at pH values below A), at B), and above C) the isoelectric point of α -Al₂O₃ (pH 9). Red atoms = Al, blue = O, gray = H, green = Ag, and yellow = Na. *Note: nanoparticles are not to scale.*

ICP-OES: to support the Raman analysis the difference in total silver measured before and after interaction with the suspended micro-sized corundum was interpreted as an average percent adsorbed. In other words, the silver that had adsorbed could not be

directly measured by ICP-OES and, therefore, was inferred from what silver was lost in a reacted colloid. *Analysis*—quantitative measurements of the total amount of silver was made at each pH for each control and samples. As seen in Figure 3.4, no apparent adsorption dependency on pH was observed. This is likely attributable to multiple mechanisms occurring simultaneously or independently at each experimental pH (Figure 3.3).

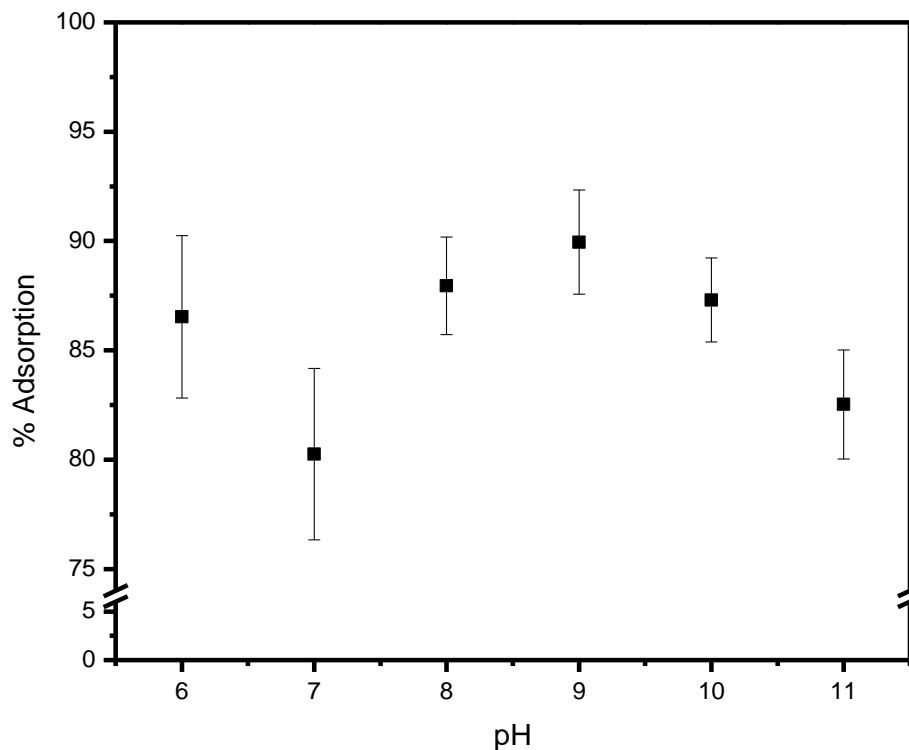


Figure 3.4. Average percent adsorption of AgNPs to α -Al₂O₃ as a function of pH as determined by ICP-OES. Error bars represent the standard deviation of nine independently prepared samples. The initial concentration of AgNPs was 1 mg L⁻¹. For each pH 1.22 g of the micro-sized corundum with a SSA of 7 um g⁻¹ was used.

AFM: Topographic profiles of corundum windows revealed a step and terrace structure on the *a*-plane surface. The surfaces originally appeared void of any nano-sized particles, although some protrusions and holes were present but without any indication of

homogeneity. A distilled water control added no additional features on the surface (Figure 3.5A), while a NaNO_3 control seemed to deposit some nanoparticles despite the absence of AgNPs (Figure 3.5B). Likewise, this result was unexpected but was attributed to the precipitation of electrolyte from a thin water film on the surface that was not completely removed with the stream of nitrogen gas. The windows were then submerged in a 1 mg L^{-1} AgNP colloid for 30 minutes (with 0.005 M NaNO_3 at pH 8) before being dried with nitrogen. The resultant AFM images of the treated windows yielded additional nanoparticles on the surface without any real indication of preferences to the step edges (Figure 3.5C). In future studies, particle counting algorithms may have to be employed to statistically conclude if more particles appear after the AgNP submersion than the NaNO_3 . Furthermore, since AFM is not a chemical technique, no identity about the particles is revealed, thus a molecular imaging technique, like Raman, would be beneficial to accompany AFM.

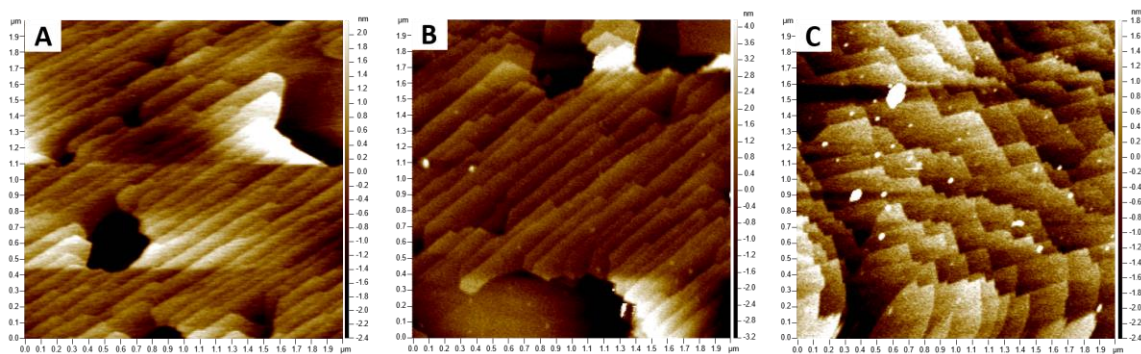


Figure 3.5. $2 \times 2 \mu\text{m}$ AFM images of macro-sized corundum window. A) Washed and annealed window imaged before any treatment was administered displays step-and-terrace structure with minimal nano-sized features. B) The Same window submerged in 0.05 M NaNO_3 for half hour yields some nano-sized precipices on the surface. C) The Same window submerged in 1 mg L^{-1} AgNPs and 0.05 M NaNO_3 yields more and larger nano-sized particles.

Label-Enhanced Raman. Muscovite—The vibrational modes associated with muscovite are identified and labeled in the supporting information (Table 3.S3⁶⁹⁻⁷³). Using MATLAB the principle component scores were displayed as a pixel color, either red or blue, creating an image that portrays the most highly correlated principle component (PC) for that spectrum collected in that location. The similarities between both principle components (PCs) in the control map are almost identical, consequently, blending both pixel colors on the map and creating an almost purple image suggesting an even distribution of both throughout the map (Figure 3.S1). Both PCs correlate directly to literature reported spectra.⁷⁰ Table 3.S3 assigns the observed experimental peaks to vibrational modes reported in McKeoen *et al.* where Raman spectra of muscovite were calculated as well as measured about two axial orientations.⁷⁰ With the addition of AgNPs, no significant differences were observed, as seen by the similarities in the PCs and the evenly colored image (Figure 3.S2). Rhodamine 6G (R6G) by itself did not display any indicative signs of its identity on its map; however, more fluorescence was observed which could be credited to its presence. The more fluorescent areas within the R6G control map (Figure 3.6 A-D) are related to PC 2, where more of a “hump” can be observed in these spectra. The map for both R6G and colloid illustrated the most noticeable differences. Specifically, two distinct PCs were computed and red areas are seen on the map (Figures 3.6 E-H) exhibit spectra more closely correlated to R6G (PC2). Thus the areas pixelated more with PC2 (red) are interpreted as R6G bound to AgNPs, while PC1 represents muscovite (blue). The SERS spectrum of R6G was assigned according to our previous studies^{37,74}. The interaction between AgNPs and muscovite is likely electrostatic, since no additional peaks were detected, suggesting no covalent bonds were formed.

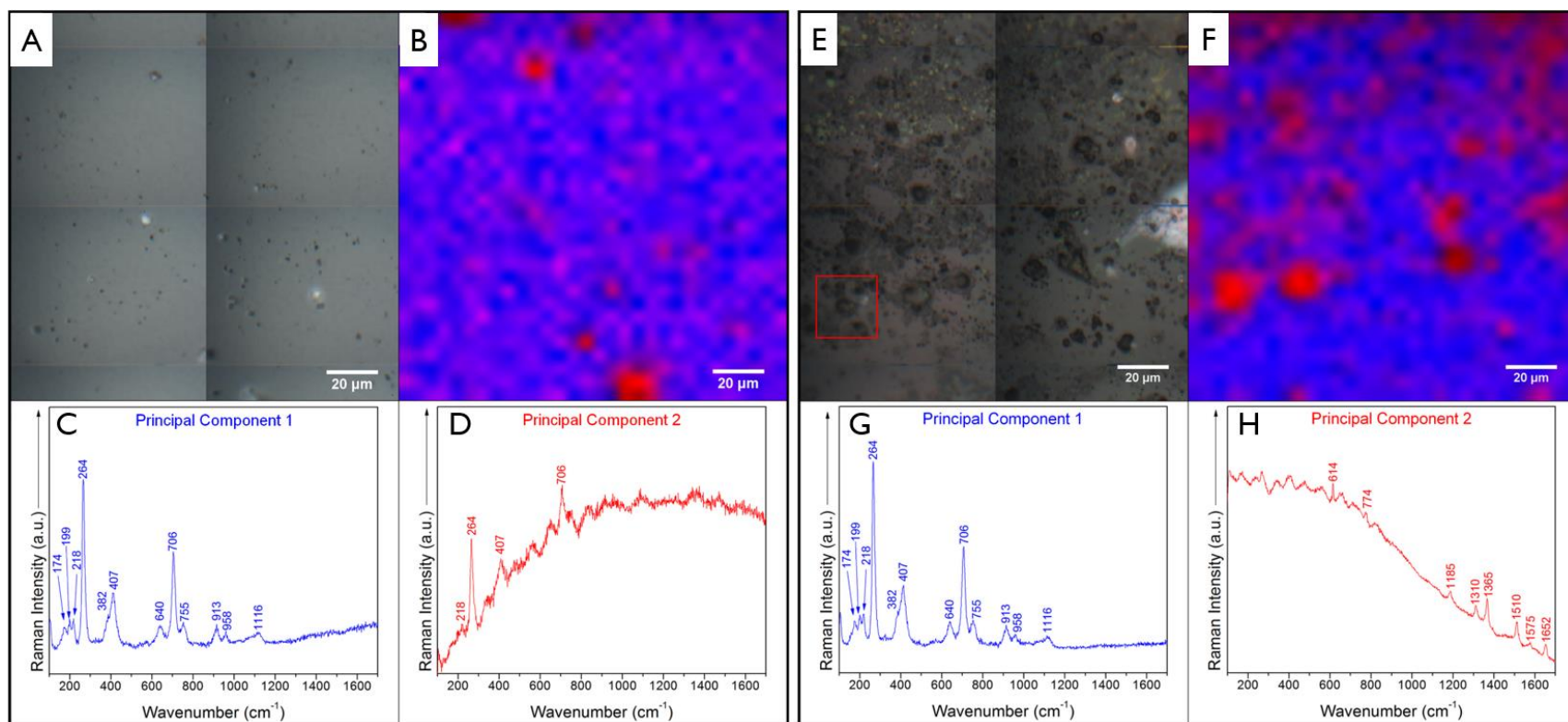


Figure 3.6. $10\ \mu\text{M}\ 10^{-3}\ \text{M}$ R6G dried on freshly cleaved muscovite (A-D) and both AgNPs and $10\ \mu\text{M}\ 10^{-4}\ \text{M}$ R6G dried on freshly cleaved muscovite (E-H). A,E) Optical image of mapped areas. B,F) Chemical images of same areas from optical image constructed from PC 1(blue) and PC 2 (red) C,G) Principle component one correlates to muscovite in both (same vibrational modes are labeled) D,H) Principle component two, with no AgNPs PC2 correlates to fluorescent R6G background, however, when AgNPs are added adsorption is revealed with more red (PC2) which correlates to R6G enhancement spectra. Note R6G marker bands labeled in H but absent in D.

CONCLUSION

Overall, the results of this study demonstrate that Raman is suitable in identifying both physisorption and chemisorption mechanisms involved in AgNP interaction with minerals, namely muscovite and corundum. However, AgNPs behave differently in the presence of different minerals, and Raman analysis may demand a SERS probe to help “visualize” AgNP adsorption. In contrast, the oxidized form of AgNPs is already Raman active and can be directly “seen”. In addition, Raman molecular imaging offers a distinct advantage over traditional point spectra by increasing confidence in identifying adsorption mechanisms as well as offering information into their distribution. These sorts of attractions can be revealed and analyzed with a variety of software and hyperspectral analysis. Lastly, although ICP-OES and AFM are suitable for supporting adsorption experiments additional verification is required for increased chemical information. In conclusion, future fate and transport studies involving silver nanoparticles may find prudent to use label-free and label-enhanced Raman imaging to characterize AgNPs adsorption behavior on hydrated mineral surfaces.

ACKNOWLEDGEMENTS

Garrett VanNess and Joseph Solch are thanked for their assistance in the maintenance and operation of the ICP-OES system at WSU.

REFERENCES

- (1) Nanotechnology - Project on Emerging Nanotechnologies
<http://www.nanotechproject.org/>.
- (2) Benn, T.; Cavanagh, B.; Hristovski, K.; Posner, J. D.; Westerhoff, P. J. *Environ. Qual.* **2010**, *39* (6), 1875–1882.
- (3) Luoma, S. N. **2008**, No. September. PEN15-Silver Nanotechnologies and the Environment: Old Problems of New Challenges? Woodrow Wilson International Center for Scholars. 2008; http://www.nanotechproject.org/process/assets/files/7036/nano_pen_15_final.pdf.
- (4) Evanoff, D. D.; Chumanov, G. *ChemPhysChem* **2005**, *6* (7), 1221–1231.
- (5) Kim, D.; Moon, J. *Electrochem. Solid-State Lett.* **2005**, *8* (11), J30.
- (6) Mueller, N. C.; Nowack, B. *Environ. Sci. Technol.* **2008**, *42* (12), 4447–4453.
- (7) Fabrega, J.; Fawcett, S. R.; Renshaw, J. C.; Lead, J. R. *Environ. Sci. Technol.* **2009**, *43* (19), 7285–7290.
- (8) Stevenson, L. M.; Dickson, H.; Klanjscek, T.; Keller, A. A.; McCauley, E.; Nisbet, R. M. *PLoS One* **2013**, *8* (9), e74456.
- (9) Fabrega, J.; Luoma, S. N.; Tyler, C. R.; Galloway, T. S.; Lead, J. R. *Environ. Int.* **2011**, *37* (2), 517–531.
- (10) Asharani, P. V.; Lian Wu, Y.; Gong, Z.; Valiyaveetil, S. *Nanotechnology* **2008**, *19* (25), 255102.
- (11) McShan, D.; Ray, P. C.; Yu, H. *J. food drug Anal.* **2014**, *22* (1), 116–127.
- (12) Johnston, H. J.; Hutchison, G.; Christensen, F. M.; Peters, S.; Hankin, S.; Stone, V. *Crit. Rev. Toxicol.* **2010**, *40* (4), 328–346.
- (13) Dobias, J.; Bernier-Latmani, R. *Environ. Sci. Technol.* **2013**, *47* (9), 4140–4146.
- (14) Liu, J.; Hurt, R. H. *Environ. Sci. Technol.* **2010**, *44* (6), 2169–2175.
- (15) Batley, G. E.; Kirby, J. K.; McLaughlin, M. J. *Acc. Chem. Res.* **2013**, *46* (3), 854–862.
- (16) Levard, C.; Reinsch, B. C.; Michel, F. M.; Oumahi, C.; Lowry, G. V.; Brown, G. E.

- Environ. Sci. Technol.* **2011**, *45* (12), 5260–5266.
- (17) Lok, C.-N.; Ho, C.-M.; Chen, R.; He, Q.-Y.; Yu, W.-Y.; Sun, H.; Tam, P. K.-H.; Chiu, J.-F.; Che, C.-M. *J. Biol. Inorg. Chem.* **2007**, *12* (4), 527–534.
- (18) Akaighe, N.; MacCuspie, R. I.; Navarro, D. A.; Aga, D. S.; Banerjee, S.; Sohn, M.; Sharma, V. K. *Environ. Sci. Technol.* **2011**, *45* (9), 3895–3901.
- (19) Kanel, S. R.; Flory, J.; Meyerhoefer, A.; Fraley, J. L.; Sizemore, I. E.; Goltz, M. N. *J. Nanoparticle Res.* **2015**.
- (20) Pidwirny, M. (2006). "Introduction to Soils". *Fundamentals of Physical Geography*, 2nd Edition. September 2016. <http://www.physicalgeography.net/fundamentals/10t.html>
- (21) Prasad, M.; Saxena, S.; Amritphale, S. S.; Chandra, N. *Ind. Eng. Chem. Res.* **2000**, 3034–3037.
- (22) Mikutta, R.; Baumgärtner, A.; Schippers, A.; Haumaier, L.; Guggenberger, G. *Environ. Sci. Technol.* **2012**, *46* (7), 3866–3873.
- (23) Zaunbrecher, L. K.; Cygan, R. T.; Elliott, W. C. *J. Phys. Chem. A* **2015**, *119* (22), 5691–5700.
- (24) Arvidsson, Rickard; Molander, Sverker; Sandén, Björn A.; Hassellöv, M. *Hum. Ecol. Risk Assess.* **2011**, *17* (1).
- (25) Dale, A. L.; Lowry, G. V.; Casman, E. A. *Environ. Sci. Technol.* **2013**, *47* (22), 12920–12928.
- (26) Davis, J. A.; Kent, D. B. *Surface Complexation Modeling in Aqueous Geochemistry*, 23rd ed.; 1990.
- (27) El Badawy, A. M.; Luxton, T. P.; Silva, R. G.; Scheckel, K. G.; Suidan, M. T.; Tolaymat, T. M. *Environ. Sci. Technol.* **2010**, *44* (4), 1260–1266.
- (28) Bickel, P.; Diggle, P.; Fienberg, S.; Krickeberg, K.; Olkin, I.; Wermuth, N.; Zeger, S. *Springer Verlag* **2002**, *2*, 37–52.
- (29) Liang, S.; Singh, M.; Dharmaraj, S.; Gam, L.-H. *Dis. Markers* **2010**, *29* (5), 231–242.
- (30) Roggo, Y.; Edmond, A.; Chalus, P.; Ulmschneider, M. *Anal. Chim. Acta* **2005**, *535* (1–2), 79–87.

- (31) Lowry, G. V.; Gregory, K. B.; Apte, S. C.; Lead, J. R. *Environ. Sci. Technol.* **2012**, *46* (13), 6893–6899.
- (32) Caporali, S.; Moggi-Cecchi, V.; Pagliai, M.; Pratesi, G.; Schettino, V. *Life Detect. Extraterr. Samples* **2012**, 6001–6002.
- (33) Ossig, R.; Kwon, Y.-H.; Hubenthal, F.; Kronfeldt, H.-D. *Appl. Phys. B* **2012**, *106* (4), 835–839.
- (34) Ahamad, N. U.; Al-Amin, M.; Ianoul, A.; Ahamad, N. U.; Al-Amin, M.; Ianoul, A. *J. Nanoparticles* **2014**, *2014*, 1–9.
- (35) Yang, T.; Wang, E.; Wang, F.; Chou, K.; Hou, X. *Sci. Rep.* **2015**, *5*, 9690.
- (36) Dorney, K. M. A Chemical Free Approach For Increasing the Biochemical surface-enhance Raman Spectroscopy (SERS)-based sensing capabilities of colloidal silver nanoparticles., Wright State University, 2013.
- (37) Pavel, I. E.; Alnajjar, K. S.; Monahan, J. L.; Stahler, A.; Hunter, N. E.; Weaver, K. M.; Baker, J. D.; Meyerhoefer, A. J.; Dolson, D. A. *J. Chem. Educ.* **2012**, *89* (2), 286–290.
- (38) Pavel, I.; Mccarney, E.; Elkhaled, A.; Morrill, A.; Plaxco, K.; Moskovits, M. **2008**, 4880–4883.
- (39) Vlčková, B.; Moskovits, M.; Pavel, I.; Šišková, K.; Sládková, M.; Šlouf, M. *Chem. Phys. Lett.* **2008**, *455* (4), 131–134.
- (40) Waterhouse, G. I. N.; Bowmaker, G. a.; Metson, J. B. *Phys. Chem. Chem. Phys.* **2001**, *3* (17), 3838–3845.
- (41) Nie, S. *Science (80-.)*. **1997**, *275* (5303), 1102–1106.
- (42) Xu, H.; Bjerneld, E. J.; Käll, M.; Börjesson, L. *Phys. Rev. Lett.* **1999**, *83* (21), 4357–4360.
- (43) Michaels, A. M.; Nirmal, M.; Brus, L. E. .
- (44) Manahan, S. E. *Environmental Chemistry*, ninth.; Taylor and Francis Group: Boca Raton, 2010.
- (45) Dietrich, R. V. Mica <https://www.britannica.com/science/mica> (accessed Aug 30, 2016).
- (46) Tolaymat, T. M.; El Badawy, A. M.; Genaidy, A.; Scheckel, K. G.; Luxton, T. P.; Suidan, M. *Sci. Total Environ.* **2010**, *408* (5), 999–1006.

- (47) US EPA. Secondary Drinking Water Standards: Guidance for Nuisance Chemicals.
- (48) Yan, L.; Englert, A. H.; Masliyeh, J. H.; Xu, Z. *Langmuir* **2011**, *27* (21), 12996–13007.
- (49) Sverjensky, D. A. *Geochim. Cosmochim. Acta*, **1994**, *58* (14), 3123–3129.
- (50) McLaren, R. G.; Cameron, K. C. *Soil Science*, Second.; Oxford University Press, 1996.
- (51) Creighton, J. A.; Blatchford, C. G.; Albrecht, M. G. *J. Chem. Soc. Faraday Trans. 2* **1979**, *75*, 790.
- (52) Mulfinger, L.; Solomon, S. D.; Bahadory, M.; Jeyarajasingam, A. V.; Rutkowsky, S. a.; Boritz, C. *J. Chem. Educ.* **2007**, *84* (2), 322–325.
- (53) Foose, D. P.; Sizemore, I. E. P. **2016**.
- (54) Martina, I.; Wiesinger, R.; Schreiner, M. *e-Preservation Sci.* **2012**, *9*, 1–8.
- (55) Yong, C. W.; Warren, M. C.; Hillier, I. H.; Vaughan, D. J. *Phys. Chem. Miner.* **2003**, *30* (2), 76–87.
- (56) Agency, U. S. E. P. A. *Fed. Regist.* **1994**, *4*.
- (57) Environmental Monitoring Systems Laboratory; McDaniel, W. *Methods for the Determination of Metals in Environmental Samples*. 1996, pp 24–30.
- (58) Montano, M. D.; Ranville, J.; Lowry, G. V; Blue, J.; Hiremath, N.; Koenig, S.; Tuccillo, M. E.; Gardner, S. P. **2014**, No. August, 186.
- (59) Hanson, N.; Harris, J.; Joseph, L. A.; Ramakrishnan, K.; Thompson, T. *Off. Insp. Gen. Epa* **2011**, No. 12, 1–23.
- (60) Dorney, K. M.; Baker, J. D.; Edwards, M. L.; Kanel, S. R.; O'Malley, M.; Sizemore, I. E. *P. J. Chem. Educ.* **2014**, *91* (7), 1044–1049.
- (61) Badawy, a. M. E.; Luxton, T. P.; Silva, R. G.; Scheckel, K. G.; Suidan, M. T.; Tolaymat, T. M. *Environ. Sci. Technol.* **2010**, *44* (4), 1260–1266.
- (62) Porto, S. P. S. *J. Chem. Phys.* **1967**, *47* (11), 1009.
- (63) Zhu, W.; Pezzotti, G. *J. Raman Spectrosc.* **2011**, *42* (11), 2015–2025.
- (64) Pezzotti, G.; Zhu, W. *Phys. Chem. Chem. Phys.* **2015**, *17* (11), 2608–2627.

- (65) Zabinski, J. S.; McDevitt, N. T. *Raman Spectra Inorg. Compd.* **1996**.
- (66) About Precision Sapphire Technologies Ltd. <http://www.sapphire.lt/sapphire/>.
- (67) Hass, K. C.; Schneider, W. F.; Curioni, A.; Andreoni, W. *Science* (80-.). **1998**, 282 (5387), 265–268.
- (68) Janeček, J.; Netz, R. R.; Flörsheimer, M.; Klenze, E.; Schimmelpfennig, B.; Polly, R. *Langmuir* **2014**, 30 (1), 2722–2728.
- (69) Ulcinas, A.; Valdre, G.; Snitka, V.; Miles, M. J.; Claesson, P. M.; Antognozzi, M. *Langmuir* **2011**, 27 (17), 10351–10355.
- (70) McKeown, D.; Bell, M.; Etz, E. S. *Am. Mineral.* **1999**, 84, 1041–1048.
- (71) Ostendorf, F.; Schmitz, C.; Hirth, S.; Kühnle, A.; Kolodziej, J. J.; Reichling, M. *Nanotechnology* **2008**, 19 (30), 305705.
- (72) Tlrrynme, H. **1977**, 62, 534–539.
- (73) Cyr, R. D. Saint; Words--dichroism, K.; Infrared, F.; Moment, T. **2000**, 48 (4), 433–438.
- (74) Trefry, J. C.; Monahan, J. L.; Weaver, K. M.; Meyerhoefer, A. J.; Markopolous, M. M.; Arnold, Z. S.; Wooley, D. P.; Pavel, I. E. *J. Am. Chem. Soc.* **2010**, 132 (32), 10970–10972.
- (75) Li, W.; Wang, Y. B.; Pavel, I.; Yuan, Q.; Ye, Y.; Fu, E. Q.; Luo, M. D.; Hu, J. M.; Kiefer, W. *J. Phys. Chem. A* **2005**, 109 (12), 2878–2886.

ASSOCIATED CONTENT

SUPPORTING INFORMATION

Supplementary information includes additional figures and tables supporting the Raman results.

RESULTS AND DISCUSSION

Table 3.S1. Summary of controls and samples for both minerals and the instrumental method they were analyzed with (denoted by ✓). Both forms of corundum (except the “as received” control) were reacted with a total volume of 100 mL for 30 min each.

		<u>Corundum</u>		<u>Muscovite</u>
		As fused micro-sized spherical particles	As large flat sapphire windows	As freshly cleaved
Controls		As received	As received	As received
		Water (pH adjusted to 8 with 30 μ L 0.1 M NaOH)	Cleaned (HNO ₃) and annealed (@ 1250°C)	10 μ L HQ water (hydrated)
		pH 6 and 7 (HNO ₃)		
		pH 9, 10, and 11(NaOH)	DI water (30 min)	10 μ L 10 ⁻³ M R6G
		5 mM ISA (@~pH 8)	5 mM ISA (30 min)	
Samples		1.0 mg L ⁻¹ AgNPs ⁻ + 5 mM ISA @ pH 6, 7, 8, 9, 10 and 11	1.0 mg L ⁻¹ AgNPs ⁻ + 5 mM ISA	10 μ L 15.4 mg L ⁻¹ AgNPs ⁻
				10 ⁻⁴ M R6G + 15.4 mg L ⁻¹ AgNPs ⁻
Analysis	Non-labeled Raman	✓	✓	✓
	Labeled Raman			✓
	ICP-OES	✓		
	AFM		✓	

Table 3.S2. Tentative assignments of the Raman vibrational modes observed for α -Al₂O₃.

Experimental Raman modes (cm⁻¹)	Literature Raman Shift (cm⁻¹)	Tentative assignment
378 (m)	378	<i>E_g</i> external
416 (s)	416	<i>A_{1g}</i>
429 (m,sh)	429	<i>E_g</i> external
451 (w)	451	<i>E_g</i> internal
574-576 (w)	576	<i>E_g</i> internal
644 (m)	644	<i>A_{1g}</i> <i>zz</i>
750 (m)	750	<i>E_g</i> internal

Table 3.S3: Vibrational modes, and tentative assignments of muscovite Raman spectrum about the A_g in-plane rotation (normal to 001 plane). Tentative assignments are taken from McKeown et. al. 3627⁷⁰ and 3657 cm^{-1} assigned from Wang et. al.⁷⁵ Experimental reference spectrum obtained with a 633 nm HeNe Laser with a 1 second acquisition time.

Vibrational Mode (cm^{-1})	Experimental Reference	Tentative Assignment
85		Sheet yz-trans. + K y-trans.
124	122	Sheet xz-trans. + K xy-trans. (minor)
172	170	M2-OH stretch (M2 z-trans.)
198	195	M2-OH stretch + Od xz-trans.
217	215	OH-M2-OH bend + M2-Oa stretch
265	262	Ob, OH y-trans. + Oc,e z-trans. + K y-trans.
265		T1-Oa z-trans. + T2-Ob -z-trans. + M2 xy-trans. + K xy-trans.
295		M2-OH stretch + M2-Oa stretch
316	317, w	M2-OH stretch + M2-Ob stretch + tetrahedral rot. z
382	382, sh	M2 z-trans. + Oc z-trans. + Od,e -z-trans.
411	408	M2 xz-trans. + Od z-trans. + Oc,e xz-trans.
442		Oa-M2-Ob bend + Oc,e z-trans. + Od xy-trans.
527		T-Obr-T xy-bend
583		M2 xy-trans. + T z-trans.
583		Od,e xy-trans. + T y-trans. + K xy-trans.
638		Onb yz-trans. + Obr -yz-trans.
703	702	Onb z-trans. + Ob r -z-trans. + M2-Ob stretch
754	752	Oa-M2-Ob bend
800		T-Oc,d-T bend
811		T-Oc,e-T bend
913	912	Tetrahedral breathing
958	956	T-Onb stretch (n1)
1024	1020	T-Onb stretch (n1) + Obr in/out tetr. base center
1098	1079	T1,2-Oc,e xy-stretch (n10)
1116	1116	T1,2-Oc,d xy-stretch (n10)

Abbreviations: M2 – Octahedral site occupied by Al^{+3} (M1 site is vacant). T – Tetrahedral. Onb - non-bridging O atoms. Obr - bridging O atoms. sh – shoulder.

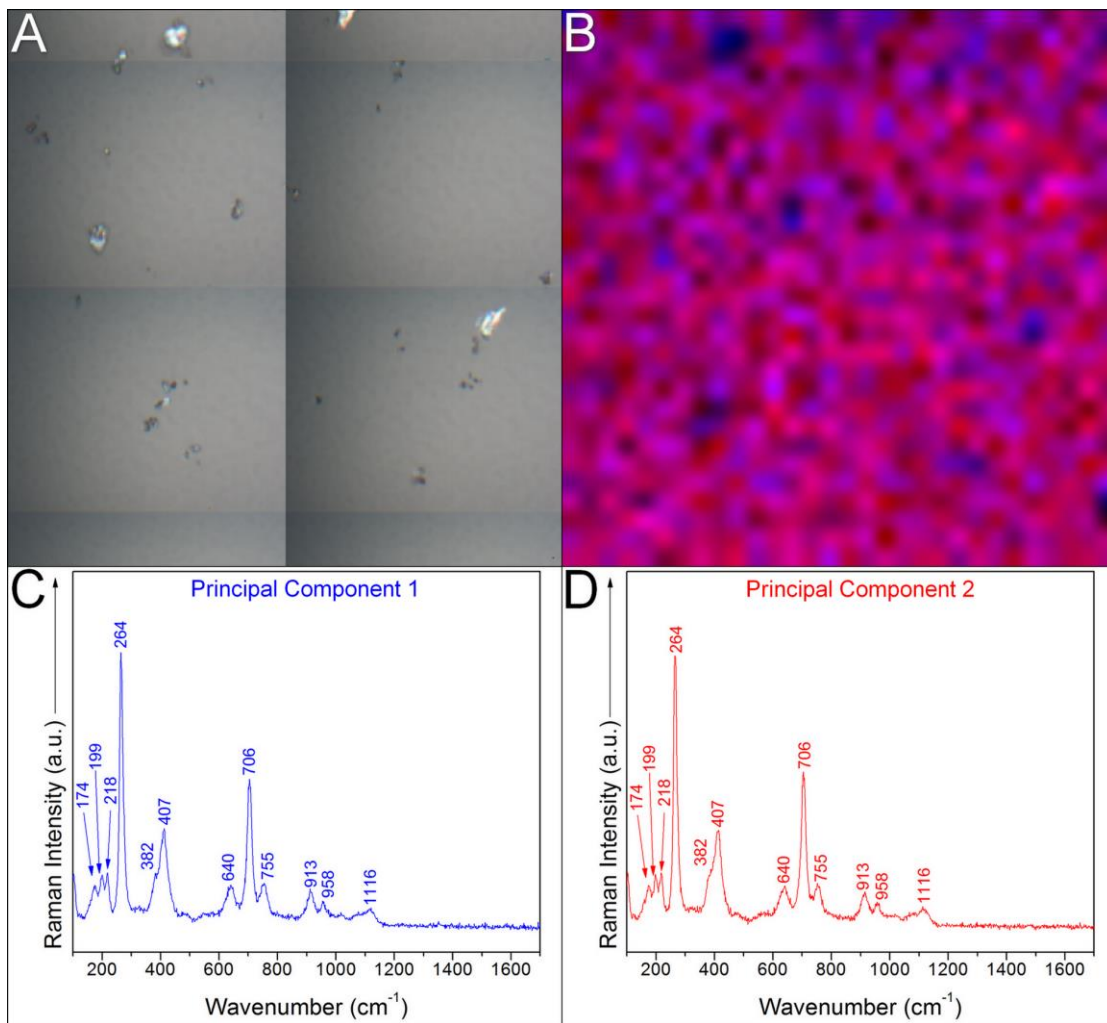


Figure 3.S1. Raman Map of Bare Muscovite Surface. 150×150μm Map collected over 5μm intervals with an 1 second acquisition time and measured over a spectral range of 100 to 1700 wavenumbers cm⁻¹. (A) Image of mapped area (B) Image of same area constructed from PCA (C) Principle component one (D) Principle component two, both correlating to muscovite.

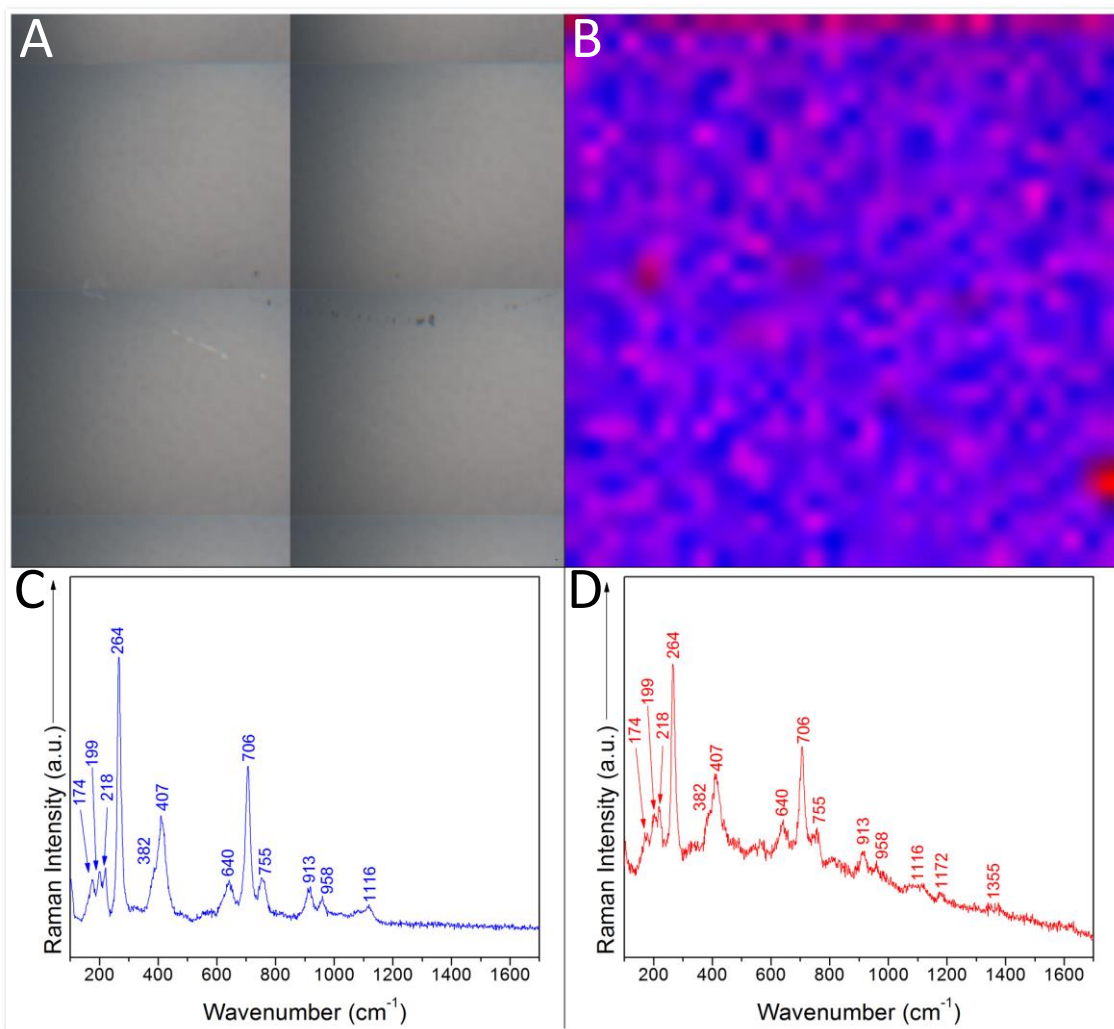


Figure 3.S2. Silver Nanoparticle Colloid on Muscovite. 150×150μm Raman Map collected over 5μm intervals with an 1 second acquisition time and measured over a spectral range of 100 to 1700 wavenumbers cm⁻¹. (A) Image of mapped area (B) Image of same area constructed from PCA (C) Principle component one (D) Principle component two both correlating to muscovite.

CHAPTER 4

**MEASURING THE SILVER COMPOSITION OF NANOCOLLOIDS BY
INDUCTIVELY COUPLED PLASMA–OPTICAL EMISSION SPECTROSCOPY:
A LABORATORY EXPERIMENT FOR
CHEMISTRY AND ENGINEERING STUDENTS**

*Seth W. Brittle, Joshua D. Baker, Kevin M. Dorney, Jessica M. Dagher,
Tala Ebrahimian, Steven R. Higgins, and Ioana E. Pavel Sizemore*

Department of Chemistry, Wright State University,
3640 Colonel Glenn Hwy., Dayton, OH, 45435

COPYRIGHT PERMISSION

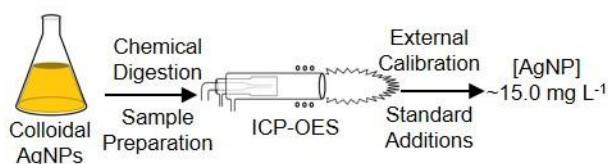
The proceeding chapter is reproduced from a published *Journal of Chemical Education* manuscript authored by Seth W. Brittle. The article, “*Freshwater crayfish: a potential benthic-zone indicator of nanosilver and ionic silver pollution*” was accepted with a set of minor revisions. Permission to use this work in its entirety for this thesis/dissertation has been granted by the JCE editorial staff. The full citation for access article is the following:

Brittle, S. W.; Baker, J. D.; Dorney, K. M.; Dagher, J. M.; Ebrahimian, T.; Higgins, S. R.; Pavel-Sizemore, I. E. Measuring the Silver Composition of Nanocolloids by Inductively Coupled Plasma–Optical Emission Spectroscopy: A Laboratory Experiment for Chemistry and Engineering Students. *J. Chem. Educ.* 2015, 92, 1061–1065; DOI 10.1021/ed500707k.

SUMMARY OF INVOLVEMENT

Seth Brittle was primarily responsible for drafting and editing the manuscript and associated figures, tables, and supporting information. This included interpreting and analyzing student evaluations and assessments in addition to verifying experimental measurement. In addition, he helped implement the experiment by setting up lab materials, teaching recitations, and answering questions with other co-authors. He also helped students with chemical digestions and interpreting their measurements obtained from ICP-OES.

GRAPHICAL ABSTRACT



ABSTRACT

The increased worldwide exploitation of nanomaterials has reinforced the importance of introducing nanoscale aspects into the undergraduate and graduate curriculum. To meet this need, a novel nano-laboratory module was developed and successfully performed by science and engineering students. The main goal of the experiment was to accurately quantify the total silver composition of a nanocolloid with modern inductively coupled plasma–optical emission spectroscopy (ICP-OES) instrumentation in conjunction with two well-established methods that are heavily employed in both research and industrial settings. Specifically, undergraduate and graduate students estimated the total silver composition of Creighton colloidal nanoparticles via the external calibration method ($16.3 \pm 4.7 \text{ mg L}^{-1}$) and the standard addition method ($14.9 \pm 4.2 \text{ mg L}^{-1}$) at two emission wavelengths (328.068 and 338.898 nm). The assessment of basic laboratory skills and the class assignments showed that the students successfully mastered the various aspects of sample/standard preparation, the operation of the ICP-OES instrument, and the data analysis. Students’ interest and experience in this laboratory were highly rated in the anonymous student evaluations.

Keywords

Upper-Division Undergraduate • Graduate Education/Research • Laboratory Instruction •
Interdisciplinary/Multidisciplinary • Hands-On Learning/Manipulatives •
Nanotechnology • Colloids • Instrumental Methods

INTRODUCTION

In the last two decades, the nanoscience and nanotechnology sectors have exponentially proliferated across the world.¹ It is expected that by 2020, approximately six million people will be employed in nanofields.¹ In response to this workforce demand, many universities have now established curricula, in particular at the graduate level, to introduce students to the themes originating within the nanoareas.² Furthermore, current National Science Foundation (NSF) solicitations for proposals³ encourage the introduction of nanoscale science, engineering, and technology into the undergraduate education.

Many of the unique properties of nanomaterials derive from their size, shape, and surface charge,^{4,5} but the elemental composition is one of the most important characteristics because it directly relates to the controlled, safe, and efficient use of nanomaterials as well as to their toxicity.^{6,7} Inductively coupled plasma - optical emission spectrometry (ICP-OES), also commonly referred to as ICP - atomic emission spectroscopy (ICP-AES), is a well-established analytical technique that offers both qualitative and quantitative forms of elemental analysis.⁸ In addition, ICP-OES can detect up to 70 elements⁹ and exhibits better detection limits (down to the ppb level⁹) than other traditional techniques such as flame atomic absorption/emission spectroscopy (FAAS or FAES) and ultraviolet-visible (UV-Vis) absorption spectroscopy. Thus, ICP-OES offers suitable quantification of a wide range

of elements in a relatively fast, single analysis and without the expense of a more costly mass spectrometer (ICP-MS).^{9,10}

This new laboratory module aimed to familiarize students enrolled in upper-level *Instrumental Analysis* and *Experimental Nanomaterials and Nanoscience* laboratory courses (3 credit hours each course) with two well-established calibration methods, namely the external calibration method and the standard addition method, for the accurate quantification of the total silver composition of nanocolloids. In this context, both science and engineering students were introduced to the theoretical and experimental aspects of ICP-OES including, sample/standard preparation, the operation of modern ICP-OES instrumentation, and data analysis. The proposed experiment module takes at least two three-hour lab periods and a possibly a third one may also be necessary if students fabricate their own colloidal nanoparticles. Additional organizational details and suggestions for various laboratory time periods are provided in Supporting Information. The two calibration methods were compared for a widely-used Creighton colloid of silver nanoparticles (AgNPs) by relating the actual yield to the theoretical yield of the reaction. The external calibration approach was selected to demonstrate the rapid analysis of a large set of colloidal samples, while the standard addition method was recommended for the analysis of complex, colloidal samples, where matrix effects are considerable.^{11,13} For further comparisons, two emission wavelengths were utilized in both calibrations (the main and secondary lines of Ag (I) ion at 328.068 nm and 338.898 nm, respectively). It is important to introduce students to the possibility of employing multiple emission wavelengths for the same elemental ion to avoid possible spectral overlaps, to interrogate different concentration ranges, or to confirm the results obtained by a specific wavelength.

A more detailed explanation could elaborate upon the ionization energies associated with different ions. While the external calibration method in combination with quality control measurements is endorsed by the U.S. Environmental Protection Agency (EPA), the standard addition method is preferred for increased confidence.¹³ Thus, this laboratory experiment closely followed the U.S. EPA Method 200.7 with some minor modifications to fit the allotted time period (outlined in the Supporting Information). This approach effectively exposed students to the two methods frequently employed in research and industrial settings.

ICP-OES-based laboratory experiments for the quantification of nanomaterial composition has been introduced before into the academic curricula, but it focused on the external calibration approach. For example, Metz *et al.* designed an ICP-OES experiment for non-STEM students to estimate AgNP accumulation in the Wisconsin Fast Plants, *Brassica rapa*.¹⁴ Numerous ICP-OES and FAAS laboratory modules encourage the utilization of both calibration methods, but these educational experiments are not relevant to nanomaterial characterization (*e.g.*, multivitamins, teeth, motor oil, and so on).¹⁵⁻¹⁷ The experiment reported here is unique in that it introduces students to more than one calibration method to accurately quantify the total silver composition of colloidal AgNPs using modern, ICP-OES instrumentation.

MATERIALS AND METHODS

Chemicals: All chemicals in this laboratory experiment were purchased as high-grade analytical reagents from Fisher Scientific, and were used without further modification (Supporting Information). High quality (HQ) water (resistivity > 18 M Ω •cm) was the solvent in the AgNP synthesis, the quantitative dilutions of the digested samples,

and the method blank. A SPEX CertiPrep ICP OES grade Ag^+ standard ($1,000 \pm 5 \text{ mg L}^{-1}$) and OPTIMA grade nitric acid (HNO_3) for trace metal analysis were employed for the standards preparation and chemical digestions.

Synthesis of Creighton Colloidal AgNPs: Colloidal AgNPs were synthesized in advance via a modified Creighton method¹² through the titration reduction of Ag^+ in silver nitrate (AgNO_3) with sodium borohydride (NaBH_4) at $\sim 0^\circ\text{C}$ (Supporting Information).¹⁹ This nongreen synthesis was rigorously described by our group together with other green and nongreen bottom-up fabrication methods for silver and gold nanoparticles in a recently published, complementary nano laboratory experiment.²⁰ Any of these nanocolloids could be utilized in the proposed ICP-OES-based laboratory experiment. The Creighton colloid was wrapped in aluminum foil, stored at $\sim 10^\circ\text{C}$, and used within one week in order to avoid the potential release of Ag^+ ions from AgNPs. This oxidation process may occur over time (6 to 125 days), in the presence of dissolved O_2 and H^+ , and is temperature dependent (ion release rate increases with temperature, $0\text{-}37^\circ\text{C}$).²¹

Chemical Digestion of AgNPs: Students digested $0.500 \pm 0.001 \text{ mL}$ of colloidal AgNPs in 2.0 mL OPTIMA grade HNO_3 . A “cold digestion” was employed first, where the solutions were allowed to sit for 15 min, followed by a “hot digestion” at $\sim 180^\circ\text{C}$. The samples were allowed to evaporate until a minimal amount of liquid remained ($\sim 200 \mu\text{L}$), and the beakers were removed from the hot plate. The digested samples were then diluted to a total volume of $100.00 \pm 0.08 \text{ mL}$, and a final 2% HNO_3 matrix by volume was established. A method blank (MB) of HQ water was prepared in the same manner.

Blanks and Standards Preparation: *External calibration method*—External standards were prepared from the standard Ag^+ solution that ranged from $0\text{-}150 \mu\text{g L}^{-1}$, in

25.0 $\mu\text{g L}^{-1}$ increments. A matrix blank, consisting of HQ water and 2% HNO_3 was used as a calibration blank for 0.0 $\mu\text{g L}^{-1}$. *Standard addition method*—A standard addition calibration was performed by spiking five 5.0-mL samples of digested and diluted AgNPs with known volumes of a 10.0 $\mu\text{g mL}^{-1}$ of Ag^+ standard in the following amounts: 0.0, 25.0, 50.0, 75.0, and $100.0 \pm 0.1 \mu\text{L}$, and then diluting to 10.0 mL.

All digested samples, blanks, and standards were prepared with a final 2% HNO_3 matrix.

ICP-OES measurements: A Varian 710-ES ICP-OES instrument having an axially positioned torch was employed for the elemental quantitation of total Ag within the digested, colloidal AgNP. Other ICP-OES instrument models such as Optima8x00 (Perkin Elmer) and Ultima Expert (Horiba Scientific) may also be utilized for this experiment. Optimized acquisition parameters included a replicate read time of 15 s, an internal stabilization delay of 45 s, a sample uptake delay of 40 s, a peristaltic pump rate of 2 mL min^{-1} (~30 rpm) and a rinse time of 15 s. Each sample was measured in triplicate using the two emission lines for Ag employing an autosampler (Varian SP3) and a wide dynamic range CCD detector. Light intensities were transduced into electrical signals, and a resultant spectrum was created by plotting the emitted intensities versus wavelength.

Hazards: The toxicity of AgNPs is still under investigation;^{6,7} thus, care should be exercised when working with any AgNPs. Aqueous solutions of corrosive NaBH_4 should be used in less than one week and stored in loosely fitted containers without agitation. Silver nitrate (AgNO_3) should be identified as a possibly toxic and corrosive chemical. Concentrated HNO_3 is extremely corrosive and should be handled carefully, especially during high-temperature digestions. All sample-related activities should be carried out in a

chemical fume hood to avoid build-up of flammable gas (hydrogen gas evolved during AgNP synthesis) and toxic inhalations (oxides of nitrogen evolved during AgNP digestion). The operation of the ICP-OES should be performed under the supervision of trained personnel, and should closely follow a standard operating procedure (SOP). Personal protective equipment should be worn at all times during the experiment.

RESULTS AND DISCUSSION

Student results: The theoretical yield of the Creighton AgNPs was estimated through simple, stoichiometric calculations (sample calculation in Supporting Information). Briefly, 50.0 mL of 1 mM AgNO₃ was reduced to 300.0 mL of 2 mM NaBH₄, yielding 350.0 mL of Creighton colloid. Given the atomic weight of Ag (107.8682 g mol⁻¹), the total Ag amount present in the colloid was estimated to be 15.4 mg L⁻¹. Next, small aliquots of colloidal AgNPs and HQ water were chemically digested by each student group and quantitatively diluted to fit within the Ag concentration range of the calibration curves based off the estimated theoretical yield. Students then individually analyzed the external calibration and standard addition standards.

External calibration method—Students constructed the external calibration curve by plotting the instrument response (*i.e.*, the emission intensity) as a function of the known Ag concentrations (*i.e.*, the concentration of each external standard), and used a linear least square analysis to fit the data. A sample curve is shown in Figure 4.1A for the main emission line of Ag at 328.068 nm. Unknown Ag composition in the colloidal samples of AgNPs was then interpolated according to their signal response from the calibration curve. For example, one student group obtained an intensity of 1626.2 a.u. for the Creighton sample. This emission value (*y*) was found to correspond to a total Ag amount of 11.1 mg

$L^{-1}(x)$ after solving the regression equation and considering the 200-fold dilution factor (sample calculation in Supporting Information). Standard deviations across the two courses are presented in Table 4.1.

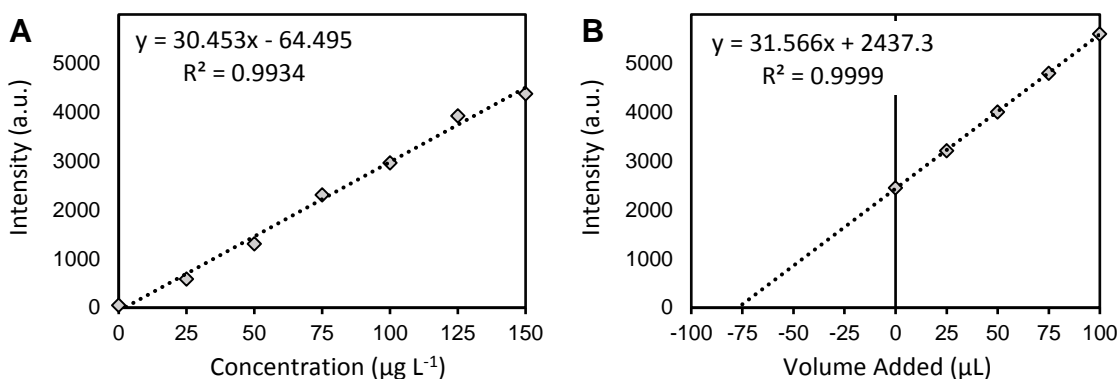


Figure 4.1. Sample external calibration curve (A) and standard addition curve (B), which were constructed by students for the main emission line of Ag at 328.068 nm.

Standard addition method—In this calibration approach, students measured the instrument response for five samples spiked with various amounts of an Ag standard. The emission intensities (y) were then plotted as a function of the volume of standard solution added (x). A sample curve is shown in Figure 4.1B for the main emission line of Ag at 328.068 nm. Subsequently, a linear regression was performed to determine the total Ag amount of the Creighton colloidal samples. For example, one student group estimated the amount of Ag in their colloidal sample as being 15.4 mg L^{-1} after solving for x when $y = 0$. The dilution factor and concentration of the standard added were also taken into consideration (sample calculation in Supporting Information).

Comparison of the external calibration and standard addition methods for the determination of the total Ag composition of nanocolloids: Both calibration methods were effective in quantifying the total Ag composition of the Creighton colloid. Average Ag amounts and standard deviations across the two courses are presented in Table 4.1, while percent errors are given in Table 4.S2 (Supporting Information). The percent error were determined by comparing the class average values (*i.e.*, the actual yield for both courses) to the theoretical yield for the Creighton reaction, which was estimated from stoichiometric calculations (15.4 mg L^{-1}). This value was assumed to correspond to an ideal 100% yield for simplicity. Overall, the standard addition method provided more accurate Ag estimates (by 1.3-8.4%) and exhibited smaller deviations (by 0.0-27.3%) than the external calibration method for the main excitation line of Ag at 328.068 nm (Table 4.1). The average Ag amount obtained via the standard addition method in the two courses was $14.9 \pm 4.2 \text{ mg L}^{-1}$ at 328.068 nm, which corresponds to a percent error of 3.3% (Table 4.S2) for the Creighton reaction. It should be noted that students were also asked to calculate percent recoveries and percent error in order to compare both calibrations and both emission lines (Supporting Information). It was found that the improved precision of the standard addition method may be attributed to the consideration of matrix effects.

Table 4.1. Class average values and standard deviations for the total Ag composition of Creighton colloids as obtained by students through ICP-OES.^a

Course name	External Calibration		Standard Addition	
	328.068 nm	338.898 nm	328.068 nm	338.898 nm
<i>Instrumental Analysis</i>	14.6 ± 6.5	10.5 ± 4.0	14.8 ± 2.3	7.9 ± 4.9
<i>Experimental Nanomaterials and Nanoscience</i>	13.7 ± 2.9	13.6 ± 3.7	15.0 ± 2.9	11.5 ± 8.0

^aAll amounts are reported as mg L⁻¹ (ppm). Error is reported as 1σ.

In considering both emission lines, the 328.068 nm wavelength performed better than the 338.898 nm wavelength for both calibration methods (Table 4.1). It should be noted that the external calibration method led to more accurate Ag amounts than the standard addition method for the 338.898 nm emission line (Table 4.S4). The statistical weights of the states corresponding to the emission wavelengths could be quite different and lead to the greater intensity observed for the 328.068 nm line (from an increased population in this state). Given the proximity of the two states on an energy scale, even a subtle difference in statistical weights could explain the observed differences. Because the lower energy state electronic configuration is the same for both emission lines (namely, [Kr]4d¹⁰5s¹), the ground state has the same energy and the same term symbol ²S_{1/2}. However, upon excitation, the electronic configuration changes to [Kr]4d¹⁰5p¹. This upper state electronic configuration has two possible term symbols, namely ²P_{3/2} for the 328.068 nm line and ²P_{1/2} for the 338.898 nm line, due to LS coupling. Thus, recombination to this excited state configuration would be more favorable and have a higher population of excited Ag atoms than that of the ²P_{1/2} state (corresponding to emission at 338.898 nm).^{9,10}

Formative Assessment: The knowledge gained by the undergraduate and graduate students was assessed through pre- and post-laboratory assignments (Supporting Information), which showed that the proposed educational goals were successfully achieved in both courses. Briefly, before performing the proposed experiment, students were graded on their ability to correctly answer a set of pre-lab questions using the relevant material, which was made available to them in advance. After the completion of the experiments, students prepared a full laboratory report and were graded with the help of a rubric including the topics that were interrogated in the pre-lab assignment. The achievement of the proposed educational goals was further substantiated by the excellent ratings of a set of laboratory skills (#*S1-S6*) that were performed by the instructor and were identified as vital for the successful completion of the experiment (Table 4.2). Students were found capable of *S1*- correctly performing the cold and hot digestions, *S2*-performing the appropriate dilutions of the digested samples for ICP-OES analysis, *S3*-completing all necessary safety checks and operation of the ICP-OES equipment, noting any irregularities and reporting them as directed, *S4*-setting the instrument computer to the appropriate data collection parameters, *S5*- loading the autosampler with the appropriate number of blanks, standards, and samples in the correct order, and *S6*-taking into consideration the conditions/parameters that must be met to allow for accurate sample analysis. Furthermore, anonymous evaluations were administered to examine students' interest in the laboratory before (*Q1*) and after its completion (*Q2*) as well as the overall experience in the performed experiment (*Q3*). The high ratings in Table 4.3 and anonymous comments showed that students found the new laboratory experiment stimulating and enjoyable.

Table 4.2. Results of the anonymous evaluations of several laboratory skills (S1-S6) performed by the instructors in the *Experimental Nanomaterials and Nanoscience* course.

Laboratory Skill	Instructor Ratings ^{a,b,c}		
	Fall 2012	Fall 2013	Average
S1	2.7 (0.3)	2.3 (0.3)	2.5 (0.5)
S2	2.7 (0.4)	2.2 (0.4)	2.5 (0.5)
S3	3.0 (0.0)	2.0 (0.0)	2.5 (0.5)
S4	2.2 (0.3)	2.7 (0.3)	2.5 (0.5)
S5	3.0 (0.0)	2.0 (0.0)	2.5 (0.5)
S6	2.7 (0.3)	2.2 (0.3)	2.5 (0.5)

^a Values in parentheses represent standard deviations of 1σ . ^b Each section contained eight groups $N=8$ groups of students. A total of 14 and 15 students completed the laboratory course in the Fall 2012 and Fall 2013 semester, respectively. ^c A rating of 3.0 indicates that student groups always met the laboratory goal, while ratings of 2.0 and 1.0 indicate that student groups sometimes and never met the laboratory goal, respectively.

Table 4.3. Results of the anonymous, student evaluations of several laboratory aspects (Q1-Q3) in the two courses.

Laboratory Aspect	Student Ratings ^{a,b,c}	
	<i>Instrumental Analysis</i>	<i>Experimental Nanomaterials and Nanoscience</i>
Q1: Pre-Interest	2.7 (2.5)	8.4 (1.8)
Q2: Post-Interest	8.5 (2.3)	8.5 (2.1)
Q3: Overall Experience	8.2 (2.4)	8.5 (2.4)

^a Values in parentheses represent standard deviation (1σ) of assessments and responses. ^b $N = 13$ students who volunteered to answer the questions for both courses. ^c On a scale from 1 to 10, 1 corresponds to the lowest score assigned by students, while 10 is the highest score.

CONCLUSION

As nanoparticle research and applications continue to grow, young scientists and engineers must be exposed to the fundamentals of nanotechnology and nanoscience. This

laboratory experiment successfully introduced a diverse population of science and engineering students to one of the most important aspects in the characterization of metallic NPs: the accurate quantification of the metal composition of nanocolloids by ICP-OES. It should be noted that over 50% of the students in the *Experimental Nanomaterials and Nanoscience* laboratory class were represented by female and other underrepresented groups. In this context, students were exposed to the convenience of the external calibration method and the importance of spiked samples in the standard addition method, at different emission wavelengths. Successful fulfillment of the laboratory experiment was verified through pre- and post-laboratory assignments and the assessment of a set of basic laboratory skills. Overall, students gained the scientific knowledge and the laboratory skills to confidently employ both ICP-OES calibration methods with metallic NPs-based samples. Additionally, anonymous evaluations indicated that the proposed ICP-OES based experiment was well received and highly rated by the students. This laboratory experiment could be implemented for the ICP-OES-based quantification of other metallic NPs in chemistry, environmental sciences or engineering undergraduate curricula.

ACKNOWLEDGEMENTS

Financial support through the NSF-Nanotechnology Undergraduate Education in Engineering Program, NSF-Environmental Health and Safety of Nanotechnology, and WSU start-up is gratefully acknowledged. The authors would also like to thank Garrett VanNess and Joseph Solch, laboratory instrumentation specialists at Wright State University, for their technical support during both courses.

REFERENCES

- 1) Roco, M. C. The Long View of Nanotechnology Development: the National Nanotechnology Initiative at 10 years. *J. Nanopart. Res.* **2011**, *13*, 427-445.
- 2) Blonder, R. The Story of Nanomaterials in Modern Technology: An Advanced Course for Chemistry Teachers. *J. Chem. Educ.* **2012**, *88* (1), 49-52.
- 3) National Science Foundation - Nanotechnology Undergraduate Education (NUE) in Engineering Kronz, M. F.; Poats, M. (NUE) in Engineering. http://www.nsf.gov/funding/pgm_summ.jsp?pims_id=13656&org=NSF&sel_org=NSF&from=fund (accessed Jan 2014)
- 4) Sun, Y.; Xia, Y. Shape-Controlled Synthesis of Gold and Silver Nanoparticles. *Science*. **2002**, *298*, 2176-2178.
- 5) Fabrega, J.; Fawcett, S. R.; Renshaw, J. C.; Lead, J. R. Silver Nanoparticle Impact on Bacterial Growth: Effect of pH, Concentration, and Organic Matter. *Environ. Sci. Technol.* **2009**, *43* (19), 7285-7290.
- 6) Yah, C. S.; Simate, S.; Iyuke, S. E. Nanoparticles Toxicity and Their Routes of Exposures. *Pharm. Sci.* **2012**, *45* (2), 477-491.
- 7) Sharifi, S.; Behzadi, S.; Laurent, S.; Forrest, L. Toxicity of Nanomaterials. *Chem. Soc. Rev.* **2012**, *41*, 2323-2343.
- 8) Rouessac, F.; Rouessac, A. *Chemical Analysis Modern Instrumentation Methods and Techniques*. 2nd ed.; John Wiley & Sons Ltd: West Sussex, England, 2007; pp. 309-327.
- 9) Skoog, D.; Holler, J. F.; Crouch, S. R. *Instrumental Analysis*. 8th ed.; Brooks/Cole: India, 2008; pp. 291-316.
- 10) Nötle, J. *ICP Emission Spectrometry: A Practical Guide*. Wiley-VCH: Weinheim, Germany, 2003; pp. 105-122.
- 11) Robinson, J. W.; Frame, E. M. S.; Ii Frame, G. M. *Undergraduate Instrumental Analysis*. 6th ed.; Marcel Dekker: New York, 2005; pp. 483-505.

- 12) U.S. Environmental Protection Agency. Inductively Coupled Plasma – Atomic Emission Spectrometry. *Method 6010C*. Revision 3. **2007**.
- 13) U.S. Environmental Protection Agency. Determination of Metals and Trace Elements in Water and Wastes by Inductively Coupled Plasma – Atomic Emission Spectrometry. *Method 200.7*. Revision 4.4. **1991**.
- 14) Metz, K. M.; Sanders, S. E.; Miller, A. K.; French, K. R. Uptake and Impact of Silver Nanoparticles on *Brassica rapa*: An Environmental Nanoscience Laboratory Sequence for a Nonmajors Course. *J. Chem. Ed.* **2013**, *91* (2), 264-268.
- 15) Arnold, R. J.; Arndt, B.; Blaser, E.; Blosser, C.; Caulton, D.; Chung, W. S.; Fiorenza, G.; Heath, W.; Jacobs, A.; Kahng, E.; Koh, E.; Le, T.; Mandla, K.; C. Overcoming Matrix Effects in a Complex Sample: Analysis of Multiple Elements in Multivitamins by Atomic Absorption Spectroscopy. *J. Chem. Ed.* **2011**, *88* (4), 484-487.
- 16) Porter, V. J.; Sanft, P. M.; Dempich, J. C.; Dettmer, D. D.; Erickson, A. E.; Dubauskie, N. A.; Myster, S. T.; Matts, E. H.; Smith, E. T. Elemental Analysis of Wisdom Teeth by Atomic Spectroscopy Using Standard Additions. *J. Chem. Ed.* **2002**, *79* (9), 1114-1116.
- 17) Palkendo, J. A.; Kovach, J.; Betts, T. A. Determination of Wear Metals in Used Motor Oil by Flame Absorption Spectroscopy. *J. Chem. Ed.* **2013**, *91* (4), 579-582.
- 18) Creighton, A. J.; Blatchford, C. G.; Albrecht, G. M. *J. Chem. Soc., Faraday Trans. 2*. **1979**, *75*, 790-798.
- 19) Solomon, S. D.; Bahadory, M.; Jeyarajasingam, A. V.; Rutkowsky, S. A.; Boritz, C. *J. Chem. Educ.* **2007**, *84*, 322-325.
- 20) Paluri, S. L. A., Edwards, M. L.; Lam, N. H.; Williams, E. M.; Meyerhoefer, A.; Pavel Sizemore, I. E. *J. Chem. Educ.*, **2014**. DOI: 10.1021/ed5004806.
- 21) Liu, J.; Hurt, R. H. Ion Release Kinetics and Particle Persistence in Aqueous Nano-Silver. *Environ. Sci. Technol.* **2010**, *44*, 2169-2175.

ASSOCIATED CONTENT

SUPPORTING INFORMATION

Additional material for instructors, students, a detailed description of the ICP-OES measurements, additional safety aspects and expected laboratory outcomes.

STUDENT HANDOUT

1. SAFETY AND HAZARDS

Students should receive instructions for chemical safety, personal protective equipment, and the proper handling of nanomaterials and nitric acid (HNO_3). The toxicity of colloidal silver nanoparticles (AgNPs) is currently under extensive scientific investigation, while HNO_3 is extremely corrosive and creates toxic fumes when heated; therefore, care should be exercised at all times when handling either AgNPs or HNO_3 . Silver nitrate (AgNO_3) involved in the synthesis of Creighton AgNPs is a possibly toxic and corrosive reagent. Laboratory goggles, coats, and gloves must be worn at all times to prevent accidental exposure. Labeled waste containers should be utilized for the proper disposal of all AgNP samples.

2. INTRODUCTION

Inductively coupled plasma - optical emission spectrometry (ICP-OES) is a well-established analytical technique that offers both qualitative and quantitative forms of elemental analysis.¹ In ICP-OES, a liquid sample is introduced into a nebulizer by means of a peristaltic pump, where it is aerosolized and further transported to plasma. The plasma (argon) atomizes, ionizes, and excites the elements in the sample. The subsequently emitted

radiation is sorted by wavelength in a spectrometer, and the corresponding intensity is measured. This allows for the determination of a wide range of elements in a relatively fast, single analysis.^{2,3}

The use of silver nanoparticles (AgNPs) in both research settings and consumer products has increased over the past decade. AgNP fabrication and manipulation is a very active research area due to the countless applications of AgNPs in catalysis, photonics, electronics, biosensing, drug delivery, pharmaceuticals, and so on.⁴ As a result, an increased exposure of AgNPs to humans and the environment is expected. Thus, the accurate characterization of nanomaterial concentration is of great importance for most applications and environmental studies; of particular interest is the toxicity of AgNPs, in which the amount of nanomaterial must be known with high certainty.^{5,6}

In this laboratory, two calibration methods commonly used in research and industrial settings, namely the external calibration method and the standard addition method, will be employed to accurately quantify the silver composition of widely-used Creighton AgNPs by ICP-OES. The Creighton colloid will be synthesized in advance via the aqueous reduction of silver nitrate by sodium borohydride.^{4,7} In preparation for ICP-OES measurements, the AgNP samples will be chemically digested and quantitatively diluted. Following the sample preparation, students will acquire hands-on experience with the ICP-OES instrument and software by setting the operational parameters and experimental procedures of the two calibration methods. An ICP-OES instrument will be utilized for the silver quantification, and the main and secondary emission lines of Ag at 328.068 nm and 338.898 nm, respectively, will be used for additional efficiency comparisons.

The external calibration method will require the preparation of a series of standard solutions containing known concentrations of analyte(s) to calibrate the instrument. These standards will be prepared separately from the sample. The calibration will be based on the instrument signal response (*i.e.*, the emission intensity) as a function of the known analyte concentration (*i.e.*, the concentration of each external standard). A calibration plot will be constructed from this analysis and will be fitted using a linear least square regression. The analysis is expected to yield a linear equation, $y = mx + b$, where y is the signal response and x is the concentration. Unknown sample concentrations will then be interpolated from the calibration curve according to their signal response. The external calibration approach is used when it is assumed interference effects are negligible. In contrast, the standard addition method is recommended for the analysis of complex samples, where matrix effects are considerable.

In this laboratory, students will also utilize the most common standard addition method,⁷ which adds increments of a standard solution to sample aliquots of equal volume. In this case, the sample matrix will remain unchanged, with all constituents of the mixture being identical; the exception will be the added concentration of the analyte. The instrument response will then be measured for all solutions, and the data will be plotted as the instrument response (y) versus the volume of the standard solution added (x). Subsequently, a linear regression will be performed, and the m -slope and y -intercept of the calibration curve will be utilized to estimate the concentration of an analyte in the sample.² Measured data will then be individually analyzed by each student, and the knowledge gained throughout the experiment will be evaluated through pre- and post-laboratory student assignments.

3. EXPERIMENTAL METHOD

3.1. First 2-3 hr Laboratory Period

Recitation: During the first laboratory period, students will be introduced to the ICP-OES technique. Concepts such as the working principle of ICP-OES, the external calibration and standard addition methods, the sample preparation and analysis, the method setup through the instrument software, and data analysis together with illustrative examples will be presented and discussed. The synthesis of Creighton colloidal AgNPs will also be discussed, and the theoretical yield of the reaction will be estimated together with the instructor.

Synthesis of Creighton AgNPs: Silver nanoparticles will be synthesized in advance by the teaching assistant (TA) through the reduction of 50.0 mL of 1 mM silver nitrate solution (AgNO_3) via dropwise addition to 300.0 mL of a 2 mM of sodium borohydride (NaBH_4) solution at the temperature of ice.^{4,7} This “bottom-up” nanofabrication approach was selected due to its simplicity, low cost, stability, and relatively low amounts of post-synthetic byproducts. For a further description of the reduction process, students should refer to reference 7.

3.2. Second 2-3 hr Laboratory Period

Glassware cleaning: Before proceeding with the preparation of samples and standards, all glassware will need to be properly cleaned. Glassware should be soaked in 10% nitric acid for 24 h and rinsed with high-quality water ($\geq 18 \text{ M}\Omega\cdot\text{cm}$) a minimum of 5 times. The exposure to HNO_3 will remove possible contaminating trace metals.

Sample preparation: Each group (pairs of students) will receive a colloidal sample of AgNPs. A sample aliquot of AgNP colloid (0.5 mL) will be digested in OPTIMA grade HNO₃. Briefly, the sample aliquot will be transferred to a 50-mL beaker along with 2.0 mL of HNO₃. This solution will be allowed to sit for 15 min for a “cold digestion”. During this time period, a hot plate will be set to 225° C. Upon completion of the cold digestion; the beaker will be placed onto the hot plate for the “hot digestion”. The liquid sample will be allowed to evaporate until a minimal volume remains (~ 200 µL) and the beaker will be removed from the hot plate. Once cooled, the sample needs to be quantitatively diluted so that the expected concentration (based on theoretical yield) fits within the middle of the calibration curve. In this experiment, a 1:100 volume dilution will probably suffice.

Standards preparation for the external calibration method: A Ag⁺ stock solution of 10.0 mg L⁻¹ will be utilized to prepare the standard solutions for external calibration. This stock solution will be made in advance by the GTA from a 1,000 ± 5 mg L⁻¹ Ag⁺ standard for trace metal analysis (SPEX CertiPrep). Students will then prepare seven standard solutions of 0.0, 25.0, 50.0, 75.0, 100.0, 125.0, and 150.0 ± 0.1 µg L⁻¹ in 100-mL ± 0.08 volumetric flasks. All flasks will be diluted up to the graduation mark with 2% HNO₃ (OPTIMA grade) to prevent Ag precipitation and leaching into the glass.⁷

Standard addition method preparation: The Ag⁺ stock solution of 10.0 mg L⁻¹ will also be utilized for the Ag analysis by this second method. Students will quantitatively transfer the digested sample of AgNP colloid into a 50-mL volumetric flask and dilute it to the graduation mark using a 1:100 volume ratio. After that, 5.0-mL aliquots of this diluted sample will be transferred to five clean plastic test tubes. Exactly 0, 1, 2, 3 and 4 spikes of 25.0 µL from the 10.0 mg L⁻¹ of Ag⁺ stock solution will be added to these test tubes.

3.3. Third 2-3 hr Laboratory Period

Standards and sample analysis: Students will then analyze the standards and the sample using a 710 ES ICP-OES instrument (Varian Inc.) coupled with an autosampler (Varian SP3). Peristaltic tubing pump rates will be set to the recommended 2 mL min^{-1} value (~ 30 rpm). The following acquisition parameters will be utilized: wavelengths for Ag of 328.068 nm and 338.898 nm, a radio frequency (RF) power of 1.20 kW, a plasma flow of 15.0 L min^{-1} , an auxiliary flow of 1.50 L min^{-1} , and a nebulizer pressure of 200 kPa. Each sample will be measured in triplicate using a replicate time of 10 s, a between-measurement stabilization time of 15 s, a sample uptake delay of 40 s, and a 15 s rinse time.

4. DATA ANALYSIS

4.1. Theoretical yield of the Creighton reaction

As it was mentioned above, the Creighton colloid will be synthesized via the reduction of 50.0 mL of 1 mM of AgNO_3 with 300.0 mL of 2 mM NaBH_4 . Thus, given the atomic weight of Ag ($107.8682\text{ g mol}^{-1}$), the total Ag present in the Creighton colloid may be calculated as shown below.

$$1\text{ mM of AgNO}_3 \rightarrow 1\text{ mM of Ag}^+ \quad (1)$$

$$1\text{ mM of Ag}^+ \times \frac{1\text{ M} \left(\frac{\text{mol}}{\text{L}}\right)}{10^3\text{ mM}} \times \frac{107.8682\text{ g of Ag}^+}{1\text{ mol of Ag}^+} = \frac{1.0786 \times 10^{-1}\text{ g of Ag}^+}{1\text{ L}} \quad (2)$$

$$\frac{1.0786 \times 10^{-1}\text{ g of Ag}^+}{1\text{ L}} \times \frac{50.0\text{ mL of Ag}^+}{350.0\text{ mL total}} = \frac{1.54 \times 10^{-2}\text{ g of Ag}}{1\text{ L}} \quad (3)$$

$$\frac{1.54 \times 10^{-2}\text{ g of Ag}}{1\text{ L}} \times \frac{10^3\text{ mg}}{1\text{ g}} = 15.4\text{ mg L}^{-1}\text{ of Ag in form of AgNPs} \quad (4)$$

First, a student can think of 1 mM of AgNO₃ as containing 1 mM of Ag⁺ (eq. 1). Next, the amount of Ag⁺ (in g L⁻¹) in 1 mM of AgNO₃ will be determined by using the atomic weight of Ag (eq. 2); then, the total Ag amount in the Creighton colloid will be estimated by applying the conservation of mass rule, $M_1 \times V_1 = M_2 \times V_2$, with V_1 and M_1 being the volume and mass, respectively, of the AgNO₃ solution and V_2 representing the total volume of the Creighton colloid (eq. 3). Lastly, this concentration (g L⁻¹) will be converted into mg L⁻¹ (ppm) by multiplying by 10³ (eq. 4).

4.2. External calibration

Students will construct the external calibration curve in Excel or Origin software by plotting the ICP-OES instrument response (*i.e.*, the emission intensity) against the known concentrations of the Ag standards. A linear regression will then be performed on the data to determine the unknown Ag composition of the Creighton colloid through interpolation. For example, a student group generated the curve seen in Figure 4.1A and measured an intensity of 1626.2 a.u. for their 1:200 volume diluted sample. From here, students calculated the total Ag composition as follows:

$$y = mx + b \quad (5)$$

$$y = 30.453x - 64.495 \quad (6)$$

$$x = \frac{(1626.2 + 64.495)}{30.453} = 55.518 \mu\text{g L}^{-1} \quad (7)$$

$$55.518 \mu\text{g L}^{-1} \times 200 = 1.1104 \times 10^4 \mu\text{g L}^{-1} \quad (8)$$

$$\frac{1.1104 \times 10^4 \mu\text{g}}{\text{L}} \frac{1.11 \times 10^4 \mu\text{g}}{\text{L}} \times \frac{1 \text{ mg}}{10^3 \mu\text{g}} = 11.1 \text{ mg L}^{-1} \quad (9)$$

First, a linear regression is performed to fit a trend line to the data as a simple linear equation (eq. 5), where y is the instrument response, and x is the concentration. In this example, the student group obtained the regression equation (eq. 6) from a set of seven Ag^+ standards ranging from 0.0 to 150.0 $\mu\text{g L}^{-1}$ concentration, in 25.0 $\mu\text{g L}^{-1}$ increments. Therefore, when their digested Creighton colloid emitted a measured intensity of 1626.2 a.u, the actual Ag amount was determined by solving for x (eq. 7). Next, the 1:200 volume dilution factor was considered (eq. 8), which produced a total Ag amount of $1.1104 \times 10^4 \mu\text{g L}^{-1}$. Students then converted this value to mg L^{-1} (eq. 9) for easier comparison to the theoretical yield.

4.3. Standard addition method

Similar to the external calibration method, a linear regression will also be utilized in the standard addition method. In this approach, the emission intensities of the five samples spiked with various amounts of Ag^+ standard are plotted as a function of the volume of standard solution added (eq. 10). For example, a student group generated the curve seen in Figure 4.1B with five additions of a 10.0 mg L^{-1} of Ag^+ standard in 25.0 μL increments to a final volume of 10.0 mL (eq. 11). This curve was then used to calculate the concentration of the sample by determining the volume of the standard needed to generate the response when no standard was added. Students accomplished this by extrapolating the curve back to the x -intercept in order to generate the absolute value of the raw volume (eq. 12). Next, students determined the raw concentration using the conservation of mass formula (eq. 13), where M_1 is the concentration of the standard added and V_1 is the volume calculated. Multiplying these values together and dividing by the final volume (V_2) generates the raw concentration (M_2) of the sample (eq. 14). After considering the volume

dilution factor (eq. 15) and converting to mg L^{-1} (eq. 16), the total Ag composition of the original Creighton sample was determined.

$$y = mx + b \quad (10)$$

$$y = 31.566x + 2437.3 \quad (11)$$

$$y = 0 = \left| \frac{-2437.3}{31.566} \right| = 77.213 \mu\text{L} = V_1 \quad (12)$$

$$M_1 \times V_1 = M_2 \times V_2 \quad (13)$$

$$(10^4 \mu\text{g L}^{-1} \times 77.213 \mu\text{L}) = (M_2 \times 10^4 \mu\text{L}) \quad (14)$$

$$77.213 \mu\text{g L}^{-1} \times 200 = 1.5443 \times 10^4 \mu\text{g L}^{-1} \quad (15)$$

$$\frac{15443 \mu\text{g}}{\text{L}} \times \frac{1 \text{ mg}}{1000 \mu\text{g}} = 15.4 \text{ mg L}^{-1} \quad (16)$$

4.4. Comparison of the two calibration methods

Percent Yield and Percent Error- The percent yield of the Creighton reaction may be determined from the ratio of the actual yield to the theoretical yield multiplied by 100% (eq. 17). For example, if we consider the actual yield of 11.1 mg L^{-1} , which students determined via ICP-OES using the external calibration method, and the theoretical yield of 15.4 mg L^{-1} , which was estimated stoichiometrically, a percent yield of $\sim 72.0\%$ is obtained (eq. 18).

$$\text{Percent yield} = \frac{\text{Actual yield}}{\text{Theoretical yield}} \times 100\% \quad (17)$$

$$\text{Percent yield} = \frac{11.1 \text{ mg L}^{-1}}{15.4 \text{ mg L}^{-1}} \times 100\% = 72.0\% \quad (18)$$

The percent error may be determined by using the theoretical yield as the accepted value (eq. 19). Using the above values for the theoretical and actual yield, a percent error of ~27.9% is obtained (eq. 20). Alternatively, one may understand that percent error plus the percent yield is simply 100%; therefore, if one is determined then the other is implied.

$$\text{Percent error} = \frac{\text{Theoretical yield} - \text{Actual yield}}{\text{Theoretical yield}} \times 100\% \quad (19)$$

$$\text{Percent error} = \frac{15.4 \text{ mgL}^{-1} - 11.1 \text{ mgL}^{-1}}{15.4 \text{ mgL}^{-1}} \times 100\% = 27.9\% \quad (20)$$

Percent Difference – Students should also calculate a percent difference to verify the presence of matrix effects within a sample. This may be achieved by taking the absolute value of the difference between the external calibration value and the standard addition value, which is then divided by the average Ag amount obtained using the two methods (eq. 21). For example, a percent difference of 32.7% was determined using the two Ag amounts demonstrated here, namely 11.1 mg L⁻¹ and 15.4 mg L⁻¹. When analyzing the percent difference values, students should notice that a percent difference of less than 10% suggests that no matrix effects are present.⁹

$$\text{Percent difference} = \left| \frac{\text{Ext. Cal. Value} - \text{Std. Add. Value}}{\left((\text{Ext. Cal. Value} + \text{Std. Add. Value}) / 2 \right)} \right| \times 100\% \quad (21)$$

$$\text{Percent difference} = \left| \frac{11.1 \text{ mg L}^{-1} - 15.4 \text{ mg L}^{-1}}{\left((11.1 \text{ mg L}^{-1} + 15.4 \text{ mg L}^{-1}) / 2 \right)} \right| \times 100\% = 32.7\% \quad (22)$$

Percent Recovery – If matrix effects are present, students are encouraged to determine the accuracy of the standard addition method. This may be accomplished by calculating the percent recovery. Students should take the difference between a spiked

sample and an unspiked sample, and divide it by the concentration of the spike used in the additions (eq. 23). It is important to note that the concentrations before the consideration of the dilution factor are utilized here. Furthermore, it does not matter which spiked sample a student chooses as long as the correct concentration of the spike is calculated and the respective spiked sample concentration is used. The concentration of the spike added may then be estimated from the dilution formula. As an example, a 75.0 μL spike of a 10.0 mg L^{-1} Ag^+ standard to a final volume of 10.0 mL yielded an elemental composition of 75.0 $\mu\text{g L}^{-1}$ (eq. 24).

$$\text{Percent Recovery} = \frac{\text{Spiked Sample} - \text{Unspiked Samples}}{\text{Spike Added}} \times 100\% \quad (23)$$

$$\text{Spike Added} = \frac{(0.075 \text{ mL} \times 10 \text{ mg L}^{-1})}{10 \text{ mL}} = 7.5 \times 10^{-2} \text{ mg L}^{-1} \quad (24)$$

$$\text{Percent Recovery} = \frac{0.147 \text{ mg L}^{-1} - 0.077 \text{ mg L}^{-1}}{0.075} \times 100\% = 93.3\% \quad (25)$$

Students should note that the EPA Method 200.7 suggests optimal control limits within 85 – 115%.⁹

Pairwise t-test – Another option for students to determine if both methods are significantly different is a two-sample paired *t*-test. This can be accomplished by comparing the class means in Microsoft Excel or with a graphing calculator. For example using the course averages for the *Experimental Nanomaterials and Nanoscience* course listed in Table 4.1, both calibration methods are determined not to be statistically different at the $p = 0.05$ level. Students can select the “2-SampTTest” option under the <Stat> tab, insert their own data and determine if the resultant *p*-value is significant or not. In this example, a *p*-value of 0.385 is obtained using the provided means, the corresponding

standard deviations, and the sample size ($n = 8$). Because this value is greater than an acceptable α -level, the null hypothesis is not rejected, and the means are determined as not being significantly different.

4.5. Comparison of the primary and secondary emission lines of Ag:

A comparison of both emission lines can be made in few different ways. First students can determine another percent difference between both emission lines of their sample. Alternatively, one could compare the percent errors (Table 4. S2) and identify the emission line of a larger percent error. Another option is to directly compare the error (standard deviations) from the concentrations averages (Table 4.1). Again, a t -test could be used here similarly to the comparison between the two calibration methods.

5. POST-LABORATORY ASSIGNMENT

A formal laboratory report should be prepared by each student for this experiment. Students should compare the results obtained with both calibration methods in terms of specificity and sensitivity. Students should not forget to elaborate on the significance of the theoretical yield of the Creighton reaction, the percent error, the percent difference, and the percent recovery. Students should also explain the difference in the results obtained using both emission lines of Ag. Lastly, depending on the scope of the course, students could also compare the Ag composition of Creighton colloids measured by ICP-OES to the UV-Vis absorption estimates from the surface plasmon resonance peak of AgNPs at about 400 nm. In our previous “laboratory experiment” work,¹⁰ we provided a detailed explanation on how the silver concentration can be roughly estimated using UV-Vis absorption spectroscopy.

6. REFERENCES

- 1) Rouessac, F.; Rouessac, A. *Chemical Analysis Modern Instrumentation Methods and Techniques*. 2nd ed.; John Wiley & Sons Ltd: West Sussex, England, 2007; pp. 309-327.
- 2) Skoog, D. A.; Holler, J. F.; Crouch, S. R. *Instrumental Analysis*. 8th ed.; Brooks/Cole: India, 2008; pp. 291-316.
- 3) Robinson, J. W.; Frame, E. M. S.; Ii Frame, G. M. *Undergraduate Instrumental Analysis*. 6th ed; Marcel Dekker: New York, 2005; pp. 483-505.
- 4) Sun, Y.; Xia, Y. Shape-Controlled Synthesis of Gold and Silver Nanoparticles. *Science*. **2002**, 298, 2176-2178.
- 5) Trefry, J. C.; Monahan, J. L.; Weaver, K. M.; Meyerhoefer, A. J.; Markopolous, M. M.; Arnold, Z. S.; Wooley, D. P.; Pavel, I. E. *J. Am. Chem. Soc.* **2010**, 132 (32), 10970-10972.
- 6) Badawy, A.; Feldhake, D.; Venkatapathy, R. *State of the Science Literature Review: Everything Nanosilver and More*; 2010.
- 7) Creighton, J. A.; Blatchford, C. G.; Albrecht, M. G., Plasma Resonance Enhancement of Raman Scattering by Pyridine Adsorbed on Silver or Gold Sol Particles of Size Comparable to the Excitation Wavelength. *J. Am. Chem. Soc., Faraday Trans. 2.* **1979**, 75, 790-798.
- 8) Gaines, P., *Silver Chemical Stability*. Vol. **2012**. <http://www.inorganicventures.com/silver-chemical-stability>
- 9) U.S. Environmental Protection Agency. *Determination of Metals and Trace Elements in Water and Wastes by Inductively Coupled Plasma – Atomic Emission Spectrometry*. Method 200.7. Revision 4.4. **1991**.
- 10) Dorney, K. M.; Baker, J. D.; Edwards, M. L.; Kanel, S. R.; O'Malley, M.; Sizemore, I. E. P. Tangential Flow Filtration of Colloidal Silver Nanoparticles: A “Green” Laboratory Experiment for Chemistry and Engineering Students. *J. Chem. Educ.*, **2014**, 91 (7), 1044–1049.

NOTES FOR INSTRUCTOR(S)

- For shorter laboratory time periods, the TA can prepare in advance the colloid, the standards, the glassware, and even operate the instrument. Even when omitted, the details of these procedures should be discussed with the students during the recitation period.
- If larger time periods are available, the colloidal nanoparticles should be synthesized together with the students by following any of the green or nongreen procedures described in the laboratory experiment from reference 20 of the manuscript.
- It should be noted that the U.S. EPA Method 200.7 was slightly modified to fit the allotted time period at our institution. Instructors are encouraged to follow as closely as possible the original U.S. EPA method if time and resources permit. This means that the silver stock solution should be prepared according to the U.S. EPA guidelines instead of purchasing it, and additional quality controls and assurances (QA's/QS's) should be included to increase confidence in the experimental results. In our laboratory experiment, we opted to increase the level of confidence by constructing an entire standard addition calibration curve rather than spiking a single sample. This offered more hands-on practice to our students and helped them better understand the spiking concept.
- All glassware utilized in the experiment should be thoroughly cleaned in a nitric acid bath (10% v/v), followed by a sodium hydroxide (1.25 M) in ethanol bath (80% v/v). Glassware should be rinsed with HQ H₂O (>18 MΩ cm) after each step.

- If an ICP-OES instrument is unavailable, a FAAS or GFAAS instrument can be employed as long as an Ag lamp is available. These options are outlined below:

Flame Atomic Absorption Spectroscopy (FAAS) –As long as a silver lamp is available this is probably the most attractive alternative. FAAS operation is fairly simple and may fit within the budget of most course allocated funds. Higher calibration standards may be necessary depending on the sensitivity of the instrument; likewise, a 1:100 dilution of the digested sample may be too large and should be reduced accordingly so that the expected concentration falls within the calibration curve. Additionally, the experiment can be elaborated with the exploration of different burner path-lengths and oxidant options if resources are available.

Graphite Furnace – Atomic Absorption Spectroscopy (GFAAS) – Similarly to FAAS, GFAAS is a suitable alternative without much-added cost. GFAAS has similar detection limits to ICP-OES, and the samples/standards may be prepared in the same manner. One distinct advantage is that GFAAS does not require as much sample as either FAAS or ICP-OES. However, the generation of reproducible results may be sometimes challenging.

- A tentative time schedule of the proposed activities is given in Table 4.S1.

Table 4.S1. Tentative time schedule for the proposed laboratory experiment. *Italics denote optional activities.*

Laboratory Period	Laboratory Activity	Time Period
	- Recitation	1 hr
#1	- Creighton colloid synthesis	2 hr
	- <i>UV-Vis absorption spectroscopy measurements of the colloidal AgNPs</i>	<i>30 min</i>
#2	- Chemical digestion of samples	2 hr
	- Quantitative dilution of samples	30 min
TA	- External standard preparation	1 hr
	- Standard addition preparation	1 hr
#3	- Operation of the ICP-OES	2 hr
	- <i>Data analysis together with the students</i>	<i>30 min</i>

- The average percent errors associated with this new laboratory experiment at WSU are given in Table 4.S2. The percent error for the two methods and the two emission lines of Ag were determined by comparing the actual yield for both courses to the theoretical yield for the Creighton reaction. These values were discussed in the manuscript.

Table 4.S2. Average percent errors (%) from each course, calibration method, and wavelength.

Course name	External Calibration		Standard Addition	
	328.068 nm	338.898 nm	328.068 nm	338.898 nm
<i>Instrumental Analysis</i>	5.3%	31.6%	3.9%	48.7%
<i>Experimental Nanomaterials & Nanoscience</i>	11.4%	11.8%	2.6%	25.3%

- The percent differences for each WSU student group are summarized in Table 4.S3. The wide range of values (from 0.9% to 187.2%) is probably due to the diverse student population (chemistry, physics, biology, environmental sciences, mechanical and materials engineering, and electrical engineering majors) and errors in sample preparation. The overall average of the percent difference (42.4%) is larger than the EPA recommended 10%, which supports the conclusion of matrix effects impacting the sample analysis.

Table 4.S3. Percent differences (%) calculated for each student group, for the 328.068 nm emission line of Ag.

Calibration Method	External Calibration (mg L⁻¹)	Standard Addition (mg L⁻¹)	Percent Difference (%)
<i>Experimental Nanomaterials & Nanoscience</i>	11.1	11.2	0.9
	10.1	0.3	187.2
	16.5	15.4	6.8
	17.7	15.9	10.5
	16.6	18.3	10.1
	16.9	18.4	8.6
	19.7	15.2	25.7
	15.9	8.2	63.2
	16.7	10.6	44.5
	18.2	11.4	46.5
<i>Instrumental Analysis</i>	24.3	12.2	66.6
	18.1	19.8	8.5
	21.1	15.1	32.9
	17.0	17.4	2.2
	5.7	23.5	122.3
<i>Average</i>	16.4	14.2	42.4

- Table 4.S4 summarizes the percent differences obtained in the two courses at WSU by comparing the results corresponding to the primary and secondary emission lines of Ag. These results were discussed in the manuscript.

Table 4.S4. Percent differences (%) between the primary and secondary emission lines of Ag based off course averages.

Calibration Method	Wavelength (nm)	Experimental			
		Nanomaterials & Nanoscience		Instrumental Analysis	
		[Avg.] (mg L ⁻¹)	% <i>Difference</i>	[Avg.] (mg L ⁻¹)	% <i>Difference</i>
External Calibration	328.068	13.65	0.49	17.42	35.09
	338.289	13.58		12.22	
Standard Addition	328.068	15.00	26.11	14.82	74.81
	338.289	11.53		6.75	

Laboratory supplies required for the proposed experiment

- Varian 710 ICP-OES instrument (or other atomic spectrometer equipped for Ag analysis)
- Micropipettes and disposable micropipette tips capable of volumetric uptakes in the 100 - 1,000 μL range.
- Chemical reagents:
 - Silver nitrate (Ultrapure Grade, 99.5%)
 - Sodium borohydride (99%, powder)
 - Optima nitric acid
 - $>18 \text{ M}\Omega\cdot\text{cm}$ water
 - $1,000.0 \pm 5.0 \text{ mg L}^{-1}$ of stock Ag^+ standard for ICP-OES analysis
- 50-mL beakers for digestion
- 50-mL and 100-mL Grade A volumetric for dilutions
- Hot plates
- 15-mL ICP-OES test tubes (if using autosampler)
- Glass funnels

Formative Assessment

The knowledge gained by the undergraduate and graduate students in this new laboratory experiment was assessed through written pre- and post-laboratory assignments.

Pre-Laboratory Questions

- 1) Why are the atomic emission methods with an ICP source better-suited for multi-element analysis than the flame atomic absorption methods?
- 2) Briefly, explain the two modes in which the ICP torch may be oriented and why one mode is better suited for lower detection limits than the other.
- 3) How many concentric quartz cones make up the ICP torch and what flows through each?
- 4) Briefly explain the standard addition method and indicate for which type of application it is suitable.
- 5) Name two advantages and two disadvantages of the ICP-OES method.

Answer Key for Instructors

- 1) The high-temperature plasma source of the ICP (up to ~ 10,000 K) compared to that of flame atomic absorption sources (2000-3000 K) make it better suited for multi-element analysis, as it can populate a large number of different energy levels for multiple elements simultaneously. This allows all excited atoms and ions to emit their characteristic radiation (wavelength) at approximately the same time. Another advantage is that atomic emission methods with an ICP source do not require element specific hollow cathode lamps for multi-element analysis when compared to flame atomic absorption methods.
- 2) The ICP torch may be oriented in the axial or radial position. The axial orientation is better suited for lower detection limits owing to a higher radiation intensity achieved through its longer path length. The axial orientation also offers greater precision compared to the radial orientation.
- 3) Three: the sample flows through the innermost cone, the tangential argon plasma support flows through the middle cone, and the auxiliary argon gas flows through the outer cone.
- 4) The standard addition method is a type of calibration that is used when matrix interferences in a sample are considerable. It consists of producing identical replicates of an equal volume of a digested sample and spiking them with increased amounts of a standard of known analyte concentration. The instrument response may be plotted against the volume of the standard added to each sample replicate, and a regression analysis is performed. The x -axis intercept corresponds to a zero addition, *i.e.*, a sample replicate that is not spiked. The product of the raw analyte

concentration in the sample and the volume of the sample replicate is equal to the product of the x -intercept and the concentration of the standard solution used for spiking.

- 5) Advantages: increased sensitivity (low detection limits), simultaneous emission lines or multi-elemental analysis due to the high plasma temperature.

Disadvantages: not applicable to most non-metals, relatively extensive preparation for analysis and possibility of chemical or spectral interference for multi-elemental matrices.

CHAPTER 5

CONCLUSIONS AND FUTURE DIRECTIONS

The benefits associated with silver nanoparticles will not be ignored. AgNPs have already proven themselves in many antimicrobial, conductive, and optical applications. This is likely to continue, despite the risks to human and environmental health. While toxicological studies have come a long way, most now generally agree AgNPs possess at least some sort of toxicity, either inherently or through the release of Ag^+ ions. Consequently, the worldwide expansion of silver nanotechnologies now demands responsive research to assess their environmental impact, determine techniques to monitor their persistence and transformation, and establish ways to spread awareness about the associated risks. Thus, the intent of this dissertation was aimed to assert the significance of nanoparticle research.

In chapter 2, freshwater crayfish was demonstrated as a potential benthic-zone indicator of freshwater silver pollution in its ionic or nano form by measuring total accumulated silver within the gills and hepatopancreas of exposed specimen. Chapter 3, established Raman spectroscopy as a possible methodology to characterize the physisorption and chemisorption mechanisms involved in the adsorption of AgNPs to hydrated mineral surfaces, namely, muscovite and corundum. Lastly, chapter 4 acknowledged the importance in educating future STEM students about evolving nanotechnologies and associated measurements involving in their characterization, such as ICP-OES and two calibration methods. Together these conclusions offer insight into AgNPs future and how to compromise between nanotechnological progress and unfamiliar environmental risks.

In future studies, it is perhaps most important for researchers to consider other types of silver nanoparticles. In each of these projects, the Creighton synthesis was chosen for its relative simplicity, low-cost, and popularity. Furthermore, Creighton AgNPs act almost as a AgNP “standard” since they do not contain many functional groups or stabilizing agents found in many others and they also exist in the world’s most popular solvent, water. However, in future studies, another synthesis should be considered because not one formula is used within industrial and consumer applications.

Another important future consideration involves more accurately identifying the forms or states of silver that derive from modern anthropogenic sources. In other words, research needs to go beyond comparisons between Ag^+ and AgNPs. The environment is never that simple. For example, controls with silver sulfides, chlorides, and even different oxidation states should be considered as these are likely terminus pathways for silver within freshwater environments. Likewise, the nature of these measurements usually involve x-rays and more sophisticated instrumentation and therefore introduce a whole other realm of variables that were not considered in any of these studies.

Lastly, confidence in almost all scientific results demand reproducibility, but instead of merely repeating experiments other variables should be tested and explored. For example, different benthic specimens could be tested to establish if crayfish are truly unique or if it is merely their location. Also, other minerals could be tested to demonstrate AgNPs tendency to complex more readily with one mineral surface over another. Or perhaps, other laboratory modules could be expanded to include other analytical techniques used in nanoparticle characterization and see if the same interest is generated.

In conclusion, the story of AgNPs fate and transport within freshwater environments will not end here, but it was never intended to. Nanotechnologies will continue to grow and will infiltrate our lives in ways never imagined before, and, as with any emerging contaminant, researchers must strive to keep up and continue to answer the questions others neglect or ignore. Hopefully, these projects will offer directions and insights into some of these future studies and, ultimately, help others in the development of their own studies and conclusions.

CHAPTER 6

CURRICULUM VITAE

SETH WILLIAM BRITTLE

EDUCATION

- Wright State University - Dayton, OH *September 2012 – December 2016*
Advisor: Dr. Ioana E. P. Sizemore Anticipated Ph.D. in Environmental Science
- Marist College - Poughkeepsie, NY *September 2008 – May 2012*
Advisor: Dr. Zofia Gagnon B. S. in Environmental Science

RESEARCH EXPERIENCE

Oak Ridge Institute for Science and Education Student Research Participant

U.S. Air Force Institute of Technology *September 2016 – Current*

- Detection and measurements of radiation with ORTEC analog NIM modules
- Developed and optimized positron annihilation lifetime spectrometer to measure defects

Graduate Research Assistant

Wright State University *August 2012 – Current*

- Synthesis of silver, gold, iron, and titanium dioxide nanoparticles for various applications
- Size selection, concentration, and purification of colloidal nanoparticles via tangential flow filtration
- Characterization of solid and liquid analytes with Raman spectroscopy and micro-Raman imaging
- Surface-enhanced Raman spectroscopy with functionalized nanomaterials
- UV-vis spectrophotometry for plasmonic characterization of colloidal nanoparticles
- Fluorescence spectrophotometry used to examine the emission spectra of fluorescent dyes
- Chemical digestions of aqueous, biological, and sediment samples
- Quantification of total elemental composition of nanometal colloids with inductively coupled plasma optical emission spectroscopy and flame atomic absorption spectrophotometry
- Quantification and size measurements of nanoparticles with transmission electron microscopy
- Topographical characterization of mineral surfaces with atomic force microscopy
- Surface area measurements of various minerals and nanomaterials with BET surface analyzer

Research Assistant,

Marist College *September 2011 – May 2012*

- Histological tissue preservation
- Single cell gel electrophoresis
- Flame atomic absorption spectroscopy
- Oxidative damage determined with bioassays
- Serotonin analyses via bioassays
- Electrochemical water measurements

TEACHING EXPERIENCE

Graduate Teaching Assistant, *Wright State University*

- Experimental Nanomaterials and Nanoscience *Fall 2012, 2013*
- Environmental Chemistry *Fall 2013*
- Instrumental Analysis *Spring 2014, 2015*

STEMM Camp Volunteer Instructor, *Wright State University*

- Exploring the Nanoworld of Precious Metals *Summer 2013, 2014, 2015*

Teaching Assistant, *Marist College*

- Plant Biology *Fall 2010, 2011*

SKILLS AND CERTIFICATIONS

- **Technical Skills:** ICP-OES, FAAS, TEM, FTIR, AFM, PALS, GC/MS, HPLC, IC, BET surface analyzer, UV-Vis spectroscopy, fluorescence spectroscopy, Raman spectroscopy, SERS, TFF, Water quality measurement (w/ YSI quarto probe multimeter). Bottom-up fabrication and characterization of colloidal silver, gold, and TiO₂ nanoparticles.
- **Computer Skills:** Microsoft Office 2016, Origin Pro 8.5, SigmaPlot 12.0, MatLab R2015b, SPSS 21.0, R 3.1.1,
- **Certifications:** Currently certified by WSU's Environmental Health and Safety Department in the following: Laser, Lab, and Biological Safety, Bloodborne Pathogens, and Radiation Safety Awareness. Completed OSHA's HAZWOPER training.

PUBLICATIONS

- Seth W. Brittle, Sessa L. A. Paluri, Daniel P. Foose, Matthew T. Ruis, Matthew T. Amato, Nhi H. Lam, Bryan Buttigieg, Zofia E. Gagnon, and Ioana E. Sizemore. Freshwater Crayfish: A Potential Benthic-Zone Indicator of Nanosilver and Ionic Silver Pollution. *Environmental Science and Technology*.
- Seth W. Brittle, Joshua D. Baker, Kevin M. Dorney, Jessica Dagher, Tala Ebrahimian, Steven Higgins, and Ioana E. P. Sizemore. Measuring Silver Nanoparticle Concentration by Inductively Coupled Plasma Optical Emission Spectroscopy: A Laboratory Experiment for Instrumental Analysis and Nanoscience. *Journal of Chemical Education*.
- Sushil R. Kanel, Heath Misak, Dhriti Nepal, Shankar Mall, Seth W. Brittle, Ioana E. Sizemore, David M Kempisty, Mark N. Goltz. Application of Carbon Nanotube Yarns as a Filter Media to Treat Nitroaromatic-contaminated Water. *New Carbon Materials*.

PRESENTATIONS

- Oral Presentation – 2016 Fall AGU Meeting *December 2016*
“Spectroscopic Methodologies for Characterizing the Adsorption Behavior and Distribution of Silver Nanoparticles to Hydrated Mineral Surfaces”

Seth W. Brittle, Kevin O’Neil, Daniel P. Foose, ... Steven R. Higgins, and Ioana E. P. Sizemore

- Poster Presentation – 47th ACS Central Regional Meeting *May 2016*
“Fate and Transport of Colloidal Silver Nanoparticles in a Saturated Porous Media: A Laboratory Experiment for Chemistry and Engineering Students”

Seth W. Brittle, Sushil Kanel, Jessica Dagher, Allie Meyerhofer, Ioana E. P. Sizemore

- Oral Presentation – 249th National ACS Conference *March 2015*
“Bioaccumulation of ionic silver and silver nanoparticles within freshwater crayfish using inductively coupled plasma optical emission spectroscopy”

Seth W. Brittle, Daniel P. Foose, ... Zofia E. Gagnon, and Ioana E. P. Sizemore

- Poster Presentation – 249th National ACS Conference *March 2015*
“Measuring silver nanoparticle concentration by inductively coupled plasma optical emission spectroscopy: A laboratory experiment for chemistry and engineering students”

Seth W. Brittle, Joshua D. Baker, Kevin M. Dorney, ...Steven R. Higgins, and Ioana E. P. Sizemore

- Oral Presentation – 8th Cleveland State Interdisciplinary Research Conference *Nov. 2014*
*“Bioaccumulation of Silver Nanoparticles within Hudson River Crayfish (*Orconectes virilis*)”*

Seth W. Brittle, Daniel P. Foose, ... Zofia E. Gagnon, and Ioana E. P. Sizemore

- Poster Presentation – 8th Cleveland State Interdisciplinary Research Conference *Nov. 2014*
“Quantifying Silver within Nanocolloids by Inductively Coupled Plasma Optical Emission Spectroscopy using two Widely Accepted Calibration Methods”

Kevin A. O’Neil, Seth W. Brittle, Joshua D. Baker, ...Steven R. Higgins, and Ioana E. P. Sizemore

- Oral Presentation – 246th ACS National Conference *September 2013*

“Optimizing silver nanoparticle size and excitation wavelength for single-molecule SE(R)RS-based detection”

Kevin M. Dorney, Joshua D. Baker, Austin J. Williams, Adam C. Stahler, Seth W. Brittle, Trevor M. Bobka, and Ioana E. P. Sizemore

RELEVANT COURSEWORK

- *Wright State University* (Graduate): Environmental Statistics, Environmental Genes Organisms and Ecosystems, Instrumental Analysis, Experimental Nanomaterials and Nanoscience, Chemical Processes in the Environment
- *Marist College* (Undergraduate): General Chemistry, Organic Chemistry, Environmental Chemistry, General Biology, Plant Biology, Plant Physiology, Physics, Toxicology, Ecology, Geology, Intro. to GIS

HONORS AND AWARDS

- Presidential Scholarship - Marist College *2008 – 2012*
- Eagle Scout *2007*

MEMBERSHIPS

- American Association for the Advancement of Science *2011 – current*
- American Chemical Society *2013 – current*
- American Geophysical Union *2016 – current*

EMPLOYMENT

- ORISE Student Participant at US AFIT - Dayton, OH *September 2016 –present*
- Graduate Research Assistant - Dayton, OH *2012 –present*
- Marist Science Summer Researcher - Poughkeepsie, NY *Summer 2011*
- Marist College Campus Student Security Guard - Poughkeepsie, NY *2008 – 2012*
- Northern Tier High Adventure Base Interpreter - Ely, MN *Summer 2010*
- Philmont Scout Ranch Ranger - Cimarron, NM *Summer 2009*